Technische Universität München

Fakultät für Maschinenwesen

Lehrstuhl für Fahrzeugtechnik

Active Cell Interconnection for Improved Battery Utilization in Electric Vehicles

Dipl.-Ing. Univ. Felix Römer

Vollständiger Abdruck der von der Fakultät für Maschinenwesen der Technischen Universität München zur Erlangung des akademischen Grades eines

Doktor-Ingenieurs

genehmigten Dissertation.

Vorsitzender:	Prof. Dr.-Ing. Michael Zäh
Prüfer der Dissertation:	1. Prof. Dr.-Ing. Markus Lienkamp
	2. Prof. Dr. Sebastian Steinhorst

Die Dissertation wurde am 14.01.2021 bei der Technischen Universität München eingereicht und durch die Fakultät für Maschinenwesen am 02.06.2021 angenommen.

Acknowledgement

This dissertation and relevant studies were conducted during my time as a research associate at TUMCREATE, Singapore, and as a Ph.D. candidate at the Institute of Automotive Technology (FTM), Technical University of Munich (TUM), Germany. This dissertation is funded by the National Research Foundation (NRF) of Singapore, under its Campus for Research Excellence And Technological Enterprise (CREATE) program. Therefore, first, I would like to show my gratitude to the organizations above. Without the support of these organizations, the studies in this dissertation could not be conducted.

Beside of the supporting organizations, I also would like to express my appreciation of the support from individual persons and groups.

First to mention hereby is the much appreciated support and supervision of my thesis supervisor, Prof. Dr.-Ing. Markus Lienkamp. He gave me the opportunity to go a path I never would have chosen otherwise, to develop skills I never thought I would ever learn, and to improve myself to a level I never thought I would reach. He entrusted me with the responsibility to work on several prototypes, being in charge of a research team in critical times and develop a research idea that fitted my interests and previous projects. His supervision was a perfect compromise of freedom to develop my ideas and guidance, when I needed it.

Secondly, I would like to thank Prof. Dr. phil. nat. Sebastian Steinhorst as my second supervisor of this thesis. His inputs gave me precious insights how to handle the topic and this thesis to bring it to a completion in time.

A special acknowledgement I want to express to my friend and colleague Dr. Fengqi Chang, who is also the author of the concurrent thesis. The whole idea and implementation of this thesis is based on our numerous meetings, conversations, and discussions. All his help to develop myself in a more scientific direction is much appreciated. In addition, his inputs as a proofreader were a priceless contribution to improve this work.

I would like to thank TUMCREATE with its management and all staff for their support to employ me all the time and to entrust me with tasks of big responsibility, where I was able to learn a lot.

Dr. Aybike Ongel as my mentor and principal investigator helped me as well to improve my scientific methods and my writing style for various scientific papers and this thesis. Her comments are much appreciated.

Without the teams in Singapore, especially IMVS and DAM, this thesis probably never would have reached this stage and for sure would not have been the same fun! The collegial cooperation and enjoying life beyond work made my stay in Singapore pleasant every day. Especially thankful I am for the effort of Mr. Olaf Teichert for his inputs while proofreading this thesis.

In addition, the Electric Powertrain Research Group in Munich with all their current and previous members should be mentioned, where always an open ear for current challenges was found and many tips on a successful completion of a thesis.

During my time as a PhD candidate, I supervised numerous students. Their contribution to this thesis as well as to the multiple other successful projects I worked on is much appreciated.

On a personal side, I would like to express my unmeasurable thankfulness towards my wife, Mrs. Shu Long. Without her, literally none of my major life achievements would have been possible, starting from my master thesis, graduating university, the great time in Singapore, many successful projects, this thesis, and, far above everything else, our wonderful son Luan with all his ups and downs.

My deep gratitude goes to my parents for all their support on my whole path so far.

Also to mention are the various friends both in Singapore and Germany, which made the endeavor of this thesis an enjoyable one.

Finally, I would like to express my gratitude to all the individuals and organizations, whom I have failed to cover in this short acknowledgement.

Singapore, December 2019

Felix Römer

Table of Contents

Abbreviations

AC	Alternating Current
ANN	Artificial Neuronal Network
APOD	Alternative Phase Opposition Disposition
ASM	Asynchronous Motor
BEV	Battery Electric Vehicle
BMS	Battery Management System
CAN	Controller Area Network
CC	Constant Current
CCV	Closed-Circuit Voltage
CHB	Cascaded H-Bridge
CoC	Coulomb Counting
CSP	Chip Scale Packaging
CV	Constant Voltage
DC	Direct Current
DOD	Depth of Discharge
ECM	Equivalent Circuit Model
EES	Electrical Energy Storage
EMI	Electromagnetic Interference
EOL	End of Life
EV	Electric Vehicle
FCEV	Fuel Cell Electric Vehicle
FTP	Federal Test Procedure
GHG	Greenhouse Gas
HEV	Hybrid Electric Vehicle
HV	High Voltage
ICE	Internal Combustion Engine
IGBT	Insulated-Gate Bipolar Transistor
IIR	Infinite Impulse Response
IPD	In Phase Disposition

IR	Impulse Response
KF	Kalman Filter
LCA	Life-Cycle Assessment
LCO	Lithium Cobalt Oxide
Li-ion	Lithium-ion Battery
LMO	Lithium Manganese Oxide
LO	Luenberger Observer
LFP	Lithium Iron Phosphate
LV	Low Voltage
M2B	Modular Multilevel Battery
ML	Multilevel
MMC	Modular Multilevel Converter
MOSFET	Metal-Oxide-Semiconductor Field-Effect Transistor
NCA	Lithium Nickel Cobalt Aluminum Oxide
NEDC	New European Driving Cycle
NiCd	Nickel–Cadmium
NiMH	Nickel–Metal Hydride
NMC	Lithium Nickle Manganese Cobalt Oxide
NYCC	New York City Cycle
OCV	Open-Circuit Voltage
OEM	Original Equipment Manufacturer
PCB	Printed Circuit Boards
PDPWM	Phase Disposition Pulse Width Modulation
POD	Phase Opposition Disposition
PSM	Permanent Magnet Synchronous Motor
PSCPWM	Phase-Shifted Carrier Pulse Width Modulation
PWM	Pulse Width Modulation
RMS	Root Mean Square
SEI	Solid Electrolyte Interphase
SM	Sub Module
SOC	State of Charge
SOH	State of Health
SOI	State of Inhomogeneity
SVM	Space Vector Modulation
TCO	Total Cost of Ownership

THD	Total Harmonic Distortion
UDC	Urban Driving Cycle ECE-15
USD	United States Dollar
VSI	Voltage Source Inverter
WLTP	Worldwide Harmonized Light Vehicles Test Procedure

Symbols

Symbols	Unit	Description
α	-	Temperature coefficient
$\Delta C_{\text{components}}$	USD	Cost difference between IGBT inverter and CHB inverter
ΔC_{Energy}	USD	Cost for energy consumption difference
ΔC_{pack}	USD	Cost difference between battery packs
ΔSOC	%	Difference of real SOC compared to observer SOC
$\Delta SOC_{\max}$	%	Maximum divergence between the SM SOC
Δx_{minmax}	A h or Ω	Maximum spread of parameter x
ε	-	Energy cost factor
μ_x	A h or Ω	Mean value of parameter x
σ_{die}	USD mm^{-2}	Specific price per die area
σ_x	A h or Ω	Standard deviation of parameter x
τ	s	Desired smoothing time constant
a	-	Phase indicator of the first phase in a 3-phase system
A_{die}	mm^2	Die area
ap_{c}	%	Accessible potential of the capacity
b	-	Phase indicator of the second phase in a 3-phase system
c	-	Phase indicator of the third phase in a 3-phase system
c_{act}	A h	Actual capacity
c_{cell}	A h	Battery cell capacity
$c_{\text{cell},j}$	A h	Capacity of j-th battery cell in parallel
C_{CHB}	USD	Costs of CHB inverter including switches
C_{contact}	USD	Cost of contactors
C_{die}	USD	Cost of die
$C_{\text{GD1}} = C_{\text{GD}}(U_{\text{DD}})$	F	Gate-drain capacitance when the voltage is U_{DD}
$C_{GD2} = C_{GD}(R_{DS(on)}I_{on})$	F	Gate-drain capacitance when the voltage is $R_{DS(on)}I_{on}$
C_{IGBT}	USD	Costs of IGBT inverter

$\cos\theta$	-	Power factor
c_{nom}	A h	Nominal battery cell capacity
c_{pack}	A h	Battery pack capacity
C_{package}	USD	Package price including die integration and bonding
c_{parallel}	A h	Capacity of parallel connected batteries
$c_{\mathrm{parallel},j}$	A h	Capacity of j-th parallel battery cells in series
C_{relBat}	USD kW^{-1} h^{-1}	Cost per kWh for the battery on pack level
$C_{\mathrm{relEnergy}}$	USD kW^{-1} h^{-1}	Cost for the electric energy
c_{res}	A h	Remaining (or residual) electric charge
C_{SC}	USD	Cost of semiconductor
CV_x	%	Coefficient of variation
D	km	Total distance driven over the lifetime
E	-	Expected value
E_{Consum}	W h	Energy consumption for the respective inverters
E_{loss}	W h	Energy losses
E_{pack}	W h	Energy of the battery pack
f	Hz	Sine frequency
i	A	Current
$i(t)$	A	Time variable current
i_{cell}	A	Battery cell current
I_{D}	A	Drain current
I_{on}	A	MOSFET current
i_{pack}	A	Battery pack current
i_{ref}	V	Reference current
i_{SM}	A	Battery submodule current
k_{B}	-	Voltage correction gain
k_x	-	Kurtosis of parameter x
l	-	Indicator of lower modules
M	N m	Torque
m	-	Number of battery cells connected in series
N	-	Sample size/Population size
n	-	Number of battery cells connected in parallel
f_{rot}	rev min^{-1}	Rotational speed
o	-	Sample number
p	-	Number of configuration

p_{c}	%	Maximum usable potential of the capacity
P_{real}	W	Power
q	-	Number of switch
Q_{rr}	A s	Recovered charge of the anti-paralleled diode
R	km	Range requirement
R_{D}	Ω	Dynamic resistance of the anti-paralleled diode
$R_{\mathrm{DS(on)}}$	Ω	Drain-source on resistance
SOC	%	State of Charge
$SOC_{\mathrm{parallel},j}$	%	SOC of j-th parallel battery cells in series
SOH	%	State of Health
SOI_x	%	State of inhomogeneity (SOI) of parameter x
sp_x	A h or Ω	Relative maximum spread of parameter x
s_x	-	Skewness of parameter x
t	s	Time
t_{fi}	ms	Current fall-time during turn-off
t_{ri}	ms	Current rise-time during turn-on
T_{s}	s	Sample time
u	-	Indicator of upper modules
u	V	Voltage
u_{cell}	V	Battery cell voltage
$u_{\mathrm{cell},l}$	V	Voltage of l-th battery cell in series
$u_{\mathrm{cell,max}}$	V	Battery cell end-of-charge voltage
$u_{\mathrm{cell,min}}$	V	Battery cell cutoff voltage
U_{D0}	V	Diode on-state zero-current voltage
U_{DD}	V	Converter supply voltage of MOSFET
u_{ECMOP}	V	Calculated over potential of the ECM
u_{n}	V	Neutral point voltage
u_{OCV}	V	Battery cell open circuit voltage
U_{P}	V	Plateau voltage
u_{pack}	V	Battery pack voltage
u_{ref}	V	Reference voltage
u_{RMS}	V	RMS voltage
u_{SM}	V	Sub module voltage
u_{sum_x}	V	Sum of all available submodule voltages of the x phase
u_{zs}^{*}	V	Commanded voltages of z phase

u_{zy}	V	Voltage between phase z and y
v	m s^{-1}	Speed
V_{DS}	V	Drain-source voltage
x	A h or Ω	Parameter representing either capacity or resistance

1 Introduction

Mobility is and will remain a key challenge for humanity. It is a requirement for economic and individual progress to be able to transport persons and goods in a timely manner. There are varying requirements depending on the travelled distance and there are diverse approaches for the usage of different modes for transportation. However, all require an energy source, storage, and conversion. The currently most prevailing solution is the usage of fossil fuel burning internal combustion engines (ICE) [1]. However, this solution causes the emission of greenhouse gasses (GHG) and other pollutants and results in road vehicles contributing to 20 % of overall human pollution [2]. Due to increased urbanization, these emissions are concentrated in metropolitan areas, which leverages the effect of pollution even more [3].

As a current and future solution, battery electric vehicles (BEV) are promising due to their scalability, high efficiency, and significantly reduced local emission levels [4]. Firstly, by replacing ICE vehicles with BEV, the energy generation during the use phase is moved away from the application area, e.g., the roads of a city, to the location where the electrical power is generated, e.g., the power plant. While the electricity generation is still mainly based on fossil fuels in most countries [5], such a shift removes the source of the emissions away from the majority of people at many places. Additionally, power plants achieve a higher conversion efficiency [6] and include a better flue gas scrubbing compared to individual ICE in vehicles [7]. Secondly, with the usage of renewable energy sources to generate electricity, BEV can be used without producing any energy conversion related emissions. A trend is currently visible to increase the usage of renewable energy sources around the world [8]. A third argument for BEV is their intrinsic higher efficiency compared to ICE vehicles due to their ability to recuperate and therefore they have lower losses during braking. This plays an even more important role, if the vehicle is driven in an urban area with repeated accelerations/decelerations [9]. Hence, even with additional losses of the electricity infrastructure and during charging, a BEV still uses less energy for driving compared to an ICE vehicle [6].

The highlighted benefits caused a number of countries to introduce new laws and guidelines to enable an accelerated introduction of BEV. For example, several countries provide tax incentives or directly subsidize the usage of BEV [10]. Other countries or regions introduced permission quotas, where the total number of vehicles on the roads is limited and an ICE/BEV ratio has to be maintained [11]. An alternative incentive is granting advanced rights to BEV, where they for example can park for free or use priority lanes [12]. Some governments even went one step further and decided to fully ban new ICE vehicle registrations in the future with clear deadlines [13]. This causes existing vehicle manufacturers to increase their production capacities and product portfolios in favor of BEV [14]. Moreover, many new automotive startups, especially from countries without a strong production background, such as China, try to enter this market as well, since such a disruptive technology change may enable new players on the market [15].

Altogether, this indicates the current and future relevance of battery electric vehicles and supports the necessity of further research in this area.

1.1 Motivation

The main bottleneck for an even faster expansion of battery electric mobility is the high cost for current battery technologies, since they contribute up to 50 % to the overall initial vehicle costs [5]. This results in the situation that currently even the five most cost effective BEV have a base price of United States dollar (USD) 15,474 plus additional USD 52.43 per km of range [16]. With a minimum range expectation of 194 km per charge [17], this results in a minimum price of USD 25,645.42 for a new BEV in contrast to on average USD 20,943 for comparable compact cars with an ICE [18]. The high costs for the batteries are mainly caused by the used materials [19]. So even if the demand for batteries increases drastically in the future, no major price drops are expected due to economy of scale. For some of the materials even an opposite effect can happen, where the increased demand leads to a drastic increase of the market price [8].

On top of that, the environmental impact caused by the production of the battery has to be considered. Certain raw materials, for example aluminum, require high amounts of energy to be produced. In addition, the battery cell assembly has a high energy demand to produce the sensitive cells in the required quality. Since the energy in most countries is still generated by burning fossil fuels [5], it increases the GHG emissions for a BEV in a life-cycle assessment (LCA) almost up to the same level of an ICE vehicle with the same size, depending on the overall distances driven [20], [21]. This fact can only be mitigated in the future with a higher penetration of renewable energies during production, but cannot be fully avoided. For the environmental impact, besides of GHG emissions, also other factors, such as consumption of resources, acquisition of raw materials from debatable sources, and fresh water usage, have to be considered.

Both arguments combined are amplified with the consideration that the battery significantly contributes to the weight of the vehicle [5] and therefore its energy consumption [22]. This effect might be reduced in urban environments, where due to recuperation much energy is conserved, but plays a more important role for longer distances on expressways with fewer stops.

Yet another challenge for electromobility is the aging of the batteries. As it will be explained in detail in Section 2.1.2, the parameters of batteries, mainly the capacity and inner resistance, are deteriorating over time and during usage. Since aged batteries at a certain point cannot fulfill the minimum range requirements of the vehicle anymore, the battery has to be replaced. Often this is not economical, because of which a new vehicle is purchased instead.

As a conclusion of the four mentioned arguments, it can be stated that the battery must be used as efficient and as long lasting as possible for an increased market penetration rate of BEV. An improved efficiency would enable a smaller and therefore more cost-efficient battery, which may increase the willingness to buy while reducing the environmental impacts. The time until end of life (EOL) of the battery can be increased by reducing the Depth of Discharge (DOD) with which the battery is cycled. A battery cycle herein refers to one complete charge and discharge depending on the individually defined limits. However, a smaller DOD reduces the usable capacity of the battery, which in turn results in increased battery size. Therefore, there is a need to increase the usable capacity of the battery without increasing the battery size and cost or reducing the battery lifetime. This research investigated active cell interconnections for improved battery utilization, i.e., increased usable capacity without compromising the battery aging. The improved utilization would allow for a smaller and hence more cost effective and environmentally friendly battery for a given range requirement with the same lifetime of a conventional battery. The outcome of this research will still be relevant once less costly battery technologies and cars that are more efficient are available, since it will still improve the initial and operating costs of the vehicle.

1.2 Problem Statement

The current way of addressing high energy storage costs in BEV is to increase the overall vehicle efficiency, which allows installing a smaller battery capacity without reducing the range capabilities. This is done by either reducing the required consumption of the vehicle (improved air drag, low energy thermal comfort, reduced auxiliary losses, etc.), or by achieving a higher efficiency during the energy conversion in the powertrain (motor efficiency, power electronics, etc.). An additional way to reduce energy storage costs is increasing the battery utilization, which means getting access to already existing capacity resources, which are not utilized by current technology. State of the art batteries are not fully utilized due to the way battery packs are constructed: a big number of small cells, sometimes several thousand, are connected in parallel and series to increase the capacity, voltage, and current rating of the pack according to the requirements. Due to production tolerances, cells, even from the same batch, have a certain variation in their parameters, mainly their capacity and inner resistance [23]–[25]. Their individual current charge level and voltage level are strongly interconnected and the used chemistry defines a voltage range with strict limits [26] as otherwise increased aging or safety problems caused by over-(dis)charge of that cell occurs (see Section 2.1.2). The variations in capacity and inner resistance are causing a relative voltage/charge level drift amongst the in series connected cells during use. As the overall charge and discharge must stop once the first series connected cell/module reaches its voltage limits, the relative drift increasingly reduces the usable capacity down to eventually zero, as illustrated in Figure 1.1a). This effect accelerates with a high number of series connected cells and with frequent, small cycles, which happens likely in stop-and-go traffic [27].

While the drifting problem still can be handled with a technological method called balancing, which will be explained in Subchapter 2.2, the cell variation still will cause the cells with the smallest capacities in series connection to limit the overall usable capacity [28], as shown in Figure 1.1b). Parallel connections of cells with different parameters result in self-balancing currents between the respective cells, which cause additional losses and aging [29]. Additionally, cells with different initial capacities in a battery pack age differently over time and the variation of capacities becomes wider [30]. It can be caused by the weaker cells degrading faster as compared to the healthier ones under the same load. This limits the performance of the whole battery pack and reduces its lifetime [31].

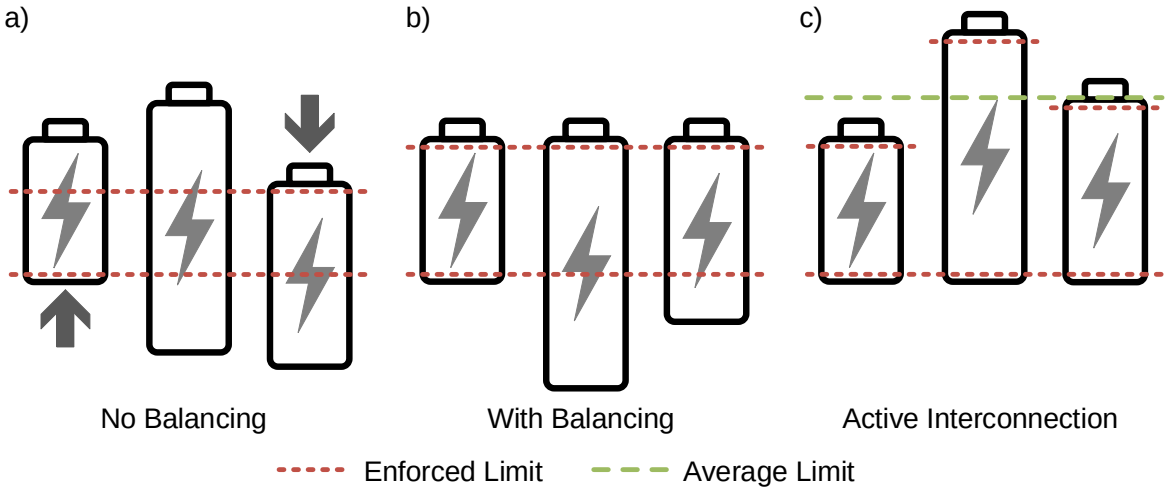

Figure 1.1: Symbolic representation of battery tolerances and their usable capacity in series connection. The size of the cell symbols represent the capacity of the series connected cells/modules and their position the relative voltage levels compared to each other.

1.3 Aim and Objectives

The aim of this thesis is to evaluate the performance of an active cell interconnection for batteries in automotive applications. The active cell interconnection is expected to enable a higher battery utilization as shown in Figure 1.1c), which can lead to a decreased battery pack size while still fulfilling the range requirements. Such a new pack would be lighter, more cost-efficient and have a lower environmental impact. However, the interconnection system should not compromise the efficiency, aging, or costs of the overall vehicle including the running costs. The system also should be parametrized in such a way that an implementation in an electric vehicle is feasible today or in the near future.

To fulfill the aim, the following objectives are defined:

- Define the most promising method to access the additional potential.
- Evaluate the potential of unutilized battery capacity due to battery cell variations with a focus on, but not limited to, large automotive battery packs.
- Conduct a total cost of ownership (TCO) comparison for the active interconnected battery with conventional BEV as an optimization and evaluation criteria.
- Investigate the impact of the selected method on energy efficiency including a higher utilization of the inhomogeneous capacity of the cells.

The scope of this dissertation is to evaluate, to which extent and with which methods the battery tolerances can be utilized to extract more energy from a battery pack. This additional accessible energy is used to make the battery smaller. The economic feasibility is evaluated by comparing the saved battery costs to the adjusted costs of the new technology. For this, an investigation is required, which tolerances can be expected and what are their consequences. Various circuits of active cell interconnections are evaluated, and a preferred one is selected. An in-depth analysis shows how this circuit can be controlled to utilize the sub-units in an individual way while ensuring the overall functionality of the vehicle. To do so, a clear awareness of the current states of the sub-units is required, so a suitable state estimator has to be defined. With all the inputs described, the preferred circuit is analyzed and parametrized in detail. Here, also the costs and feasibility play an important role. After the results are demonstrated, some general considerations towards the implementation of such a system are given. In the end, the best-case realistic benefits of an active interconnection can be highlighted.

Not within the scope of this dissertation are the aspects of the overall efficiency, detailed cost comparison, battery aging under the focus of a different modulation and the reliability of the electronics. These are covered in the complementary dissertation of Mr. Fengqi Chang [32]. For the efficiency, he focused on the functionality of the smallest subcomponents, the switches, and put them in comparison with currently used components and other future potential technologies. In his cost analysis, he conducted a detailed cost breakdown of all the involved components and cost contributors with comparisons to current costs and future alternatives. He analyzed the battery aging in extensive experiments to verify that the high frequency modulated discharge is not causing additional aging. In his reliability studies, he showed with a methodical approach that the new circuits have the potential to outperform conventional circuits. Wherever the present dissertation leverages on his research or skips the investigation of a question due to the existing coverage, it is mentioned in the text.

The contribution and novelty value of this dissertation is the definition of the possible improvements to the battery pack achieved by using a cell interconnection approach compared to a conventional electric powertrain. It can be used as a guideline for researchers, developers, and engineers interested in battery technology as well as in vehicle engineering. For the batteries, this dissertation shows the potential of improved battery utilization by investigating the existing tolerances for different cell types. Different methods to access an increased amount of energy from a pack are presented and evaluated. The most promising topology is then investigated in detail to parametrize it in an optimal way, including an economic consideration. The results are shown including recommendations of the overall configuration within an automotive use case. In conclusion it shows, to which extend it is worth to increase the efforts on reducing the battery tolerances, especially from a monetary perspective. Moreover, for vehicle engineering, it indicates the potential gains on implementations of active interconnection systems. This research gives answers, which additional considerations are necessary to access the full potential of the battery and therefore increase the vehicle value.

1.4 Structure of the Dissertation

The structure of this research follows an adaption of the “V-Model”, which is often used in mechatronic and software development [33], [34]. For that, the different work packages are placed in a way that it is shaping a “V”. On the left side of the “V” with each package downwards, the system is further decomposed and the work steps are described in a deeper layer and detail, starting from high-level questions down to detailed queries about individual components. On the right side of the “V”, the re-composition, integration, and verification steps are sorted in a way that they answer the respective questions on the corresponding layer.

In this dissertation, the first step is the definition of the high-level relevance of the topic. This includes the motivation behind the research, the definition of the problem and a depiction of the aim and objectives. In addition, the structure of the thesis is explained. This is described in Chapter 1 and in Figure 1.2 it can be found as the first work packages in the V-Model.

In Chapter 2, firstly some fundamental aspects of BEV and their relevant components are discussed to introduce a common terminology for the rest of the thesis. A focus is laid on the energy storage systems and the power electronics of the powertrain. Later, currently existing solutions to handle battery variations in packs are described. Here, both commercial and research approaches are investigated, and the limitations of these technologies are discussed. The most promising solution is determined, for which the current disadvantages are highlighted as well. With this, the research gap is identified.

In the following Chapter 3, the methodology is described, which represents the lowest level of the V-Model, where the details of the implementations are explained. This work package is divided in four subchapters: Battery Tolerance Analysis (Subchapter 3.1), Control Strategy (Subchapter 3.2), Module State Estimation (Subchapter 3.3), and Optimization of the Inverter Configuration (Subchapter 3.4). In the first part, an extensive review of the current understanding of battery parameter variations and tolerances is given and evaluated. This enables a good insight of the magnitude of the problem and therefore the maximum potential capacity gain of any solution. The second part conducts an investigation, how the selected circuit can be controlled in the best way to achieve an individual load on the submodules of the battery pack. Different modulations are compared to each other in terms of their efficiency, overall implementation of

motor control and their ability to achieve a balance between the cells. A preferred one is selected and is then further used for the third subchapter, which looks into the topic that balancing of the modules requires an awareness of their current states. This is a challenging task for active cell interconnections, since there is no way to measure the states and parameters of battery cells directly, but this information is required with high sampling rates. Current state estimators and new ideas are compared to identify a solution to be able to balance the modules as close as possible. The selected estimator is then used in the fourth subchapter, where the optimal configuration of the selected circuit is identified. To conduct this, various configurations are simulated and compared to each other in regards of their efficiency and costs.

Beginning with Chapter 4, a re-composition of the system details is started to define the overall system and therefore benefits. It merges all the results from the previous work packages. Therefore, it firstly evaluates and describes the real variations found in the review of current batteries parameters. Then, it indicates the results for the system optimization, where optimal sorting and state estimations are presented. With these results, the possible utilization improvements are possible to be quantified. That in turn leads to the results of the overall configuration optimization and its improvements compared to a conventional BEV powertrain.

In Chapter 5, the presented results are discussed to indicate the probability of an actual commercial vehicle implementation including the limits and feasibility. In the first part, the different results of the four subtopics presented in the methodology are discussed separately to identify influencing factors and their impact on the results. In the second part, recommendations are given, which lessons can be drawn from the results. This is started from the smallest unit, the cell, and then is re-composed to module level, pack level, and in the end recommendations on novel applications on networks of packs featuring the increased utilization circuit including their first life in vehicles and second life applications. In the end, challenges of the presented active cell implementation are presented and an outlook suggests the direction of further research that would complement the present dissertation.

The final Chapter 6 presents an overall conclusion and summary of the conducted research. It rounds up, which of the questions from the first chapter can be answered with the proposed approach and which problems can be solved.

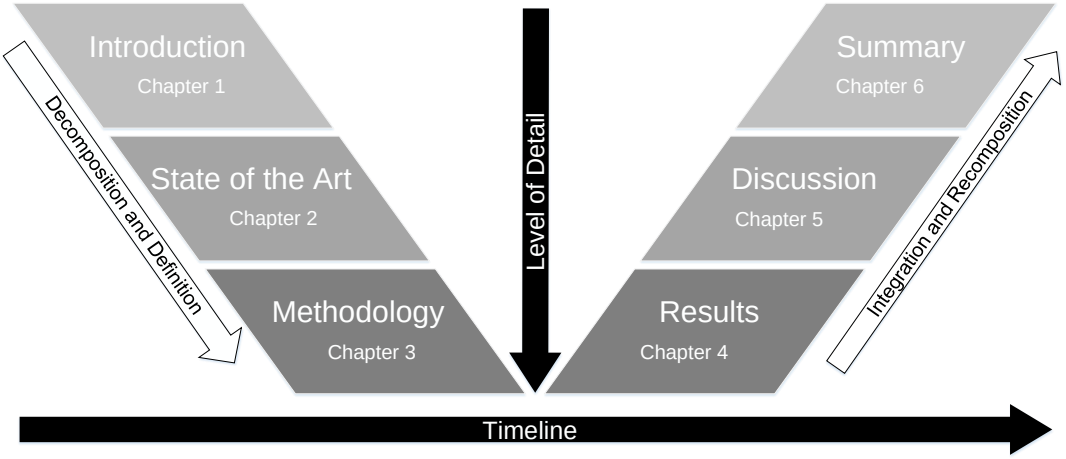

Figure 1.2: Structure of the dissertation showcased in a V-Model

2 State of the Art

This chapter gives an overview of how the problem related to the battery cell variations is currently handled in literature and commercial applications. First, some fundamental aspects of BEV with a strong focus on the powertrain and the electrical energy storage (EES) system are specified. After that, the current commercial solution of this problem, battery cell balancing, is described and discussed in detail. It is followed by a description of different alternative solutions proposed in literature. For each, the advantages and disadvantages are discussed and summarized in a ranking. The preferred method is selected, which is then investigated in detail for the rest of the dissertation. The state of the art chapter concludes with a definition of the research gap, which the current literature cannot answer until now and therefore it highlights the necessity of the conducted research of this dissertation. This chapter refers to the second work package in the V-Model described in Subchapter 1.4, and the structure is shown in Figure 2.1.

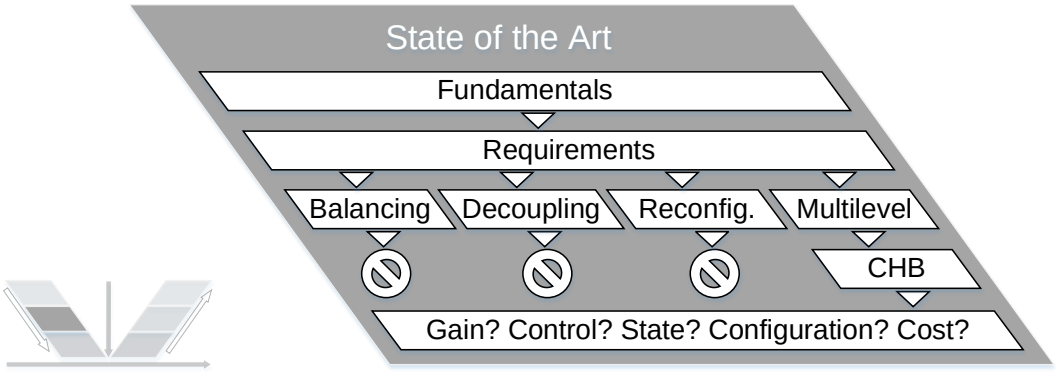

Figure 2.1: Structure of Chapter 2

2.1 Fundamentals of Battery Electric Vehicles

BEV are a specific subcategory of electric vehicles (EV), which are defined as vehicles with an electrified powertrain. “Vehicle” in these definitions is a machine that transports people or cargo and ranges from small micro-mobility solutions, such as e-scooters and bicycles until large vehicles like busses, trains, or even airplanes. In this dissertation, “vehicle” only refers to road-based cars, since they are responsible for 52 % of all transportation related energy consumption and they therefore have the greatest relevance [35, pp. 605–610]. In addition, smaller vehicles such as micro-mobility vehicles have much less battery cells in their packs and therefore the issues with tolerances are less severe. Nevertheless, the described approach is not limited to medium sized road-based cars, because especially for bigger vehicles, for example heavy-duty vehicles, busses, etc. with larger battery packs, a higher utilization rate could be even more beneficial.

Other examples of EV would be the fuel cell electric vehicle (FCEV), which is using hydrogen as an energy storage, or the hybrid electric vehicle (HEV), where different forms of energy storage are combined [36]. For this dissertation, only pure BEV are considered where a battery pack is the sole source of energy supply for an electric motor that drives the car. The reason for that are the advantages of BEV compared to HEV, which requires at least two storages and conversion systems. That in return increases the costs and decreases the reliability of such a vehicle. Additionally, FCEV have a larger carbon footprint compared to BEV, since the source of the hydrogen gas is either fossil fuels or generated with significant losses [4]. However, the solutions investigated in this dissertation can be applicable for alternative architectures as well, since many of them still use batteries: HEV as one of the storage systems and FCEV as a buffer for high power demand periods.

2.1.1 Electric Vehicle

In general, an EV powertrain consists of four major components: the EES system, which will be explained in Section 2.1.2, a converter implemented with power electronics, which will be explained further in Section 2.1.3, an electric motor, and a drivetrain. The connection between them can be seen in an exemplary configuration in Figure 2.2. Each component has its specific losses, which have to be considered for the overall vehicle efficiency. In the following sections these loses will be explained in detail for the power electronics and EES. The losses of other components are shortly mentioned as a reference.

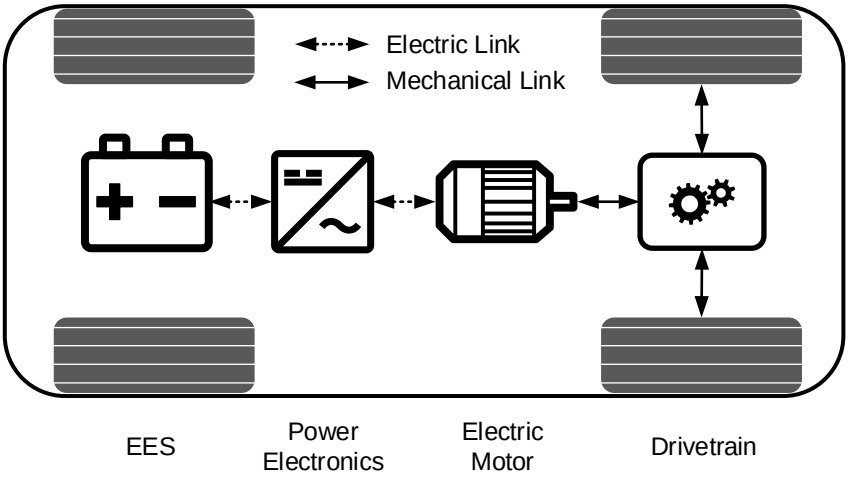

Figure 2.2: Exemplary configuration of an EV powertrain

The electric motor converts the electrical energy into mechanical energy with a rotating force vector using the principle of electromagnetism. While these motors can be powered by direct current (DC), most motors used for EV are running with alternating current (AC) [37]. Two different types are most commonly used in EV: permanent magnet synchronous motors (PSM) and asynchronous motors (ASM) [37]. Both can be designed with multiple numbers of phases, but three-phase motors are used in almost all applications. Each technology has its own advantages, but since the control is the same, for this dissertation the details are not relevant. A common feature is the ability to reverse the energy flow direction and generate electrical energy, when an external torque is applied. This is called recuperation or regenerative braking and is used during deceleration phases of the vehicle. It contributes majorly to the high energy efficiency of EV [9].

The drivetrain sometimes includes a gearbox with a gear reduction, but can also directly connect the motor to the wheels over the drive shafts. There can be more than one powertrain system, with several car models having two motors, one for each axle, or even four independent motors, where each wheel is driven separately. If two wheels are driven from the same motor, normally a differential gear is used to split the torque evenly.

The input and therefore the load on the system depends on the driver and traffic situation and is different compared to static power conversion applications. There can be high peak demands for short times, and even the direction of energy flow can change fast in a stop-and-go traffic situation with a lot of recuperation. The energy demand pattern also depends on which road the vehicle is driven, e.g., urban and expressway driving. To be able to compare vehicles and components, standardized driving cycles are defined. In such a cycle, speed over time profiles are specified with a fixed resolution. In the more relevant transient driving cycles, the patterns try to mimic a human driver on average roads as close as possible in the contrary to a modal driving cycle, where different constant speed levels are used one after another. Driving cycles can be used as an input to simulations or test benches and have a big impact on the overall rating of the efficiency. They can be generated specific for a single city and vehicle type or more general, e.g., for homologation purposes. Especially, when the vehicles are tested in an urban driving cycle, the efficiency values can be way lower than the rated efficiency [38]. Examples of commonly used cycles are summarized in Table 2.1 [39].

Table 2.1: Selection of common driving cycles [39]

Type	Name	Distance in m	Duration in s	Avg. speed in km/h	Max. speed in km/h
Urban	New York City Cycle (NYCC)	1903	598	11.5	44.6
	Urban Driving Cycle ECE 15	995	195	18.4	50
Combined	New European Driving Cycle (NEDC)	11,017	1180	33.6	120
	Federal Test Procedure (FTP)-75	17,787	1874	34.2	91.25
	Worldwide Harmonized Light Vehicles Test Procedure (WLTP) C3	23,266	1800	46.5	131.3
Highway	Artemis 130	28,737	1068	96.9	131.4
	Artemis 150	29,547	1068	99.6	150.4

2.1.2 Electrical Energy Storage System

In this section, the fundamental aspects about EES systems are described. Therefore, first the smallest units, the cells are explained. In the next part, the cells are combined to form a battery pack and the necessity of this combination is illustrated. Additionally required hardware to operate a battery pack is mentioned as well. The last part gives a summary of the battery aging process.

Battery Cell Technology

BEV have high requirements on their EES in regards of energy content, lifetime, gravimetric/volumetric energy density, and safety. Therefore, the used technology has a major impact on these factors, and it influences the cost for the storage considerably. The basic structure of the smallest component of a battery pack, the battery cell, is independent from the selected technology [40]. It represents an electrochemical cell, which consists of two electrodes, the cathode (“plus pole”) and the anode (“minus pole”) that are isolated from each other by an electrically isolating separator. Due to an electrochemical redox reaction, which involves the two electrodes and the electrolyte, an electric potential is built up between the electrodes. During discharging, this potential is dissipated by an electrical conducting path between the two poles. The reaction continues until the active material is fully converted into another stage. If the cell afterwards has to be discarded as some of the reactions cannot be reversed, it is called a primary cell. In contrary, in secondary cells, the reaction can be reversed, which is then re-forming the initial chemical material and therefore charging the cell. The maximum available potential mainly depends on the used active materials and their individual electronegativity potential, but also changes depending on the ratio of remaining available unconverted active material. Only secondary cells are further considered in this work, as primary cells have no relevance for BEV.

For the used chemicals, different combinations are possible with different benefits and limitations. The most common categories, which are relevant for automotive applications, are lead–acid batteries, nickel–cadmium batteries (NiCd), nickel–metal hydride batteries (NiMH), and lithium-ion batteries (Li-ion) [27]. In the past years, the Li-ion battery technology almost totally replaced all the other categories due to its higher energy density and other beneficial behaviors [41], which is why this thesis will only focus on it. There is a lot of research conducted about future battery technologies based on different chemistries. However, it will still take more time until it is commercially available [42]. Nevertheless, the in this dissertation investigated problem and solution is not specifically bound to the battery technology and still can be used for other batteries. The benefit might be not as significant, but it will not become obsolete.

Within the category of Li-ion batteries, several sub-groups are commercially established, which are normally characterized by the chemical compound of the cathode, since the anode is graphite in most cases [43]. The active material of the cathode in common batteries is made with lithium metal oxides, such as lithium cobalt oxide ($LiCoO_2$ or LCO), lithium manganese oxide ($LiMn_2O_4$ or LMO), lithium nickel manganese cobalt oxide ($LiNiMnCoO_2$ or NMC), lithium nickel cobalt aluminum oxide ($LiNiCoAlO_2$ or NCA), and lithium iron phosphate ($LiFePO_4$ or LFP) [44]. These materials are causing different properties, such as nominal voltage, energy density, safety, aging, and cost, which makes them suitable for different applications as described in Table 2.2. The safety is of particular importance, since large battery packs form a safety hazard due to their high energy content. Additionally, materials used in Li-ion cells may be highly flammable, as some of them even supply their own oxygen and are therefore hard to extinguish once ablaze [26]. If a certain temperature is reached, side reactions in the cell cause the temperature to rise further from within, which is called thermal runaway. For some chemistries, this runaway temperature can be as low as 150 °C (LCO) [45]. It therefore has to be ensured at all times that the temperatures of the cells remain within the permitted range by avoiding internal (too high currents) or external (hot components) heat sources.

The electrochemical potential between the two electrodes, referred to as the cell voltage u_{cell}, depends beside on the already mentioned cathode chemistry also on the state of charge (SOC), current load, and, with limited effects, the temperature of the cell. If there is no external load and

therefore no current for an extended time, the open-circuit voltage (OCV) u_{OCV} is a characteristic indicator for the SOC, as there is an increasing, non-linear trend of the voltage with the SOC, the so called OCV curve [40]. If the cell is discharged beyond a certain voltage value, the cutoff voltage $u_{\mathrm{cell,min}}$, irreversible damaging effects occur, so this must be strictly avoided [46]. Same applies for charging, where the end-of-charge voltage, $u_{\mathrm{cell,max}}$, must not be exceeded, as otherwise harmful side reactions start to damage the cell, even up to levels where a thermal runaway can happen [46]. Both values are defined by the cell manufacturers and stated in the datasheets. To charge the battery, normally a constant current (CC) is applied, until the end-of-charge voltage is reached. Sometimes, to increase the usable capacity, a constant voltage (CV) charging phase is added afterwards. This is mostly done in experiments and on cell level, where also CC or CC/CV discharges are performed to measure the capacity.

Table 2.2: Different cathode materials and their properties [44], [47], [48].

Type	Nominal Cell Voltage	Specific capacity in mAh/g	Advantage	Disadvantage	Application
LCO	3.60 V	155	High specific energy and good cycle life	Limited specific power and thermal stability	Consumer electronics
LMO	3.70 V	120	Good thermal stability and power capability	Moderate cycle life and lower energy density	High power applications (power tools)
NMC	3.65 V	160	Specific energy, power, cycle life, and thermal stability	Patent issues and high cost	EV (*BMW*, *VW*) and high power applications
LFP	3.2 V	160	Excellent thermal stability and cycle life	Lower energy and difficult state estimation	High power applications, EV (*BYD*)
NCA	3.60 V	180	Good energy, power, and cycle life	Thermal stability and high cost	EV (*Tesla*)

The capacity of the cell c_{cell} is the amount of electric charge it can deliver starting from the end-of-charge voltage until the cutoff voltage at a certain temperature and with a certain current [49]. This capacity c_{cell} is measured in ampere-hour (A h) and it depends on the size of the cell and its specific capacity of the used materials. The nominal capacity c_{nom}, sometimes also referred to as the rated capacity, defines the capacity declared by the manufacturer of a new cell with defined conditions of current, temperature and voltages [50, p. F-8]. The density of the charge and discharge current can be expressed as the C-rate, which is the ratio between the nominal capacity and the time of fully charging/discharging the cell. This allows to characterize batteries with different sizes and to compare the obtained results [49]. Since the cell has an internal resistance, there is a limit on the maximum allowed C-rate to avoid exceeding the temperature limit or degrade the cell too fast. The maximum allowed C-rate can be increased by reinforcing the internal structures of the cell like conductors and chemical composition of the active materials, which reduces the internal resistance – at the cost of the energy density. Because of this limit, there are medium powered cells available with optimized energy content and, for special use cases, high power cells with higher possible C-rates and lower capacity. To define the remaining energy content, the SOC value is used. While there is no general accepted SOC definition [26], a common way to describe it is the ratio of the remaining (or residual) electric charge c_{res} and

actual capacity c_{act} [51], as shown in Eq. (2.1). The remaining electric charge is the integrated current $i(t)$ subtracted from the actual capacity.

$$SOC = \frac{c_{\mathrm{res}}}{c_{\mathrm{act}}}\ 100\,\% = \left(1 - \frac{\int i dt}{c_{\mathrm{act}}}\right) 100\,\% \tag{2.1}$$

Independent from other parameters, the cells come in different packages. Until now, mainly three packages are used in automotive applications: the cylindrical cell, prismatic cell, and pouch cell [45], as depicted in Figure 2.3. In a cylindrical cell, the stacked layers of anode, separator, and cathode, typically around 1 m long, are rolled up and then the roll is put in a metallic cylindrical enclosure. The top and bottom of the cylinder are functioning as the two connection poles. It makes the cell rather simple to manufacture and therefore achieves lower costs, but the energy density of the battery pack is not the best due to the round shape and the cooling of the cells is challenging [41]. The prismatic cells are also made of coiled layers, but here the winding is done around a flat core, so that the flat wrap can be inserted in a rectangular cuboid case. The two poles are normally connected internally to two contact areas on the top of the case. This is more challenging to manufacture and therefore increases the cell production costs. However, the pack manufacturing and cooling is good and the energy density can be maximized [52]. For the last package, the pouch cell, the layers are normally stacked, or sometimes z-folded, and then the stack is sealed with a foil made of a deep-drawn aluminum-polymer-compound, a so-called pouch foil. This again is an inexpensive method compared to the other two packages, but leaves the cell vulnerable for impacts or even penetrations, which is a safety concern. The cooling can be handled in an efficient way due to the large surface area and the energy density for the pack is moderate compared to the other packages, as the cells can be stacked, but have an unusable area around the package, where the top and bottom foils are sealed together [43].

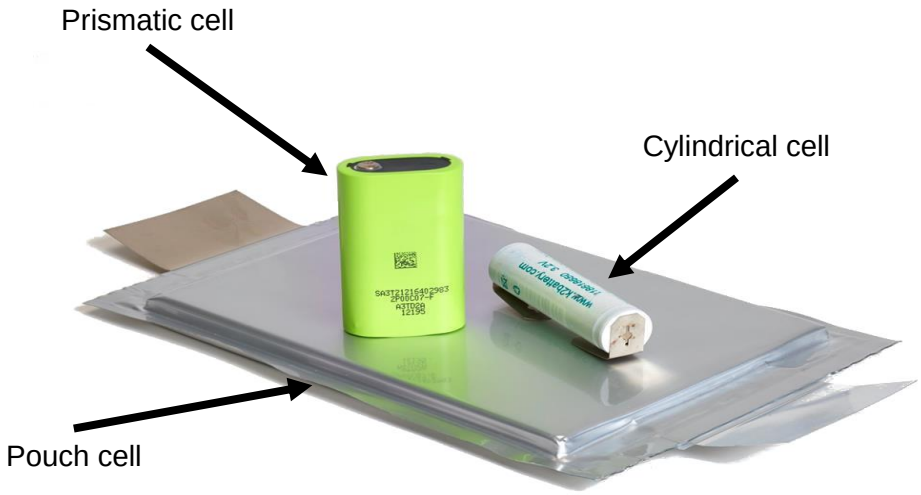

Figure 2.3: Commercial Li-ion cells in the three common packages, adapted from [53, p. 5]

The size of the individual cells is not directly related to the packaging. A range of miniature cells with a capacity of just a few mA h for hearing aids up to enormous cells of 1 kA h is possible [54]. Cells, which are too small for their application have the problem of a low efficiency and low energy density in a battery pack due to the multiple contacts and individual cell packaging. Battery packs with oversized cells, however, can be difficult to be cooled, since the cooling cannot directly reach the inside of a cell, and cell defects have more severe consequences. For a detailed investigation of the optimum cells size the research work of Mr. Matthias Kerler [55] is recommended.

Many of the cell parameters mentioned here are affected by tolerances [56]. Of main concern are the individual cell capacities and the internal resistances, since they affect the overall behavior of the vehicle. The tolerances can be minimized with additional effort during manufacturing, but this results in higher production costs. The cell size is a factor for the tolerance consideration, since an increased amount of cells in a pack leads to a higher chance of bad cells. However, the impact of tolerances for the vehicle is worse for larger cells. A detailed analysis of these variations and their consequences is missing in current literature and therefore conducted in Subchapter 3.1.

Battery Pack Configuration

A single cell is not sufficient to supply power to the motor in vehicle applications. Firstly, the cell voltage u_{cell} is insufficient to drive a car, as extremely high currents would be required to achieve the power in the magnitude of several kW. That is why m cells are connected in series to increase the voltage of the pack u_{pack}, as shown in Eq. (2.2):

$$u_{\mathrm{pack}} = \sum_{l=1}^{m} u_{\mathrm{cell},l} \tag{2.2}$$

Typically, voltages of around 200 V to 800 V are considered for EV where a majority of vehicles uses around 400 V [57]. This requires around 100 cells connected in series. Since these voltages are above 60 V, costly high voltage (HV) protection measures are required [58].

Secondly, the capacity of a single cell cannot be increased to infinite. To reach the required capacity c_{parallel}, n equal cells are connected in parallel, as shown in Eq. (2.3):

$$c_{\mathrm{parallel}} = \sum_{j=1}^{n} c_{\mathrm{cell},j} = n\,\bar{c}_{\mathrm{cell}} \tag{2.3}$$

To increase both capacity and voltage, n m cells are connected to a battery pack. There exist two ways of implementation, which are depicted in Figure 2.4. For the msnp-topology, m cells are connected in strings, which are then connected in n parallel connections - whereas for the npms-topology, n cells are connected in parallel modules, which are then connected in m series strings. Both topologies can be used with different advantages and disadvantages, but the npms-topology has a slightly better fault-tolerance behavior and is less costly to be implemented [59].

Beside of all the cells, a battery management system (BMS) is required in a battery pack. The main function is monitoring all voltages, so that no cell would be operated outside of the allowed range [26]. Additionally, the BMS uses a current sensor to monitor i_{pack} to guarantee the maximum C-rate is not exceeded during charging and discharging. Temperature sensors are used to ensure the thermal limits are kept, control the cooling and heating system, and their values are communicated by the BMS to the motor control so it can limit the power in case the temperatures are getting close to critical. Another important aspect is the state estimation of values like the SOC and the communication of all the relevant parameters to the rest of the vehicle. Additional sensors, for example moisture, acceleration, and internal self-checkups can be integrated as well. In case of a critical fault, or when the vehicle is not used, two contactors are used to disconnect the positive and the negative HV potential of the battery from the rest of the vehicle. As a last resort, mainly for critical over currents, a fuse is normally integrated as well.

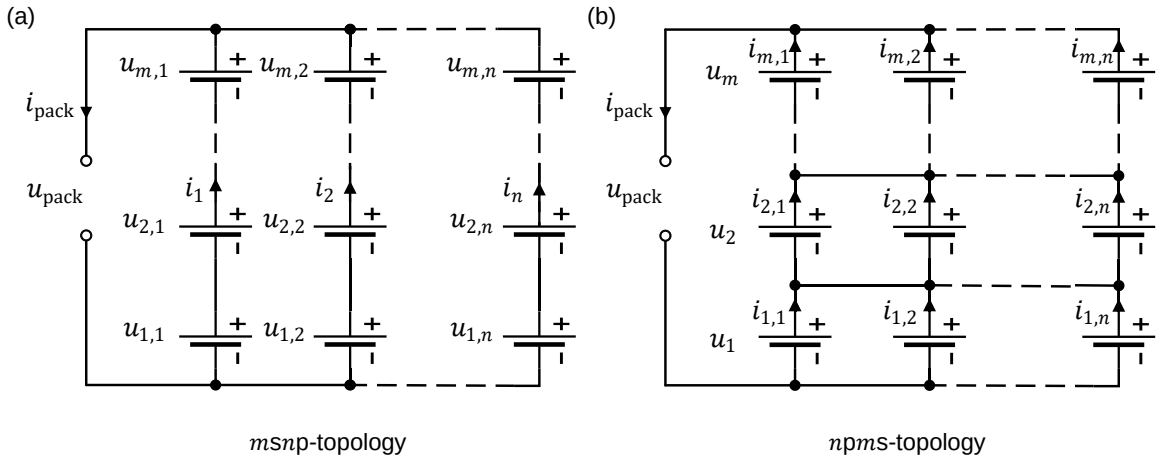

Figure 2.4: Two different battery pack topologies. (a) msnp-topology (b) npms-topology

Battery Aging

A critical aspect, especially considering the high initial costs of the battery, is battery aging. The term summarizes different forms of degradation of active material in the cell due to irreversible side reactions. This effect is already extensively covered in the literature, e.g., in [60]–[62], so in this section only the basic principles, which are relevant for the further dissertation, shall be mentioned.

Aging can be separated in two aspects: calendar aging and cycle aging. The first one describes aging effects over time, independent of the actual usage of the battery. It is influenced by the storage temperature, where a low temperature is beneficial and the SOC during the storage, which also should be low, but mainly on the time itself [63]. The cycle aging refers to how many cycles the battery has experienced and is mainly influenced by the amount for charge throughput, but is also sensitive to the temperature and depth of discharge (DOD) [61]. Both aging effects are superimposed and cause the capacity to decline and the internal resistance to increase. It can be expressed as the state of health (SOH), which is mostly calculated with the capacity reduction [49], as seen in Eq. (2.4):

$$SOH = \frac{c_{\mathrm{act}}}{c_{\mathrm{nom}}}\ 100\ \% \tag{2.4}$$

Once the SOH has reached a certain decline, the battery is considered insufficient for the intended application. This is because on the one hand, the vehicle specifications are then reduced to a level where the user would directly notice the difference, and on the other hand, there is a point, where the aging rate accelerates. This point is referred to as the aging knee [64]. Especially with the consideration of a second life use case, it is difficult to define an end of life [65], but is commonly considered between 70 % to 80 % [60], [64].

2.1.3 Power Electronics

To drive the motor with the energy from the EES system, a power electronic converter is required, which converts the DC of the battery pack to three-phased AC required by motors used for EV. Since the main energy flow direction through the power electronics is from DC to AC, the word “inverter” is widely used, while a description as “converter” is also applicable. The currently most common structure is the voltage source inverter (VSI) as depicted in Figure 2.5. It contains six active switches to generate a three-phase modified sine wave voltage with variable magnitude and frequency [66]. Two switches form what is known as a half bridge, which can be switched complementarily to apply either a positive or a negative voltage to the connected motor coil.

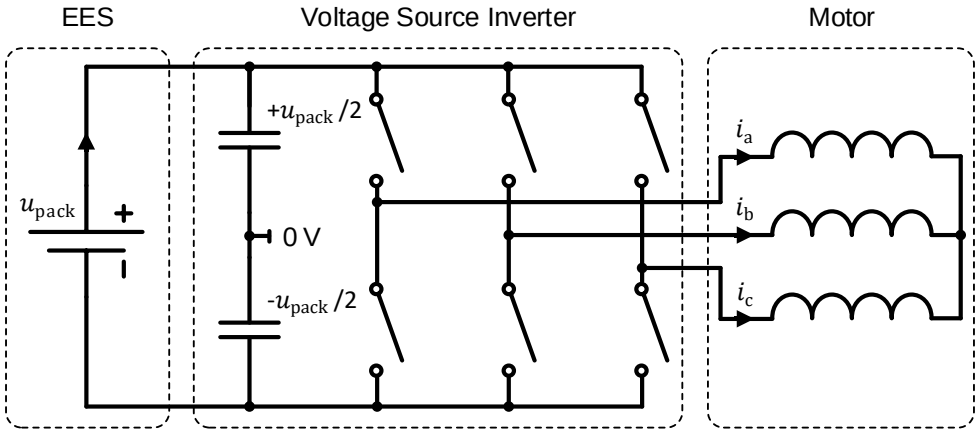

Figure 2.5: Simplified conventional voltage source inverter

The symbolic switches in Figure 2.5 are placeholders for active power electronic semiconductors. Switches for vehicle applications can be metal-oxide-semiconductor field-effect transistor (MOSFET) or insulated-gate bipolar transistor (IGBT), where the later one is most commonly used in cars due to its better ability to handle HV [67, pp. 10–14]. To create the required modified sine wave voltage, most commonly the switching sequence is determined by pulse width modulation (PWM). There, the desired sinusoidal AC voltage waveform, also known as the reference voltage, is compared to a triangular carrier waveform. This method and others are explained in detail in Section 3.2.1.

A common issue with this inverter is the low partial load efficiency [38], as the powertrain is designed to handle high peak load conditions, but vehicles are often driven in partial load conditions, i.e., city traffic. This can lead to inverters rated at 97 % efficiency achieving only 80 %, depending on the driving cycle [68]. Additionally, electromagnetic interferences (EMI) can appear due to the switching of the whole voltage u_{pack} in short times. A required dead time between half bridge switching brings distortion to the AC output current, which results in torque ripples. Moreover, total harmonic distortions (THD), which is caused by the PMW generation of the sine wave, is causing losses and higher stress for the components. To achieve a reduction of electromagnetic interferences, THD, and pulsing current, filtering is necessary [69], [70]. One component to do so is the input capacitor of the inverter, which alone can amount up to 30 % of total inverter volume and cost, respectively [71]. A more comprehensive analysis of the common IGBT VSI including its efficiency and drawbacks is conducted by the complementary dissertation of Chang [32].

2.2 Cell Balancing

As indicated in Subchapter 1.2 and 2.1.2, the cell tolerances in both parameters, capacity and resistance, cause the SOC of the in series connected cells to drift apart within a few cycles. Since an over-(dis-)charge destroys lithium-based batteries immediately and even bears a big safety risk, it must be avoided at any time. The most common way to work with this issue is the implementation of a cell balancing system, which tries to equalize the energy among the cells. This feature is integrated in the BMS and it extends its basic functionalities explained in Section 2.1.2. In common literature, there is a differentiation about the way the balancing is executed. It is either possible by dissipating the unbalanced energy (passive balancing), or, at least partially, by shifting it to other cells (active balancing) [72].

2.2.1 Passive Cell Balancing

The principle of passive balancing is to remove excess energy from selected cells. This is mainly done by dissipating heat using resistors to radiate the energy surplus [73]. Each shunt resistor needs its own switch and is connected in parallel to the cell or parallel cells it is balancing. If the switch is on, a current is drawn from the connected cells discharging them or, if applied, limiting the charging current. Therefore, the resistor needs the ability to handle the heat generated by the current and must be dimensioned accordingly. Often the printed circuit boards (PCB) are equipped with thermal sensors to ensure the components are not overheating and therefore pausing the balancing if the temperature gets too high. As the balancing dissipates energy, this solution is normally only activated during charging, and then usually towards the end. This is because close to the end of the charging cycle, the internal resistance values are stable and therefore the additional expected drift is lower. The cell voltage is used to equalize them, which indicates the different SOC. Analog dissipative shunting works with the same principle, just that instead of resistors, it uses transistors [74]. It therefore is able to control the current, compared to the normal resistor, which is switched either on or off.

While it is an effective way to minimize the drift in a simple and therefore cost effective way with a small amount of additionally required components, the balanced energy is wasted and the system needs to be able to dissipate the generated heat. Depending on the design, there is a maximum capacity spread such a system can handle. The cell with the smallest capacity/SOC limits the overall usable amount of energy. A defective circuit leads to the inability to balance the connected cells and causes the states to drift apart during cycling resulting in a decreasing usable capacity of the pack over a few cycles.

2.2.2 Active Cell Balancing

In contrast to passive balancing, active cell balancing uses various methods to move energy from cells with higher SOC to cells with a lower SOC. For this dissertation, active cell balancing only refers to methods, where additional circuits are connected to otherwise conventional static battery packs. Different to some literature, other methods, which separate the pack into modules and introduce additional electronics in between them, are mentioned in the following sections to be able to distinguish their (dis-)advantages. To move the energy for active cell balancing, it has to be stored temporarily. In general, two different variants are described in literature: either based on capacitors or on inductors/transformers [73]. Switches on each in series connected cell control, if the temporary energy storage is either charged or discharged by this cell. Since the

capacity of this temporary energy storage is microscopic, the switches work with high frequencies. The cell voltages are used again to determine source and sink of the energy shifting. A central controller or individual cell management is possible [75]. There are many different circuits available, which are not discussed here in detail, since their principle and therefore properties are similar.

Many of the active balancing methods have in common that they only can share the energy with the neighboring series connected cells [76]. All methods require additional hardware, in general one additional circuit per cell/module in series [75], which increases the cost of the battery pack. Since the energy is shifted, there is an additional aging for the cells due to additional charging and discharging. Most circuits only allow a balancing during charging and have limited balancing capabilities [73]. Additionally, there are always efficiency losses occurring due to the involved switches and capacitors/inductors [72]. Publications indicate losses of around half of the balanced energy [77]. A defective circuit has the same effects on the vehicle as a malfunctioning passive balancing circuit.

2.3 Voltage Decoupling of Cells or Modules

Decoupling the voltage of the individual cells or modules from the battery pack is a subcategory of active balancing in many publications. However, it shall be described separately in this dissertation, because on the one hand, it requires a major change in the circuit of the pack, but on the other hand, it enables additional possibilities beyond active balancing, especially in regard of the overall vehicle efficiency. It has been shown that conventional powertrains have low partial load efficiency [68] and that such an efficiency can be increased with an adaptable DC link voltage [78]. Additionally, the SOC depended battery voltage results in changing vehicle performance depending on the SOC [79]. Because of these two effects, an SOC independent and adjustable DC link voltage is desirable.

Voltage decoupling of cells or modules can achieve this and on top of that, an individual utilization and therefore balancing is possible. It is done by equipping either each cell [80] or each module [81] of a battery pack with converters to decouple their voltages. This approach allows an adaptable load on the connected cells and additionally delivers a constant output voltage that can be optimized to keep the inverter in the best efficiency range for the respective driving situation. The differences of the battery parameters like voltage, SOC etc. can be in orders of several magnitudes, so that decoupling can be used for hybrid energy storage as well, for example the combination of batteries with super capacitors [82]. Also different capacities, chemistries, self-discharge rates, states of health, and aging behavior can be combined [83], which makes this technology a preferred candidate for second life applications [84].

The technologies used for decoupling can be based on individual DC/DC converters [80], multiple input DC/DC converter [85], or based on transformers [86]. For the first one, each cell or module is equipped with a bidirectional buck/boost converter, which can adapt the output voltage and therefore the drawn power independent from the actual cell/module voltage and SOC. The second one follows the same principle with the difference that expensive components such as the inductor and filter capacitor only have to be integrated once for the whole pack. The third option integrates a transformer for each module including an inverter and a rectifier on each side to provide the necessary AC for the transformer.

While the decoupling has many benefits especially for hybrid energy storage solutions, for the usage as a battery balancing and utilization measure it has to be highlighted that it introduces additional losses, as the conventional inverter to drive the motor is still required and the DC/DC solutions introduce an additional loss of around 7 % depending on the technology [84]. On top of that it also introduces additional costs for the EES, as the decoupling electronics must be dimensioned in a way that they are able to carry the maximum load of the powertrain [82]. The additional hardware increases the overall system complexity, which also rises the difficulty of control and costs [87]. In addition, it is important to mention that the defect of a single component leads to a total failure of the system, since the cells/modules are connected in series. Additionally, no literature was found that critically assesses the module size with an efficiency and cost evaluation. In general, it can be concluded that the decoupling approach might have benefits for the application in certain consumer electronics rather than in an automotive implementation.

2.4 Reconfiguration of Cells or Modules

In this subchapter, solutions are summarized, which enable a dynamic interconnection between the battery cells/modules. This means that individual elements can be connected either in series, parallel, or bypassed. The principle is derived from the earlier in Section 2.2.2 mentioned active balancing with the difference that here switches are able to alter the way the cells are connected to each other and not just shift energy between them [88]. It therefore allows for temporary parallel connections, during which the cells are balancing themselves as the voltage is equalized [89]. An additional function is that individual cells or modules can be deactivated and bypassed [90]. This increases the safety and reliability of the whole battery pack, as cell failures can be excluded from the pack, independent of whether it is an open-circuit or closed-circuit cell failure. Moreover, as a side effect, reconfigurable batteries can adapt their DC link voltages to increase the partial load efficiency [91]. Such an individual control enables stronger cells to be used more often and therefore increase the utilization [92] or at least achieve a constant balancing by parallelization, which drains larger and smaller cells more equally [93].

There are multiple methods and circuits described in literature. Normally, they vary with the amount of switches used with more switches enabling more functionalities but also increasing the costs and decreasing the efficiency. For this dissertation, they are not all explained in detail, but representative examples are mentioned.

Simpler solutions modularize the battery pack with the main purpose to be able to adapt the DC link voltage and to increase the reliability [78]. Few switches are required, which reduces the complexity and costs of the system, but also the possibilities are limited. The simplest approach to have increased flexibility on each cell is to equip all cells with an additional switch [89]. One additional switch is needed to bypass the parallel modules, which results in a $mn + m$ switch count, if implemented on a single cell level as proposed in the literature [89]. A lower switch count is possible, if several parallel cells are clustered. A balancing and utilization is challenging with such circuits, as the power and voltage is limited once cells are excluded. A commonly found circuit is to add three switches between each cell, resulting in a $3mn - 3$ switch count as it can be seen in Figure 2.6 [91]. This circuit allows a bypassing of cells and a parallelization of neighboring cells when a reduced DC link voltage is beneficial.

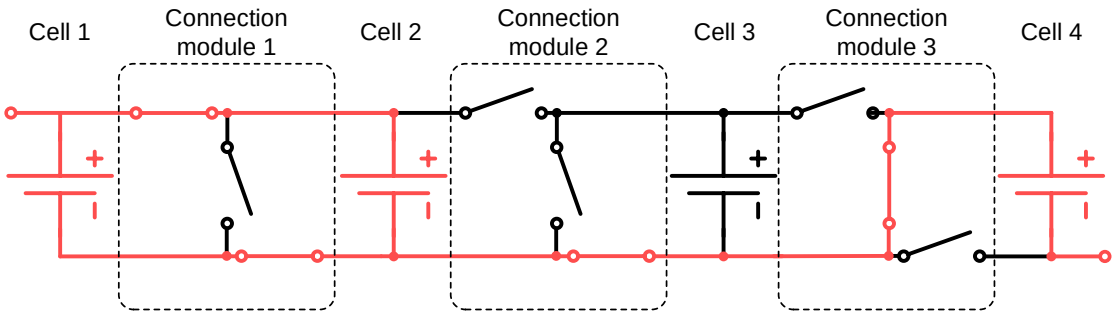

Figure 2.6: Exemplary representation of a reconfigurable battery pack. Cell 1 and 2 are connected in parallel. Cell 3 is bypassed. Cell 4 is connected in series with Cells 1 and 2. Adapted from [91].

With four switches per cell, it is already possible to parallel series strings of cells [94]. Such a circuit needs $4mn - 2$ switches for the whole circuit. Even larger circuits with for example six switches per cell ensure that if a large amount of cells are skipped, the losses due to a big number of series connected bypassing switches are not too high [92]. It therefore is then even possible to design reconfigurable modules, which are placed in reconfigurable battery packs to ensure full freedom [93]. More complex solutions include additional passive electric components and therefore combine reconfiguration circuits with DC/DC converters and the active balancing approach mentioned in Section 2.2.2 [95], [96].

The main problem of the reconfiguration approach is similar with the problem of decoupling: Additional losses and costs are introduced into the battery, which have to be at least compensated with the higher utilization and increased efficiency of the still required conventional inverter. A lot of the literature found also did not properly investigate the efficiency due to switch conduction losses, where some of them explicitly neglected those losses [89]. The costs are also not mentioned in any of the presented sources. Several circuits are proposed, but a central question, if the pack should be split up until cell level or how big the modules should be is not investigated. Bypassing of cells allows an increased reliability, but a failure of a switch still can cause the EES to become dysfunctional, if it is operating in a series connection. A critical aspect is also the dead time between the switching, which either causes a short interruption of the power delivery [78], or has to be buffered with a big DC link capacitor, which is costly and voluminous component [71]. In general it can be concluded that the reconfiguration approach is more relevant for applications with increased reliability requirements [90]. Examples are medical equipment and computer server infrastructure, where cost and losses of the EES are of secondary priority.

2.5 Multilevel Inverter

Similar to the reconfiguration methods in the previous subchapter, the multilevel inverter (ML) concept includes circuits in between the modules, which enable a dynamic reconfiguration to the extent that the load on the cells or modules can be individually controlled. The major difference for ML is that the reconfiguration now can be done in a highly dynamic way, which enables the battery to output voltages, which are almost identical to AC voltages. This feature can be used to drive an electric motor directly or to couple the battery to the electrical grid without the usage of an additional inverter. Using such method, the circuit does not introduce additional losses to the system.

An early mention of the concept appears in a patent from 1975 by cascading switched energy elements to produce an output with a similar shape of an AC voltage consisting of several stacked levels of DC voltages [97]. From there onwards, there have been multiple publications and patents to develop the idea further [98]. The main intended application can be found in medium to high power grid applications, for example reactive power compensation [99] and flexible AC transmission systems [100], with a mentioning for driving electric motors as well [101]. However, the initial main purpose of multilevel inverters was more focused on their other benefits like the lower common mode voltage and therefore lower voltage stress on the switches, lower du/dt ratio to supply lower harmonic contents in the output voltage/current and lower electromagnetic interference outputs [100]. Only in more recent research outputs the ability to balance batteries is mentioned [102] with some even mentioning an automotive application [103].

There are multiple different approaches available in literature, which shall be only summarized in this subchapter. Several multilevel converter topologies are based on single DC sources [104], which are not considered for this dissertation, as they do not provide the direct ability to put individual loads on different modules to increase the utilization. Four different ML inverter topologies are usually the most common found in literature: the diode clamped inverter, the flying capacitor inverter, the modular multilevel converter, and the Cascaded H-Bridge converter.

The diode clamped multilevel topology, also called neutral point converter, was intentionally a single DC source circuit to drive high voltage (10kV or above) industrial motors with less harmonic distortions [105]. Although it is possible to use it as a multi-source topology by replacing the necessary capacitors with battery modules, a big amount of components is required to enable a higher number of modules, as component count rises quadratic with the amount of modules [106]. Therefore, this circuit is considered not suitable, if several modules are desired. A similar conclusion can be drawn for a second topology of ML inverter, the flying capacitor ML inverters. They work in a comparable way as the diode clamped ML inverter with the difference that instead of diodes it uses capacitors to clamp the voltage to the individual levels [107]. Here, not the overall amount of components is the critical factor, as the number of required parts only rises linear with the amount of modules, but the required capacitors make the circuit less reliable and more expensive [100].

The concept of the modular multilevel converter (MMC) as an alternative can be scaled linearly since it only consists of a half bridge chopper module for each battery module, as it can be seen in Figure 2.7 [108]. Each submodule (SM) can be either bypassed or enabled, and therefore a flexible load can be implemented easily [109]. If both switches are open, the battery modules are fully disconnected from each other and therefore there is no high voltage present anywhere in the system. The required inductors to stabilize the circulating current [110] pose a disadvantage since they increase cost and volume while reducing the efficiency [111].

An analogous topology of the MMC is the Cascaded H-Bridge (CHB) converter, where, instead of the half bridge, a full H-bridge is used in each cascaded sub module as it is shown in Figure 2.8 [69]. Full H-bridges with a unipolar behavior enable a reverse polarization on each module and therefore only half of the modules are required compared to a MMC with the same amount of levels. Therefore, to achieve an n-level output voltage, $(n-1)/2$ H-bridge modules are required per phase, which results in $2n-2$ switches per phase. The inductors compared to a MMC are not required and the CHB topology is considered superior to MMC due to a better balancing possibility, component count and efficiency in low and mixed speed motors of electric vehicles [100], [112]–[114]. The main disadvantage of CHB mentioned in various literature is the requirement of isolated DC sources for each SM [106], [115]. However, this is actually beneficial to the

mentioned problem of battery tolerances, as it enables an individual control and balancing/utilization. The various benefits of the CHB circuit compared to a conventional voltage source inverter are investigated in detail in the complementary thesis of Chang [32].

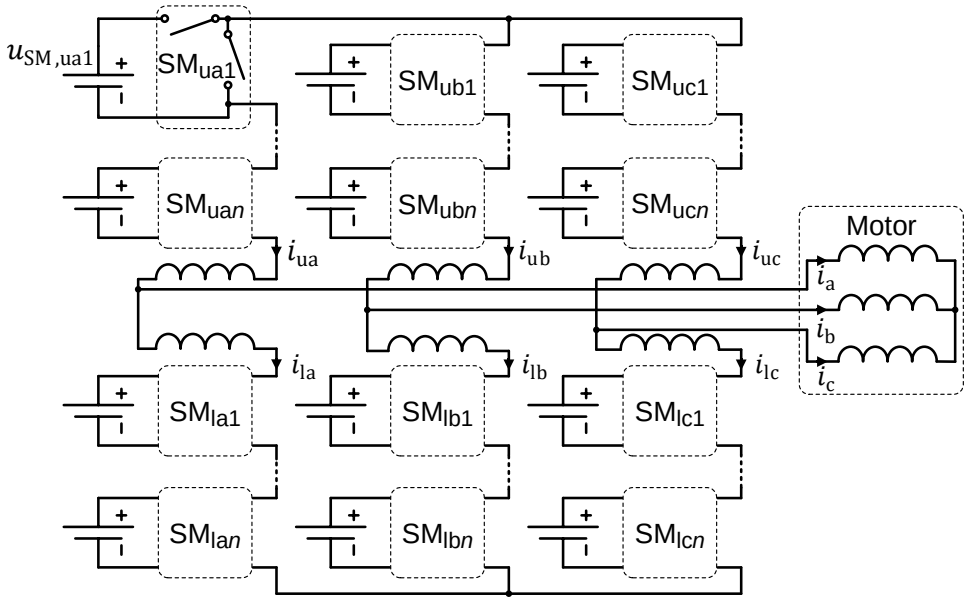

Figure 2.7: Simplified layout of a three-phase MMC to directly drive a motor, where the number of submodules can be scaled, adapted from [108].

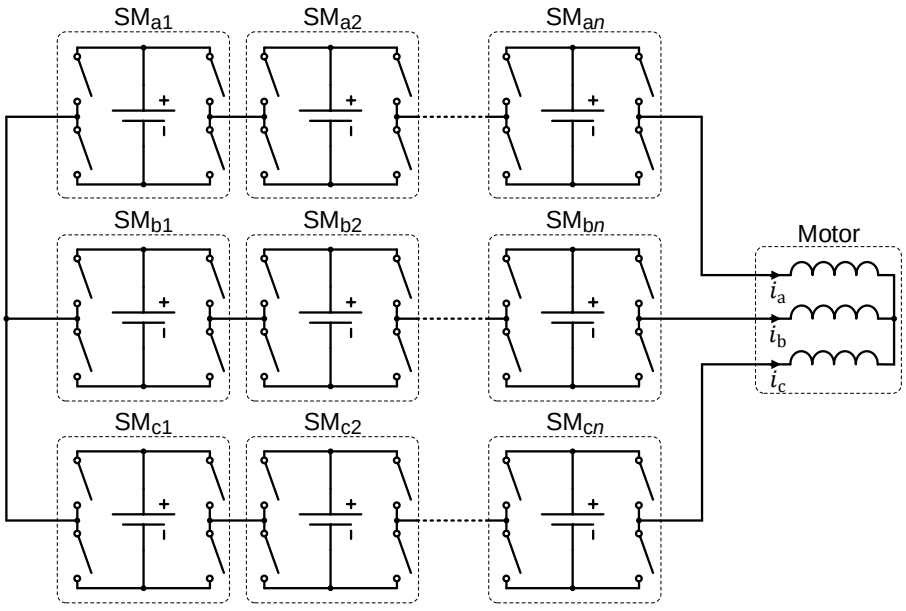

Figure 2.8: Simplified layout of a three-phased CHB inverter, where the number of submodules can be scaled

Another interesting solution worth to be mentioned is the Modular Multilevel Battery (M2B) inverter, which is based on the CHB principle, but with nine instead of four switches per module [116]. This enables a parallelization of neighboring modules with the main intention of balancing and increasing the power capability [117]. However, it has to be considered that such a circuit almost doubles the cost of the system, which makes it more suitable for stationary applications with different priorities [118]. Additionally, there are various other circuits and hybrid multilevel

converter circuits described in literature with different main purposes [106], [119]–[122]. They tend to be more complex with more involved components and commonly they are customized for other specific applications, hence not direct applicable for automotive usages and are therefore not mentioned here.

The multilevel inverter comes with specific disadvantages and uncertainties. The control of a high number of switches is challenging and the reliability has to be considered due to the high amount of components [100]. However, it can be mentioned that a bypassing of a faulty module is normally possible if cells are dysfunctional or even if a single switch is damaged. One bypassed module has only a rather limited effect on the performance of the vehicle. Depending on the overall amount of modules in the pack and the number of bypassed modules, the peak voltage and therefore acceleration are reduced and the capacity and therefore range are limited as well, but beside of that the vehicle remains operational. In general, the multilevel inverter can be competitive concerning efficiency and costs compared to a conventional powertrain, as no additional inverter is required. Not adequately discussed topics in current literature are the detailed efficiencies in relation to the module size. More small modules would enable a better balancing/utilization compared to fewer big ones, but this also would increase the losses, as the current has to pass through more modules with more conduction losses. An optimization also has to consider the costs, as the improvement could be rising disproportional to the cost of the system.

2.6 Discussions and Gap in the Literature

As shown in Section 2.1.2, batteries in EV are currently not fully utilized due to their parameter variations and the way current packs are interconnected. They therefore have some potential for improvement. The magnitude of the potential and therefore the relevance is not clearly visible in current literature. As the previous four subchapters have shown, there are already various methods available to address this issue. However, if additional hardware is introduced in an otherwise conventional powertrain, it adds additional costs and losses, which are reducing the positive effects from the higher utilization. As the battery variations only occur in small magnitudes, such a solution could make the overall efficiency worse or increase the costs to the extent that it is not viable in a commercial EV. This subchapter shall give a brief evaluation of the mentioned available methods including a rating to select the most promising one. Subsequently, the gaps in literature are identified and the contribution of this dissertation to the state of knowledge is explained.

2.6.1 Discussion on the Current State of the Art

To select the most promising method for further investigation, a qualitative comparison of the attributes of all presented methods has been conducted. A quantitative comparison is not possible since the attributes found in literature are not directly comparable, and not all values of the different methods are known. However, a qualitative comparison is found sufficient for this research, since only an indicator is required, which method should be investigated in detail. Other methods might deliver similar, but not significantly better results. A qualitative scoring system is used, where the scores range from “1” to “10” with “10” being the best given by the author based on the literature mentioned in the previous four subchapters. Seven attribute categories are compared. The utilization potential compares the ability to access not utilized energy in the cells. The

intrinsic efficiency evaluates the efficiency of the circuit itself, while the system efficiency evaluates the efficiency of the combined powertrain. Costs compare the monetary benefit based on the used components and their quantity. Reliability considers the impact, if single components including battery cells fail. The complexity analyzes the difficulty of control with the number of required control signals and requirements for alignment. The final category considers the usability for EV, which considers how comprehensive the system alternations are necessary to implement the proposed method in a vehicle. All attributes are summarized and averaged for each method in Table 2.3. The numbers are assigned in comparison to the other methods. It also has to be mentioned that the comparison only holds for EV applications and could be different for other use-cases.

Table 2.3: Rating of the existing solutions for battery balancing and increased utilization with a 1 to 10 score with 10 as the top score

Method	Utilization potential	Intrinsic efficiency	System efficiency	Costs	Reliability	Complexity	EV usability	**Avg.**
Passive Balancing	1	1	5	10	7	10	10	**6.3**
Active Balancing	6	8	6	7	6	7	8	**6.9**
Decoupling	8	7	3	4	2	6	5	**5.0**
Reconfiguration	8	7	2	3	7	2	5	**4.9**
Multilevel inverter	8	10	10	8	8	2	5	**7.3**

Table 2.3 shows that for EV applications the multilevel method achieves the highest overall score despite the high complexity in terms of circuit control. It is closely followed by the active balancing method, which allows a higher utilization with reasonable costs and low complexity, as the changes to current battery systems would be marginal.

Within the multilevel inverter method, there are also several topologies available, where again the most relevant are compared against each other in a qualitative way. For this comparison, five attribute categories are compared: the ability to increase the utilization, the system efficiency, the capability to modularize the battery pack, the amount of components required, and a cost comparison based on the components and their required quantity. Identical to the qualitative rating of the balancing methods, a scoring system is applied with “1” being the lowest score and “10” being the highest. The scores are given in a comparing way based on the literature explained in Subchapter 2.5. Table 2.4 shows the comparison between the selected ML topologies including an average value of each topology. It can be seen that for a pure utilization optimization the MMC would be the best selection, as it breaks the battery pack in even smaller modules with the same amount of switches and similar losses. However, due to the required inductors with their extra losses and costs, in total the CHB topology is considered the best alternative. There are some additional arguments in favor of this circuit worked out in the concurrent thesis of Chang [32] as an inverter with improved partial load efficiency. Due to all these advantages, the CHB topology was selected for both dissertations as the preferred topology.

Table 2.4: Rating of the existing multilevel inverter topologies with a 1 to 10 score (with 10 as the highest)

Topology	Utilization potential	Efficiency	Modularity	Comp. count	Cost	**Avg.**
Diode clamped ML inverter	8	7	3	5	3	**5.2**
Flying capacitor ML inverter	8	8	8	5	5	**6.8**
MMC	10	8	10	5	7	**8.0**
CHB converter	9	9	8	8	8	**8.4**
M2B inverter	9	7	8	4	7	**7.0**

2.6.2 Gap in the Current State of the Art

What is not found in current literature is a quantitative investigation of the actual possible gains from the battery using an active battery interconnection like the CHB inverter, especially with the requirements for an application in automotive industry and with an economical consideration.

To determine the actual possible gains, first, the theoretical possible gains have to be indicated and if they are influenced by the battery technology. Investigations of tolerances of individual batteries are not widely available and the few that can be found do not allow direct comparisons.

Secondly, a definition of the most suitable control for optimized battery utilization is required. Several different alternatives of these control strategy can be found. Most of them focus on the objective to reduce the harmonic distortions or the complexity, but not to increase the utilization.

Another missing investigation is the obtainment of the states of the individual battery modules to determine the individual loads that should be assigned to each module. Since the state of the battery pack is crucial for the functionality of an EV and other battery applications, methods for whole battery packs are available in literature in large variety. However, an increased accuracy and a much higher sampling rate is required for balancing, which can increase the complexity and therefore costs. Additionally, the state of each SM has to be known, which increases the cost of complex methods, so a suitable state estimator and its achievable accuracy is required.

Finally, current work does not include a comprehensive and holistic analysis of the efficiency and costs associated with different configurations of the CHB inverter, e.g., the number of levels, selection of switches, etc. Hence, it is currently not possible to determine if an active battery connection can actually bring benefits, which in the end can be converted into cost savings that help to decrease the total cost of ownership of a battery electric vehicle and hence potentially increase the user acceptance for the benefit of the environment.

The above-mentioned gaps in the literature lead to the derivation of the working hypotheses of this dissertation: With the usage of a Cascaded H-Bridge inverter for modularized batteries in an automotive application, there is more energy extractable with a lower total cost of ownership for the entire electric powertrain.

As a summary of this chapter, it can be concluded that a CHB inverter potentially has the best possibility to increase the battery utilization in an EV due to parameter tolerances and therefore decrease the costs. To which extend and in which implementation is examined in the following chapters.

3 Methodology

To investigate the feasibility of a CHB inverter in a battery pack of an EV, the already indicated open points in the research gap presented in the previous section are organized into four major subchapters for the methodology chapter to get a holistic, yet structured coverage. For each work package, results from the previous packages are incorporated as indicated in Figure 3.1 as a part of the V-Model, which defines the order. While the actual research work of some subchapters was done in parallel or in iterative steps, the description here follows this order and therefore in a few occasions has to anticipate results from later subchapters. Each part can be seen as a small own research project with a more detailed state-of-the-art part and an own methodology resulting in own results, that contribute to the overall research results of this dissertation. Research of some subchapters was investigated together with the support of students, who conducted master theses about their findings. Their contribution will be highlighted in each section.

The four parts are starting with the problem that the magnitude of the battery tolerances is not clearly available in literature, especially with an overview of potential correlations with other battery parameters. So in the first part, Subchapter 3.1, the tolerances are analyzed from a larger selection of available data. The next challenge is to define a way, how the modules within a CHB inverter should be prioritized to enable a full capacity contribution of each one. This sorting is conceptualized in Subchapter 3.2. To conduct the sorting in an automotive operation, the states of the modules have to be monitored during operation to an extent, where the accuracy is distinctly higher than the actual tolerances. To make sure that such a state estimator is also economical feasible, Subchapter 3.3 describes the method to find the most suitable one. The last subchapter of the methodology, Subchapter 3.4 investigates the problem that the best structure of the CHB inverter is not known, as different configurations lead to different efficiencies, utilizations, and costs.

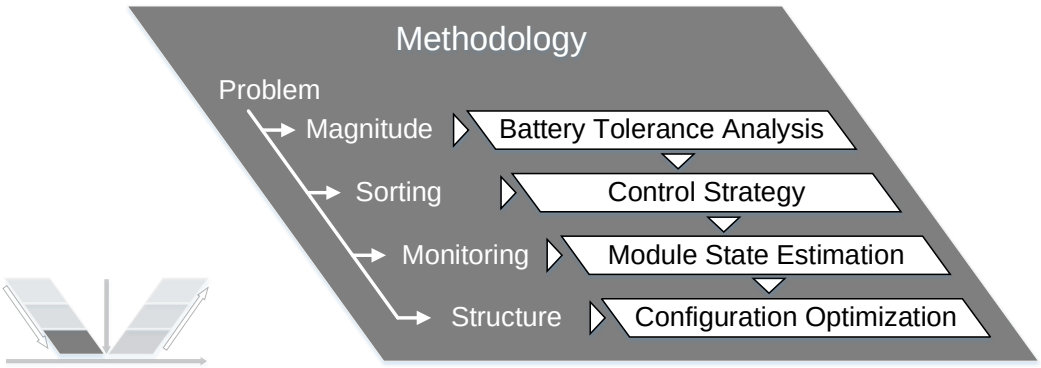

Figure 3.1: Structure of Chapter 3

3.1 Battery Tolerance Analysis

To describe the magnitude of the problem regarding the unused energy due to battery tolerances, the first subchapter investigates the actual cell variations. The cell variations are obtained from two sources, literature and self-collected data on battery cell variations, and a dataset was developed using both. The obtained results are then used as an input for the following work package to indicate the magnitude of most common variations. For that, first some general introduction is given to provide an insight of the variations. In the second step, it is explained how to calculate and analyze the data, which gives an overview of relevant statistical methods. Then a pool of different sources is explained in detail including data extraction and evaluation, which is summarized as well. The last part presents the conclusions on the cell variations, which are then used in the remaining dissertation. The results of the tolerance analysis is presented in the Results Chapter in the corresponding Subchapter 4.1.

3.1.1 Theory of Battery Tolerances

Most cell parameters indicate variations, for example also the weight and volume of the cell [56]. This dissertation however focuses on the cell capacity and the internal resistance, since only these influence the pack behavior and have the capability to improve the pack performance by utilizing current inaccessible potential. A variation in cell capacity causes the cells with a smaller capacity in a series connection to limit the overall usable pack capacity. In parallel connections, they cause balancing currents, which may affect the aging [123]. Additionally, it has to be considered that in a series connection with an equal current but a smaller capacity for a specific cell, the C-rate is higher. This is one of the main influences for the aging of the cell (Section 2.1.2). The variation of the internal resistance, in multiple publications more accurately described with impedance to include the reactive behavior of the capacitance, plays an important role as well. It causes inhomogeneous losses, which heat up the cells differently, and therefore increases the aging spread and the capacity variations as well [25].

The manufacturing process of battery cells includes several working steps, which may cause variations in the parameters of the cell. Initial variations are caused by the properties of the base materials, where the grain size distribution of the active materials, or their surface properties may vary [30]. In addition, process parameters, such as film thicknesses or drying times and cutting tolerances, electrolyte filling, and packaging variations contribute to further divergence of parameters [30]. The next step, the initial charging, where the initial solid electrolyte interphase (SEI) is formed, also adds more variation [124] due to electrical equipment tolerances. After manufacturing, varying shipping or storage conditions may further influence the variation [24]. During manufacturing of the battery pack, cells from different batches might be mixed [24], even though this is tried to be minimized with cell matching, where cells with similar properties are grouped together [125]. When the cells are connected together, tolerances in the contact resistances of the connections add to the resistance variations [126].

Beyond the initial variations, during usage there are additional influences that may further increase the overall variations. Ineffective cooling strategies may cause inhomogeneous thermal distributions and therefore a diverging aging rate [127]. External heat sources in the proximity of the pack may cause similar effects [128]. Another majorly influencing factor on the pack utilization is the unequal aging due to intrinsic variation of aging rates [129]. Yet another concern is the idea of self-propagation of the variations, where cells experience unequal loads and therefore some cells age faster [57]. While there is a scientific debate if variations in parallel connection is

causing the initial variations to directly increase [123], [130] or decrease [131], [132], it has been shown, that the overall spread of variations of the cells in a pack is in general increasing over the time [30].

The direct effect of the cell capacity variations is an overall reduction of the usable capacity for the whole pack. The capacity of a pack without active interconnections or active balancing for the cells in series connection can be calculated with Eq. (3.1) [26]:

$$c_{\mathrm{pack}} = \min_{l=1,2,..,m}\left(SOC_{\mathrm{parallel},l} c_{\mathrm{parallel},l}\right) + \min_{l=1,2,..,m}\left(\left(1 - SOC_{\mathrm{parallel},l}\right) c_{\mathrm{parallel},l}\right) \tag{3.1}$$

It is shown with Eq. (3.1) that the capacity of the whole battery pack is equal or even smaller than that of the smallest parallel capacity. Therefore, the parallel capacities should be as similar as possible and the SOC should be equalized to ensure the highest possible utilization in a static battery pack/module interconnection.

3.1.2 Parameters to Analyze the Tolerance Data

To analyze the variations, the first parameter of interest is the mean value μ_x, which can be calculated with Eq. (3.2):

$$\mu_x = \frac{1}{N}\sum_{o=1}^{N} x_o, \tag{3.2}$$

where x can be either the capacity or the internal resistance/impedance, N is the population size (sample size), and o is the sample number. By using the Kolmogorov-Smirnov test (KS-test) [133, pp. 161–168], it can be shown that not all entries in the dataset follow a normal distribution, even though most publications assume this [25], [134], [135]. However, for the comparability, the results for normal distributions are given for the whole dataset independent from the result of the KS-test.

With the mean defined, the standard deviation σ_x can be calculated, which is a representative value to describe the spread and is calculated with Eq. (3.3):

$$\sigma_x = \sqrt{\frac{1}{N-1}\sum_{o=1}^{N}(x_o - \mu_x)^2} \tag{3.3}$$

To bring the standard deviation in relation with the mean, the relative coefficient of variation is defined as $CV_x = \sigma_x/\mu_x$ in % [24].

Another factor to evaluate the magnitude of the variations is the maximum range, which is shown in Eq. (3.4):

$$\Delta x_{\mathrm{minmax}} = \max_{o=1,2,..,N}(x_o) - \min_{o=1,2,..,N}(x_o) \tag{3.4}$$

While in general a maximum range can be heavily influenced by outliners, in the case of batteries, a pre-selection by the manufacturer is assumed and the value indicates the quality of this process. It also indicates a worst-case scenario. To bring it in relation to the size of the cell, the spread ratio $sp_x = \Delta x_{\mathrm{minmax}}/\mu_x$ in % is used as the relative maximum range.

The maximum usable potential considers the fact that the smallest capacity in a series connection limits the maximum usable capacity. It is therefore a measure specifically for the problem of this dissertation. It calculates the maximum potential gain of the capacity that is possible if all cells are used to their full potential compared to the capacity in a series connection with the smallest cell limiting, as shown in Eq. (3.5):

$$p_{\mathrm{c}} = \left(\frac{\mu_{\mathrm{c}}}{\min\limits_{o=1,2,..,N}(c_o)} - 1 \right) 100\% \tag{3.5}$$

Yet another method to describe the variations is the state of inhomogeneity (SOI) introduced by Campestrini *et al.* [135], as shown in Eq. (3.6):

$$SOI_x = \frac{\Delta x_{\mathrm{minmax}}}{\max\limits_{o=1,2,..,N}(x_o)} = \frac{\max\limits_{o=1,2,..,N}(x_o) - \min\limits_{o=1,2,..,N}(x_o)}{\max\limits_{o=1,2,..,N}(x_o)} \tag{3.6}$$

For some data sets, the distribution does not follow a normal distribution. This indicates irregularities during the production, which causes the probability not to follow the normal distribution anymore. In that case, factors can be calculated to describe the shape of the distribution in a better way. One way can be an asymmetric shift around the mean value in the histogram, which is described by the skewness, as indicated by Chang *et al.* [31]. It can be calculated by Eq. (3.7) with the expected value E [25]:

$$s_x = \frac{E(x_o - \mu_x)^3}{\sigma_x^3} \tag{3.7}$$

If $s_x < 0$, the distribution is left-skewed, which means that the data is more spread to the left, for $s_x > 0$, the distribution is right-skewed, and for $s_x = 0$ it is a symmetrical distribution like the normal distribution. A right-skewed distribution for example can be explained with a manufacturer preselection of cells to ensure a minimum value of a parameter. A left-skewed distribution for example may indicate some cells aging much faster than the average.

In a similar way, the kurtosis of a distribution is used to describe its tail extremity with a divergence in how likely a value is found within the standard deviation, as shown in Eq. (3.8):

$$k_x = \frac{E(x_o - \mu_x)^4}{\sigma_x^4} \tag{3.8}$$

If $k_x < 3$, there are less extreme values expected, $k_x > 3$ stands for more extreme values, and $k_x = 3$ indicates a normal distribution. A kurtosis smaller than three indicates for example a preselection during manufacturing of the cells with a removal of both higher and lower outliers, while a kurtosis larger than three may be explained with unusual outliers, both better and worse than the average.

3.1.3 Collection of Battery Tolerance Data

The data presented here comes from two different origins: one is information found in various scientific publications and the other part is self-gathered from various research projects the author has been involved. Only larger sample sizes with more than 40 samples for new cells and at least 10 samples for aged cells were considered due to their less frequent availability. It should

be mentioned that individual cell data or statistical evaluation of the variations is not readily available in most of the literature. However, they are presented in terms of bar plots where it is possible to retrieve the variation values. Whenever this approach was used, the information in this dissertation is marked accordingly to differentiate between direct available data and extracted information. It also has to be mentioned that for both capacity and resistance/impedance, different methods of data acquisition exist. The methods are explained here to the extent what is mentioned in the literature, but the values are still directly compared in the overview due to the lack of more existing data. If several methods are used in one publication, the most similar ones compared to the other publications are selected.

Data in Literature

The oldest usable data found was published by Dubarry *et al.* [23] in 2008, where 100 new cylindrical cells in the nowadays uncommon “AAA” format (10440 according to currently common notation) with a nominal capacity of 0.3 A h were analyzed. The selected chemistry of the commercial cells is LCO, and only capacity test data is available. The for this dissertation used data is based on 0.2 C discharge rate with a 100 % DOD after a CC/CV charge with 0.5 C charge rate followed by CV until 0.005 C charge rate is reached. Accumulated test data indicates that three cells were not used for the capacity tests.

In 2012, Paul *et al.* [134] conducted an extensive analysis of 20,000 cylindrical LFP cells with a nominal capacity of 4.4 A h. No further information is given about the cells or how the tests were conducted, but capacity and internal resistance values are stated. Since no raw data can be accessed, only the values stated in the publication can be used.

The first comparison of new and aged cells was performed by Baumhoefer *et al.* [30] in 2013. They therefore acquired 48 cylindrical *Sanyo*/*Panasonic UR18650E* cells with NMC chemistry and a nominal capacity of 2.05 A h. The capacity tests were conducted with a CC/CV charge with a constant current of 2 A until 4.1 V (80 % SOC) and then a constant voltage until the charging current was less than 40 mA h. The following discharge was conducted with constant 2 A until 3 V (20 % SOC). The cycling and therefore aging of the cells was performed with 30 min discharging to 3.5 V and 30 min charging to 3.9 V, both with a current of 4 A. Within around 1000 cycles, the EOL was reached, which is defined as 84 % in this publication. This data point is used as the aged data for this dissertation, while the cycling was continued until around 1600 cycles down to an SOH of 60 %. Resistance and impedance was measured, but is not present in the publication in a usable form.

A different packaging was firstly tested by Rothgang *et al.* [136] in 2014 with 700 new prismatic automotive NMC cells of 5 A h nominal capacity. Capacity tests were performed with a defined DOD of 4.1 V until 2.7 V with different C-rates, where 1 C data was taken for the data set. Internal resistances where tested with a single pulsed current of 4 C with different durations, where the data from 10 s was used to calculate the DC equivalent internal resistance. Even though the cells were delivered as one charge, clearly two different batches with different performance can be distinguished from the data. Twenty cells seem to be excluded from the analysis, as they do not appear in the histograms.

Another data set from 2015 was generated by Keil *et al.* [60], where two clusters of identical new cylindrical NCA *Panasonic NCR18650PD* cells of 2.8 A h nominal capacity got evaluated regarding their capacity and AC resistance at 1 kHz. The first cluster of 105 cells was charged with 1 A until 4.2 V and then discharged until 2.75 V with 2.75 A. The second cluster of 175 cells was

charged in the same way, but discharged with 3 A until 2.5 V, which explains the difference between the two clusters. In total three cells were excluded from the tests.

Also in 2015, an extensive data set including real aged cells was generated by Schuster *et al.* [25] with three batches of *IHR18650A* cylindrical NMC cells produced by *E-One Moli Energy Corp*. The three batches of batteries with a nominal capacity of 1.95 A h are either new (484 units), or from two different vehicles (954 units each). One of the aged batches is used for approximately 123 cycles/21,000 km and the other one for 174 cycles/27,000 km. Capacity is measured by a CC charge with 0.5 C until 4.2 V followed by a CV charge until the current is less than 0.1 C. CC/CV discharge is conducted with 1 C until 3 V is reached and again continued until a current less than 0.05 C terminated the test. A proper impedance spectroscopy is carried out at an SOC of 50 %, where the real part of the impedance at zero crossing is used for this work as the DC equivalent internal resistance. Similar to the earlier datasets it was noticeable that in total five cells were excluded for the measurements.

The cells from a *Tesla* vehicle, the cylindrical NCA *Panasonic NCR18650B* cells, were analyzed by Devie *et al.* [124] in 2016. The nominal capacity of the 100 cells was 3.35 A h and they were assessed during a CC/CV charge cycle (0.5 C until 4.2 V and then until 65 mA) and a discharge with 0.5 C until 2.5 V. The resistance is calculated by a voltage drop, and three cells were excluded in the results.

A big sample size of 5473 prismatic NMC *Swing 5300* cells from *Boston-power* (*BPI*) was gathered by An *et al.* [137] in 2016. With a nominal capacity of 5.3 A h the cells were cycled with a CC/CV charge until 4.2 V with 0.3 C and then until 0.02 A and CC discharged with 0.2 C until 2.5 V to get the real capacities. The resistance is only tested for some cells and is therefore not included in this dissertation.

Same cell type as for Keil was tested by Campestrini *et al.* [135] in 2016. They looked into 250 units and conducted capacity tests with CC/CV charge and discharge with a charge of 0.7 A until 4.2 V and then until 0.1 A and a discharge with 3 A until 2.5 V and then again until 0.1 A. AC resistance at 1 kHz was measured at 50 % SOC.

In 2017, Rumpf *et al.* [24] acquired two batches of in total 1100 *Sony US26650FTC1* cylindrical LFP cells with a nominal capacity of 3 A h. They also followed the CC/CV charging approach with 1 C until 3.6 V and then until 100 mA. For discharge, they did several different measurements, where for this dissertation the CC capacity was selected with 1 C until 2 V. Also for the impedance, they collected several data sets, where for this work the 10 s DC pulse resistance was selected. Three cells were not included in the results.

The only pouch cell variation data found in literature comes from Barreras *et al.* [138] in 2017. Their 208 NMC *Kokam SLPB 120216216* cells with a nominal capacity of 53 A h are also among the largest. Their capacity was tested with a CC/CV charge with 1 C until 4.05 V and then until 0.05 C. Discharge was conducted with 1 C CC until 2.7 V. DC resistance is estimated by a 10 s 1 C current pulse.

Baumann *et al.* [29] were able to compare two different cell types in 2017. One batch consisted of 164 new cylindrical NMC *Panasonic NCR18650PF* cells with 2.9 A h nominal capacity and the other one consisted of 192 aged (from a BEV with 30,000 km) prismatic LMO *GS Yuasa LEV50* cells with 50 A h nominal capacity. The real capacities are measured by a CC/CV charge with 1 C until 4.2 V and then until 0.05 A followed by a CC/CV discharge until 2.5 V and then until 0.05 A again. DC resistance is calculated by a 2 s 1 C current pulse. This publication sorted out nine cells for their final results.

The publication from Devie *et al.* [139] from 2018 is one of the few sources, where an aging of the same cell batch is conducted. Here, 51 new *LG ICR18650 C2* NMC cells in a cylindrical packaging and a nominal capacity of 2.8 A h are tested, and then 15 cells are aged with 1000 1.5 C cycles and tested again. Their test methods for the capacity was a discharge down to 3.0 V with 0.5 C after a charge until 4.3 V with 0.5 C. The DC resistance was calculated after a 0.2 C pulse discharge measuring the voltage drop. Two cells were excluded from the initial 51 cells.

The latest analysis found was conducted by Lin *et al.* [140] in 2018. For that, they acquired 64 new cylindrical *IFR26650P* cells with LFP chemistry. The experimental setup is not described, but two batches are visible from the test data.

Data from Experiments

The first data set was gathered while working on the prototype of an electric taxi for tropical megacities called *EVA* in 2012 [141]. To build up the battery pack, 368 new *Dow Kokam* Model *F900-0002* pouch cells with NMC chemistry were tested for matching purpose. Their nominal capacity was 60 A h and the real capacity was tested with 1 C discharges according to the datasheet. Eight cells were sorted out due to unfitting behavior. No resistance tests were recorded. After the completion of the vehicle it was identified that one cell had a much higher self-discharge rate, which limited the usability of the whole pack significantly and initiated the idea of the research for this dissertation.

Another analysis was conducted in 2018, where 74 new cylindrical *Panasonic NCR18650PF* NMC cells with a nominal capacity of 2.9 A h were tested. The results were partly published by Chang *et al.* [31], where the author of this dissertation also co-authored. Testing methods were the same as in [29]. The cells were unused at the time, but already had a calendar age of three years. In total, 24 cells were excluded due to outlier behavior seemingly from another batch.

The latest data comes directly from the manufacturer *Melasta* for their LCO *SLPBB042126HD* pouch cells with a nominal capacity of 6.6 A h. The test configurations are unknown, but for the delivery of 367 cells, a clear indication of each cells capacity and internal resistance was included in the delivery for pack matching purpose.

Contact Resistance

Brand *et al.* [126] conducted experiments to describe the variations and magnitudes in contact resistances. They therefore analyzed spot welding, ultrasonic welding, laser welding, press contacting, and soldering. A distribution of values is clearly visible. The results can be superimposed twice on the variations of the internal cell resistances for the two poles.

3.1.4 Summary of Battery Tolerances

A summary of the relevant results from the analysis of all available capacity data sets is given in Table 3.1. The numbers in bold font are derived from extracted histogram data in literature. Different batches are noted separately. In Table 3.2, the same is done for the available results of internal resistance or impedance values and, with a separation, the different contact resistance values are added as well.

As a conclusion, in this subchapter, an extensive as possible dataset of different battery cell variations is collected. For that, first some theoretical aspects are considered about what is causing the variations and how to analyze them. Afterwards, the different data is presented, first as a description of the sources and then as detailed summarizing tables. The results of this method deliver an input, which additional capacities theoretically can be extracted with an active interconnection depending on the battery pack configuration. This finding is used to evaluate the CHB inverter efficiency on making this additional capacity accessible.

Table 3.1: Summary of cell capacity variations and statistical results (C: Cylindrical, P: Prismatic, Po: Pouch, N: New, A: Aged, Bold: derived from histogram data).

Author	Yr	Chem	Pack /Age	c_{nom} in A h	μ_{c} in A h	σ_{c} in A h	CV_{c} in %	SOI_{c} in %	p_{c} in %	s_{c}	k_{c}
Dubarry [23]	‘08	NMC	C/N	0.3	**0.299**	**0.004**	**1.48**	**7.73**	**4.27**	**-0.26**	**2.95**
Paul [134]	‘12	LFP	C/N	4.4	4.564	0.059	1.31	-	-	-	-
EVA	‘12	NMC	Po/N	60	58.97	0.665	1.13	10.78	2.97	1.25	12.9
Baumhoefer [30]	‘13	NMC	C/N	2.05	1.850	**0.005**	**0.25**	**1.06**	**0.52**	**0.38**	**2.56**
Baumhoefer [30]	‘13	NMC	C/A	2.05	1.550	**0.028**	**1.81**	**7.32**	**4.56**	**-0.18**	**2.07**
Rothgang [136]	‘14	NMC	P/N	5	5.060	0.119	**2.42**	**8.66**	**5.65**	**-0.45**	**1.66**
Keil [60]	‘14	NCA	C/N	2.8	2.678	0.014	0.52	**2.56**	**1.25**	**0.39**	**2.98**
Keil [60]	‘14	NCA	C/N	2.8	2.775	0.014	0.50	**2.49**	**1.47**	**0.00**	**2.94**
Schuster [25]	‘15	NCA	C/N	1.95	1.970	**0.016**	0.80	**4.43**	**2.42**	0.18	**2.86**
Schuster [25]	‘15	NCA	C/A	1.95	1.910	**0.043**	2.25	**10.97**	**8.31**	-0.17	**2.24**
Schuster [25]	‘15	NCA	C/A	1.95	1.850	**0.029**	1.57	**9.67**	**6.85**	-0.58	**3.97**
Devie [124]	‘16	NCA	C/N	3.35	3.177	0.025	0.80	**2.80**	**1.52**	**0.02**	**2.36**
An [137]	‘16	NCA	P/N	5.3	5.410	**0.061**	**1.12**	**5.70**	**2.27**	**0.95**	**3.52**
Campestrini [135]	‘16	NCA	C/N	2.8	2.880	**0.005**	0.16	**0.84**	**0.27**	**0.03**	**2.59**
Rumpf [24]	‘17	LFP	C/N	3.0	2.911	0.012	0.41	**1.96**	**0.96**	**-0.14**	**2.56**
Rumpf [24]	‘17	LFP	C/N	3.0	2.914	0.014	0.48	**2.69**	**1.44**	**-0.13**	**2.85**
Barreras [138]	‘17	NMC	Po/N	53	51.79	0.18	0.35	1.68	**0.65**	**0.24**	**2.41**
Baumann [29]	‘17	NMC	C/N	2.9	2.879	**0.010**	0.35	**1.72**	**0.85**	**0.12**	**2.74**
Baumann [29]	‘17	LMO	P/A	50	**46.07**	**0.506**	**1.10**	**4.56**	**1.39**	**0.92**	**3.47**
Devie [139]	‘18	NMC	C/N	2.8	2.842	0.009	0.30	1.36	-	-	-
Devie [139]	‘18	NMC	C/A	2.8	1.862	0.052	2.80	8.35	-	-	-
Chang [31]	‘18	NMC	C/N	2.9	2.913	0.007	0.25	1.23	0.65	0.25	2.85
Lin [140]	‘18	LFP	C/N	2.3	**2.072**	**0.139**	**6.69**	**17.39**	**9.85**	**0.55**	**2.01**
Melasta	‘19	-	Po/N	6.6	7.028	0.039	0.56	2.87	2.17	-1.53	5.37

Table 3.2: Summary of cell resistance variations and statistical results (C: Cylindrical, P: Prismatic, Po: Pouch, N: New, A: Aged, Bold: derived from histogram data). Separated: contact resistances.

Author	Year	Chem	Pack/ Age	μ_r in mΩ	σ_r in mΩ	CV_r in %	SOI_r in %	s_r	k_r
Paul [134]	‘12	LFP	C/N	5.03	0.29	5.77	-	-	-
Rothgang [136]	‘14	NMC	P/N	3	0.086	**2.90**	**14.06**	**0.15**	**3.06**
Keil [60]	‘14	NCA	C/N	22.5	0.3	1.30	**6.83**	**0.79**	**4.22**
Keil [60]	‘14	NCA	C/N	21	0.2	1.00	**3.78**	**0.52**	**3.48**
Schuster [25]	‘15	NCA	C/N	71.15	**1.474**	1.94	**16.12**	**0.60**	**5.89**
Schuster [25]	‘15	NCA	C/A	74.08	**1.983**	2.56	**20.63**	**0.63**	**5.35**
Schuster [25]	‘15	NCA	C/A	78.64	**2.601**	3.19	**23.98**	**0.74**	**4.33**
Devie [124]	‘16	NCA	C/N	59.6	1.758	2.95	**16.44**	**1.52**	**6.51**
Campestrini [135]	‘16	NCA	C/N	21.67	**0.155**	0.72	**3.43**	**-0.18**	**2.50**
Rumpf [24]	‘17	LFP	C/N	28.49	0.407	1.43	**7.13**	**-0.17**	**2.65**
Rumpf [24]	‘17	LFP	C/N	28.74	0.352	1.23	**5.94**	**0.09**	**2.39**
Barreras [138]	‘17	NMC	Po/N	1.64	0.08	4.88	26.83	**0.05**	**2.33**
Baumann [29]	‘17	NMC	C/N	36.04	**0.312**	0.92	**4.5**	**0.16**	**3.04**
Baumann [29]	‘17	LMO	P/A	1.01	**0.045**	4.40	**20.36**	**0.14**	**2.99**
Devie [139]	‘18	NMC	C/N	73.2	2.625	3.60	15.64	-	-
Devie [139]	‘18	NMC	C/A	112.5	5.625	5.00	14.27	-	-
Chang [31]	‘18	NMC	C/N	39.96	10.34	25.9	67.12	2.40	10.8
Lin [140]	‘18	LFP	C/N	**24.97**	**5.730**	**22.9**	**52.63**	**0.69**	**2.36**
Melasta	‘19	-	Po/N	1.26	0.039	3.15	17.99	-0.11	2.69
Brand [126]	‘17	Spot welding		**0.355**	**0.059**	**16.76**	-	-	-
Brand [126]	‘17	Ultrasonic welding		**0.471**	**0.164**	**34.88**	-	-	-
Brand [126]	‘17	Laser welding		**0.281**	**0.040**	**14.33**	-	-	-
Brand [126]	‘17	Press contact		**0.284**	**0.048**	**16.93**	-	-	-
Brand [126]	‘17	Soldering		**0.195**	**0.054**	**27.80**	-	-	-

3.2 Control Strategy

The second subchapter investigates which strategies should be used to control the CHB inverter. Since this circuit works as the motor driver, the normal motor control has to be modified so that individual loads on the cells or modules are possible without inflicting the operation of the motor and therefore the driving behavior of the vehicle. A single motor configuration is assumed. A multiple motor configuration would be possible as well, but would require further hardware and therefore results in an increased complexity of the control strategy, as discussed in Section 5.2.3.

Firstly, the theory behind the control of a conventional and a CHB inverter is explained. Then the possible adjustments to shift the individual loads during charging and discharging are examined. The two most promising balancing approaches are compared and a preferred concept is selected, which is implemented as a simulation and used for the remaining dissertation.

The described approach was developed with the support of Kakrinska [142], who contributed to the implementation of the methodology. It is assumed in this subchapter that the status of the imbalance is known exactly at any time. The method to acquire this value and the actual accuracy are explained in the following Subchapter 3.3.

3.2.1 Theory of General Inverter Control

As mentioned in Section 2.1.3, for both VSI and CHB inverter the main task is to drive the motor by supplying the required three-phase AC voltage. An overview of the inverter control structure is given in Figure 3.2, where the white blocks indicate the conventional functionality of an inverter control and the gray blocks represent the additional required functions for the active battery utilization with a CHB inverter. An overall supervisory controller converts the present driving demands like speed and torque demand under consideration of the current motor feedback (mainly the pole positions) into the commanded voltages u^*_{as}, u^*_{bs}, and u^*_{cs}, also called the reference voltages [143]. These commanded voltages have to be modulated into transistor controlling signals in a way that the inverter output corresponds to the desired phase voltages u_{as}, u_{bs}, and u_{cs} with the proportional amplitude and equal frequency. The closer the sinusoidal shape is matched for the phase voltages, the lower are the harmonic losses and the higher is the efficiency that can be achieved. The three commanded voltages have the same amplitude and frequency, but they are shifted by a phase angle of $2\pi/3$. The frequency is hereby determined by the motor speed and the amplitude regulates the requested torque. The generation and control of the commanded voltages u^*_{as}, u^*_{bs}, and u^*_{cs} are determined by the upper-level motor control algorithm and this algorithm has no influence on the battery utilization, which is why it is not further investigated for this dissertation. A basic introduction can be found for example in [66].

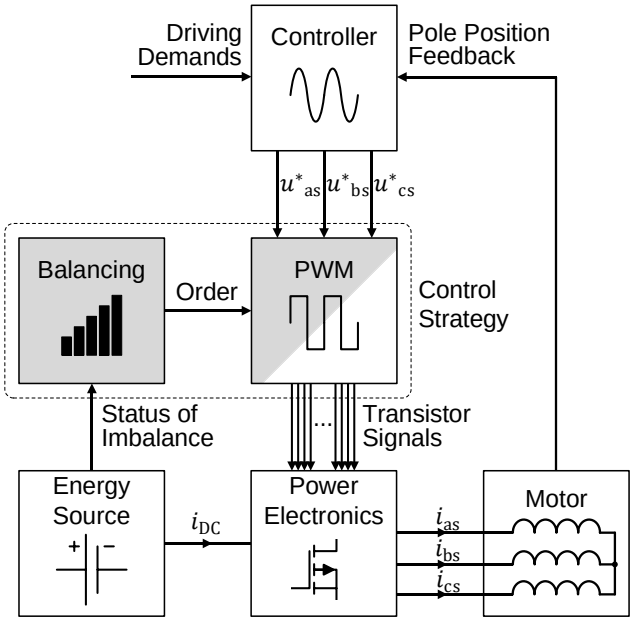

Figure 3.2: Inverter control structure. Gray blocks represent the required add-ons and modifications to enable increased battery utilization with CHB inverter.

For the modulation of the reference voltages, the PWM method is the most common method and is implemented with different variants. Because of this, it is solely considered in this dissertation. In general, PWM is a modulation technique, which encodes the amplitude of an analog signal into discrete chopped digital pulses. The PWM switching frequency is invariable and therefore the period of the modulated signal has a fixed duration. During one period, the signal is in the high state for a variable time. The ratio between high and low state duration is called the duty-cycle, which also represents on average the ratio the analogue signal amplitude is reduced from its maximum value. To modulate a sinusoidal phase voltage, the PWM switching frequency has to be much higher than the modulated frequency to avoid distortions. However, due to switching losses for each cycle, it also should not be set too high. Typical PWM switching frequency are in the range of 1 kHz to 20 kHz [67].

Common ways to generate a PWM signal for VSI and ML inverter are space vector modulation (SVM), or carrier-based PWM generation [144]. A third one, the hysteresis PWM (bang-bang PWM) can be found in some older publications as well [145]:

1. SVM is a powerful modulation scheme, where the switching states are represented by space vectors. They can be indicated in a space vector diagram in a hexagonal shape, as indicated in Figure 3.3a). Eight vectors represent the eight different possible switch pattern combinations. Each of the six active vectors make up a spoke of the diagram and the two inactive vectors, where all switches are either on or off, are plotted as null vectors in the center of the diagram. The desired output voltage vector u_{ref} is also based in the center and is sampled with the rotation frequency around it. Its concurrent location within the diagram and therefore the position in relation to the active vectors determines the switching time of each switch. SVM can be adapted for ML inverter control by adding the respective additional possible switch states caused by the additional switches in the state diagram, while the method remains the same [146].
2. Carrier-based PWM works with the comparison of the intended reference sinus wave with a carrier wave, as shown in Figure 3.3b). If the reference wave is higher than the carrier wave, the corresponding switch is in a conducting state and vice versa. The carrier signal hereby is best to be selected in a triangular shape [147] and its period defines the switching frequency. Carrier-based PWM in a ML inverter can be realized by various ways of introducing multiple carriers, so that the levels can be controlled in an aligned way.
3. A hysteresis PWM is based on the scheme where the output is allowed to oscillate between the upper and lower limit of the reference, as represented in Figure 3.3c). Its use case in ML inverter is limited due to the missing alignment of the SM.

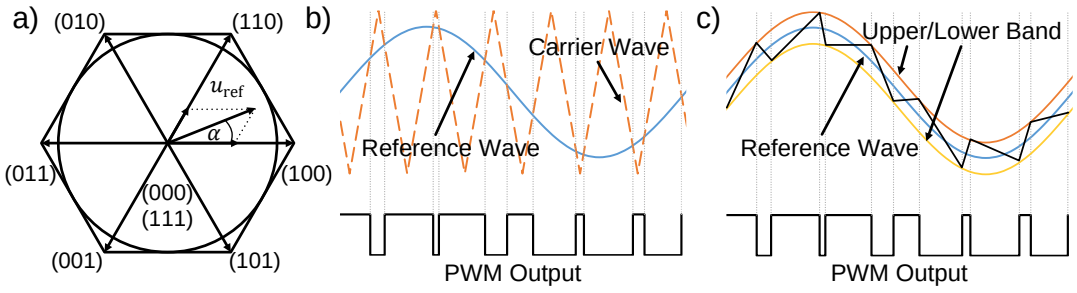

Figure 3.3: Simplified representation of PWM generation methods for s single half bridge, in detail a) SVM PWM, b) carrier-based PWM, and c) hysteresis PWM.

For the control of the active interconnection in this dissertation, the carrier-based solution is selected. The main reason for that is its common usage for CHB inverters due to simpler design considerations [100], which enables easier modifications for balancing and utilization. This is especially the case with an increased number of output levels [148], even though SVM are reported to be more efficient in avoiding harmonic distortions, as the signal can be optimized [145]. However, SVM based modulations can be transformed into carrier-based PWM, which enables carrier-based solutions to achieve the same advantages [149].

3.2.2 Theory of CHB Inverter Control

For controlling a ML inverter like a CHB inverter with a carrier-based PWM, each submodule must get its individual control signal. In this case, with a carrier-based approach selected, a multi-carrier wave comparison is required. In general, there are two possible carrier-based PWM methods commonly mentioned in the literature for ML inverters: phase disposition PWM (PDPWM) and phase-shifted carrier PWM (PSCPWM) [150], as shown simplified in Figure 3.4. For both methods, it has to be considered that the base structure of a CHB inverter, the H-bridge, has in total four usable switch configurations: the two bypassing configurations, and either a positive or negative module voltage connection. It therefore needs two separate PWM signals, one for each polarity.

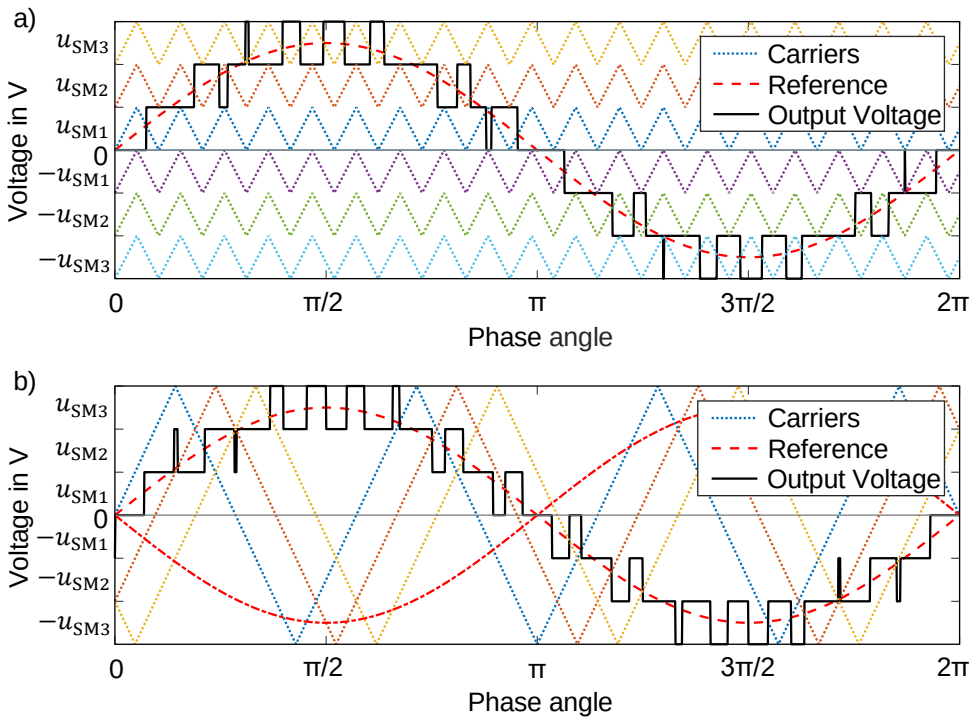

Figure 3.4: Simplified ML inverter PWM methods for a single phase and three submodules with reduced carrier frequency. (a) Phase disposition (b) Phase shift

Phase disposition PWM, originally developed by Carrara *et al.* [151] in 1992 and depicted in Figure 3.4a), is based on the principle that for each SM there are two triangular carriers with the same frequency, one for the positive and one for the negative polarity. The switching frequency of the carriers has to be significantly higher than depicted in the simplified figure. The amplitude of each carrier is the available voltage of the SM. The carriers are stacked on top of each other, the positive on the upper half of the reference wave and the negative on the lower half. Three

sinusoidal references, one for each phase and with their respective phase shifts, are then compared with the individual carriers to determine the individual switch states.

Three alternatives are commonly mentioned:

1. in phase disposition (IPD), where all carriers are in the same phase and which is shown in Figure 3.4a);
2. phase opposition disposition (POD), where the negative carriers are inverse compared to the positive ones;
3. and alternative phase opposition disposition (APOD), where each carrier is inverse from its adjacent carriers.

Based on their similarity and the suggested superiority of the IPD due to its better harmonic performance [152], only this scheme is considered for this dissertation. The major disadvantage of phase disposition PWM is that it introduces a substantial additional imbalance between the modules, because the average duty cycles of the different SM PWM during one period of the reference wave are disparate and depend on the location within the stack. As visible in Figure 3.4a), in this example SM 1 sees permanently a much higher load compared to SM 2 and SM 3 sees an even further reduced load.

Due to this big disadvantage of phase disposition PWM, the alternative scheme phase-shifted carrier PWM was introduced especially for the use case of CHB [153], which is shown in Figure 3.4b). To allow an identical load on the SM, but to avoid simultaneous change of their output voltage causing high THD, each carrier is phase shifted by 180° divided by the number of SM in each cascaded inverter phase leg. To control the negative switching state of the H-bridges, an inverse duplication of either the carriers or the reference has to be added with the latter one depicted in the example figure. The amplitudes of the carriers are all the SM voltages combined. Phase-shifted carrier PWM has no more intrinsic own unbalance of the SM, however, an increased THD can be noticed [154].

3.2.3 Balancing Principle

To achieve an equal utilization, the first step is to determine the state that should be equalized. There are two different unbalancing effects. First, due to tolerances, the cells have differentiating capacities and therefore can hold different amount of charges. Second and caused by the tolerances, but also additionally caused by other intrinsic and extrinsic differences between cells, their currently held charge differs due to drift in states over time. Both effects are causing a considerable amount of charge to remain unused in series connected cells when the first one reaches the cut-off-voltage and there is unused capacity left after the first series cell is fully charged as well. This leads to the conclusion that the charge should be the state of interest for optimized utilization. However, as it will be discussed in detail in Subchapter 3.3, the charge and remaining charge capacity are hard to determine. Furthermore, an equal charge level during charging would still result in unused capacity. To solve that, both the remaining charge and the overall usable capacity needs to be known. Two factors with two inaccuracies make the estimation even harder to achieve.

However, as by definition, an SOC of 0 % equals an available charge of 0 A h and an SOC of 100 % equals a maximum charged battery. So the SOC can be used as a single balancing criterion. An example case is shown in Figure 3.5, where initially SOC and remaining charges are different for four series cascaded SM of a phase in a CHB inverter. During discharge, until the

time t_1, the SOC are equalized. However, due to varying capacities of the SM, the available amount of charge is still not equalized and SM 4 would still limit the usable amount of energy from the pack. Nevertheless, if the SOC are kept aligned during the remaining discharge until t_2, the charge amounts are equalizing themselves and therefore the four SM reach the empty state at the same time, being all fully depleted. It only has to be ensured that $t_1 < t_2$. The same principle applies for charging, which enables a full utilization of all capacities of the modules at any time. The real value of the SOC is not required, as long as a ranking between the SM SOC can be stated and an update on this ranking is conducted with a high enough frequency.

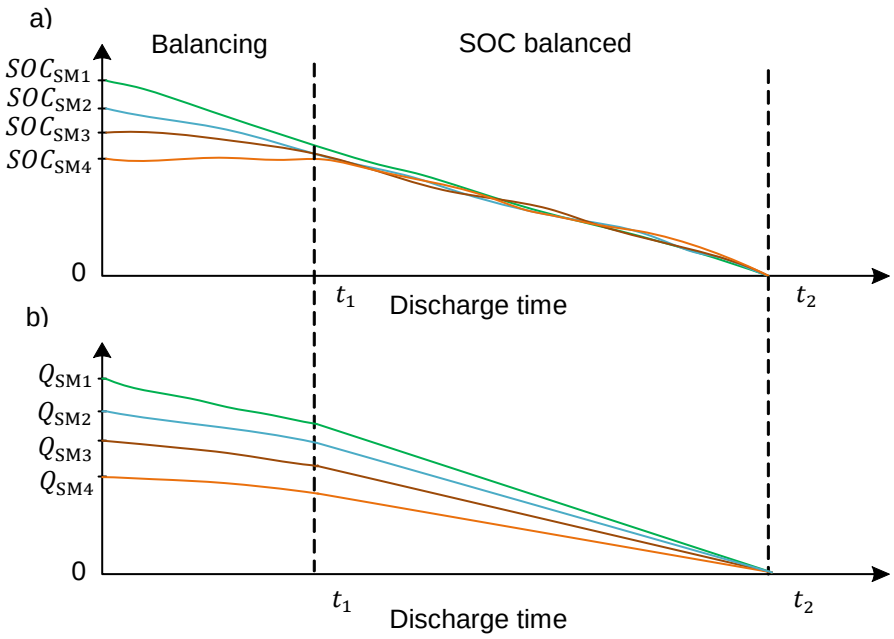

Figure 3.5: SOC balancing principle: a) SOC and b) remaining charge Q for a full discharge, adapted from [155]

3.2.4 Control Approach

With the knowledge about the states, which is explained in the following subchapter, firstly a sorting has to be conducted. This sorting is defined in a priority list, in which the states are ranked according to which SM have a higher SOC than the others. For charging, the priority list is reversed. This balancing information is then used to manipulate the PWM generation. There are two necessary balancing mechanisms required for a CHB inverter: The SM within each phase and the three phases between each other have to be balanced.

Intra-phase Balancing

Both of the two mentioned carrier-based PWM generation methods can be modified to enable different loads according to the priority list:

Phase Disposition PWM

To be able to control individual loads in a ML inverter with phase disposition PWM, first the problem of the intrinsic imbalance has to be solved. For that, the idea of module rotation was shown suitable [156]. Here, the positions of the carriers are rotated in a specific order to achieve

an equal participation in the energy contribution in one sorting cycle for the scenario of equal SM. A “sorting cycle” is defined as the amount of changes made in the switching priority list until the initial order is reached again and each SM is discharged for the same amount. As shown in Figure 3.4a), the current order is “SM 1-2-3”. The two other sorting orders within one sorting cycle therefore would be “2-3-1” and “3-1-2”. The resorting frequency should be kept as high as possible to have the best balancing results, as the energy demand for driving is fluctuating and therefore a too low resorting frequency could cause additional imbalance [157]. However, the vehicle speed profile and therefore the motor speed does not change significantly during the duration of a few periods of the engine voltage. Therefore, with updating the order of the modules in the priority list after each half-wave, additional imbalance can be minimized. A higher resorting frequency would enable an even more equal load, but at the same time would increase the switching losses, as it would add for the motor control unnecessary switch state changes. For this dissertation, different rotating schemes where explored, where the different modules are either rotated, exchanged with their neighbors, or randomly resorted. In the theoretical case of the current amplitude not changing during one sorting cycle and the presence of identical modules, this rotation would cause the phase disposition PWM to discharge the battery pack homogeneous.

To achieve a balancing between unequal SM, the simplest way is to adapt the rotating scheme in a way that they are sorted in descending/ascending SOC order for discharging/charging and no automatic rotation is applied. After every half-wave, the order is updated. It therefore firstly balances the SOC and then keeps them in equal ranges, as the SOC is not changing significantly in one sorting cycle.

Phase-Shifted Carrier PWM

When using a phase-shifted carrier PWM generation, there is no intrinsic unbalancing occurring and all SM are utilized with the same charge. The method to achieve individual loads on the SM is to adapt the carrier wave signals of the individual SM according to its SOC. Individual carriers can be mirrored, which leaves the overall output signal identical, while the energy contribution of the SM differs [158].

Inter-phase Balancing

To ensure a balancing between the phases, the neutral point shift method is selected [159], since it is direct compatible with the previously mentioned intra-phase balancing methods. The term “neutral point shift” refers to shifting the potential of the ungrounded and therefore floating neutral point of the star-configured converter away from the physical neutral point of the battery pack [160]. This is not only useful for drifts in capacity, but also, if a whole SM is disabled and bypassed due to a fault, the motor still is able to drive the vehicle. The output voltage amplitude is then reduced for each phase to the lowest summed up DC voltage. The line-to-line voltage of each phase is limited by the sum of the added up SM voltages, as shown in Eq. (3.9):

$$\left|u_{zy}\right| < u_{\mathrm{sum}_z} + u_{\mathrm{sum}_y}, \tag{3.9}$$

where u_{sum_x} is the sum of all available SM voltages of the x phase. The neutral point u_{n} then is calculated by Eq. (3.10), in which only one term is non-zero.

$$u_{\mathrm{n}} = -\max\left(u_x - u_{\mathrm{sum}_x}, 0\right) - \min(u_x + u_{\mathrm{sum}_x}, 0) \tag{3.10}$$

The reference voltages for each phase are then shifted by the neutral voltage ($u_x + u_\mathrm{n}$). This neutral voltage is not necessarily a constant value, but can be a high frequency, cyclic value. The new phase references can be directly used in the intra-phase balancing methods mentioned earlier.

3.2.5 Control Implementation

The described approaches are directly able to balance the modules and utilize them fully with the prerequisite that the SOC is known at any time and with a perfect accuracy. As this is not given, in the following work package, simulations of the here mentioned control strategies are implemented together with a comparison of selected state estimators to be able to compare the actual possible equalizations. For that, phase disposition PWM is selected due to the mentioned better THD behavior and effective balancing method by altering the sorting cycles.

As a conclusion, in this subchapter, the different ways to modulate the control of the CHB inverter are presented, which enable a differentiated load on the modules. For that, first some theory is introduced to indicate the best way to modify the motor control. In addition, a definition is given, which parameter has to be balanced to enable a full equalization. After that, several different methods are presented. Since the different methods indicate to have no direct influence on the quality of the increased utilization, the most suitable variants are selected depending on other, for this thesis irrelevant aspects retrieved from literature.

3.3 Module State Estimation

The knowledge about the SOC of the SM is an essential point of the sorting methods in the previous subchapter. However, there is no direct access to this state. It belongs to the typical functionalities of the BMS to estimate a value for the whole pack, which is mainly used for a range estimation. Nonetheless, other uncertainties, for example the selected route and driving profile, add another big indeterminacy on the calculated remaining range [161]. Therefore, a too high accuracy is normally not required.

For an increased utilization, where the cell tolerances are just a few percent, as visible in Subchapter 3.1, a much higher accuracy of the state estimation is required. The estimation error must be lower than the lowest expected tolerances for the system to function. Additionally, instead of one estimation for the whole pack, an estimation for each SM is required to achieve an increased utilization. Because of this, the cost of the system is more relevant compared to state estimators for conventional packs.

The following section first gives a short overview of existing SOC methods and summarizes them. An increased focus is put on methods, which are direct useful for the sorting in the CHB inverter. The most promising ones are selected and simulated in a holistic environment to verify their effectiveness and to quantify, how much more energy can be extracted with the selected control strategy. The best option is evaluated and its possible results regarding the increased battery utilization are then used in the following section to parametrize the CHB inverter configuration.

The work in this subchapter was developed with the support of Fundneider [155], who contributed to the implementation of the simulation including its parametrization and the evaluation of the direct results. In most parts of the simulation, a 9-level/4 SM per phase inverter is used as an example or reference, as it is a main result of the methodology in Subchapter 3.4.

3.3.1 Evaluation of Different Estimation Methods

The critical part of SOC estimation is that there are no parameters available, which can be directly measured. A cell from the outside can be regarded as a black box and only has its voltage and current accessible, which do not directly relate to the SOC. However, since the SOC is an important parameter, a significant amount of research has been conducted in this area with numerous review studies summarizing different SOC estimating methods [162]. For this work, principles with high relative accuracy between the individual SM as a sorting criteria are more important than the actual accuracy. Another aspect is the complexity, since the method should be applicable and economical in current and near future EV. All SM have to be tracked with a high sampling rate compared to just one estimation for a conventional pack with low sampling requirements. To consider the complexity, it mainly has to be evaluated, what kind of hardware is required for the necessary calculations. Another consideration must be the applicability on a high number of battery packs, as it would not be possible for a commercial vehicle manufacturer to newly parametrize the simulation model for each vehicle. It therefore has to be mentioned that this section does not give a comprehensive overview of state estimators, which already can be found in literature, but a pre-selection of methods that seem fitting for the required result. Each selected method is shortly explained, before a summarizing evaluation is given, which leads to the selection of the further investigated methods.

Open-Circuit Voltage

As mentioned before in Section 2.1.2, the OCV is a characteristic indicator for the SOC depending on the cathode chemistry following a non-linear correlation [40]. It is the most cost-efficient method, because voltage sensors come at minimal costs and are a strict requirement to determine the cutoff voltage and end-of-charge voltage for each parallel string anyways. This method also operates mostly with a high accuracy, where for some chemistries, for example LFP, a flat voltage curve can be a more challenging parameter. The main disadvantage are long waiting times until all distorting effects fully fade away, which takes up to 3 h [163]. It therefore only can be used as a periodic recalibration of other methods during longer inactive periods of the vehicle.

Closed-Circuit Voltage

The closed-circuit voltage (CCV) is the actual voltage present at the SM while a load is attached. It works with the same requirements as the OCV method, but additionally it can be measured at any time during the vehicle usage. However, due to the over potentials of the cells and the losses, the values are strongly distorted by the current, the temperature, and the SOH [51]. Due to the tolerances in the cells, especially among the internal and external resistance, even a scaled value is not directly able to indicate a SOC sorting order. In a CHB inverter, the measurement can be conducted during the current zero crossings to at least remove the ohmic over-voltages. In addition, the reverse current pulses caused by reactive power demand of the electric motor help to reduce the over-voltages making this method still being a valid option compared to conventional battery packs [164].

Pseudo-Open-Circuit Voltage

The Pseudo-OCV method takes advantage of the principle of the CHB inverter in an automotive application, where, depending on the current driving conditions, not all SM have to be active all the time to reach the required line-to-line voltage [165]. This enables timeslots, where a SM is excluded from the PWM and therefore the ohmic over-voltages are eliminated. If a SM can be excluded for a longer waiting time, also the fast transient over-voltages, which are caused by SEI layer and charge transfer with time constants of typically in the range of 0.1 s to 10 s [165], [166], can be eliminated from the measurement. This settling time enables more accurate OCV estimations compared to the CCV method. The minimum waiting time is a critical parameter, since too short times result in insufficient relaxation, while too long waiting time cause additional unbalancing, or might not even be allowed by the driving profile. In the exemplary power grid application of [165] the waiting time is chosen so that modules will not unbalance for more than 1 % SOC, resulting in a waiting period of 3 s.

Coulomb Counting

Coulomb counting (CoC) works with the bookkeeping principle by integrating the current over the time and therefore calculating the amount of charge that should be in the battery [51], [167]–[169]. With the additional information of end of charge and end of discharge, the capacity can be retrieved during a full cycle, which also delivers SOC and SOH information. The method works efficient, as only a current sensor is required, which is part of the BMS anyways to limit the maximum currents. Because of this, it is a solution often found in current commercial applications. The main limitation for its accuracy is that since it is an open-loop system, its results are prone to drift due to signal noise, sensor inaccuracy, and coulombic efficiency. To achieve higher accuracy, coulomb counting is often combined with or part of other methods [168]. For a CHB inverter, a sensor is required for each SM. However, such sensors are available at low costs.

State Observer

A state observer is a control system that estimates unmeasurable internal states based on a simulation model and feeds the error between the real system output and the simulated output back to the observer [170]. This causes the observer output state to converge eventually to the actual system state. The observer dynamics define the speed of the convergence, where a too fast adaption makes it more sensitive to noise [171], so parameter tuning is required. The key element for the SOC estimation is a battery model, where simple models lack accuracy, but highly sophisticated models increase the computational effort.

A common application and a favorite amongst the state observer for the SOC estimation in both industry and research is the Kalman filter (KF) [172], [173]. However, Kalman filters use a large number of operations and therefore result in an increased computational complexity. An alternative can be the Luenberger observer (LO), which might be less accurate, but has a lower complexity. If directly compared for the same use case of SOC estimation, the Luenberger observer requires less than half the time for one calculation step compared to the Kalman filter, but achieves a similar accuracy for the results [174].

Impulse Response

The idea of impulse response (IR) is to drain the battery with a pulse current and measure the voltage response during that time [175]. This proposal seems promising since the individual SM are drained by individual pulses of the PWM. However, the duration of the pulse is defined by the large time constants of electrochemical batteries, which imposes a restriction on the PWM switching frequency. Due to this, IR can be considered unsuitable for the SOC estimation of CHB inverters.

Artificial Neuronal Network

Artificial neuronal network (ANN) is a machine learning approach, where training data is used to determine the SOC without knowing the underlying mechanisms in the battery, but just using the measurable input parameters like voltage and current [176]. One or more hidden layers are used to process the output with the advantage that it can operate in non-linear conditions and adapt itself to factors like aging or other influences. High accuracies are achievable. However, ANN have increased requirements of the computational complexity and require significant amount of training data, which is difficult to acquire, since the ground truth has to be defined in lengthy experiments and is not directly transferable to different battery packs.

Summary of Estimation Methods

In Table 3.3 a summary of the mentioned SOC estimation methods is given with a highlight of their main advantages and disadvantages. The typical accuracy is stated as obtained from literature. With all information combined, a qualitative relevance comparison for the intended use-case of SOC sorting in a CHB inverter is derived.

Table 3.3: Comparison of preselected SOC estimation methods

Method	Pros	Cons	Accuracy	Relevance
OCV	• High accuracy possible • Simple measurement	• Long relaxation time required • Unsuitable for flat OCV-SOC curves	≤ ±2 % [177], ≤ ±3.2 % [178]	o
CCV	• Simple measurement • Comparison less sensitive	• Measurement strongly influenced by over-voltages	≤ ±2 % [164]	++
Pseudo-OCV	• Simple measurement • Comparison less sensitive • Uses CHB for higher accuracy	• Relaxing time duration unclear • Benefit compared to CCV unclear	≤ ±3.5 % [165]	++
CoC	• Simple measurement • Current in one phase equal	• Integration drift • Capacity unknown since its aging	≤ ±4 % [179], ≤ ±1 % [180]	o
LO	• Lowest computational effort among SO	• Sensor noise not considered • Model fit required	≤ ±1 % [172], ≤ ±3 % [181]	++
KF	• More accurate SO, insensitive to Gaussian noise	• Higher computational effort • Model fit required	≤ ±0.49 % [176], ≤ ±5 % [162]	+
IR	• Fast and simple measurement with extended information	• Hard to interpret • CHB pulses too short	≤ ±0.3 % [175]	-
ANN	• High accuracy • Adaptive	• Highest computational effort • Lack of training data	≤ ±0.25 % [176], ≤ ±1.25 % [162]	-

The relevance indicates a preference on CCV, Pseudo-OCV as simple methods and Luenberger observer as a more complex, but more accurate method. Luenberger observer is selected over the more common Kalman filter and other state observers, because it has the lowest computation complexity among other model-based SOC estimation methods [181].

With three solutions remaining, it is still unclear, which one would be the most preferred solution. The accuracy is only given for an absolute SOC estimation in literature, and not as sorting criteria. It has to be considered that the mentioned methods have to be optimal parametrized to be comparable. In addition, the quantified accuracy for sorting and therefore additional extractable energy remains unknown. Therefore, additional considerations are required, which are conducted in the following sections.

3.3.2 Approach of State Estimation Method Comparison

To identify the most suitable SOC method and to quantify it, a simulation approach is selected where a battery pack is cycled in a simulated vehicle using a CHB inverter with the different state estimators to generate the priority lists for the CHB inverter. *MATLAB/Simulink* is used for the simulation. Figure 3.6 gives an overview of the sub-functions of the overall model with a gray indication of components that are adapted from previous publications. Existing and validated sub-models from other publications are used whenever available to reduce the model implementation effort and to increase the universality.

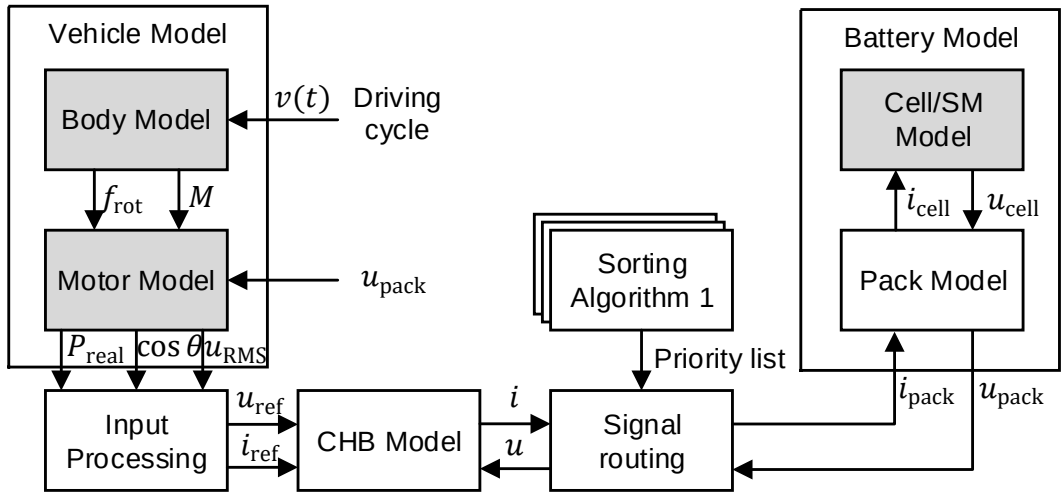

Figure 3.6: Structure of the model to compare different state estimators. Gray sub-models are based on existing models. Arrows indicate information direction.

Vehicle Model

The vehicle model consists of all relevant BEV components excluding the inverter and the battery, because these are modelled in more detail in separate models. The main input for the vehicle model is the driving cycle as explained in Section 2.1.1. For this dissertation, the worldwide harmonized light vehicle test procedure (WLTP) Class 3 transient driving cycle pictured in Figure 3.7 is used. It is selected because many countries applied it as a reference, since it includes low, medium, high and extra high speeds, which depict realistic average driving conditions [182]. The driving cycle is passed to the vehicle model as a speed profile.

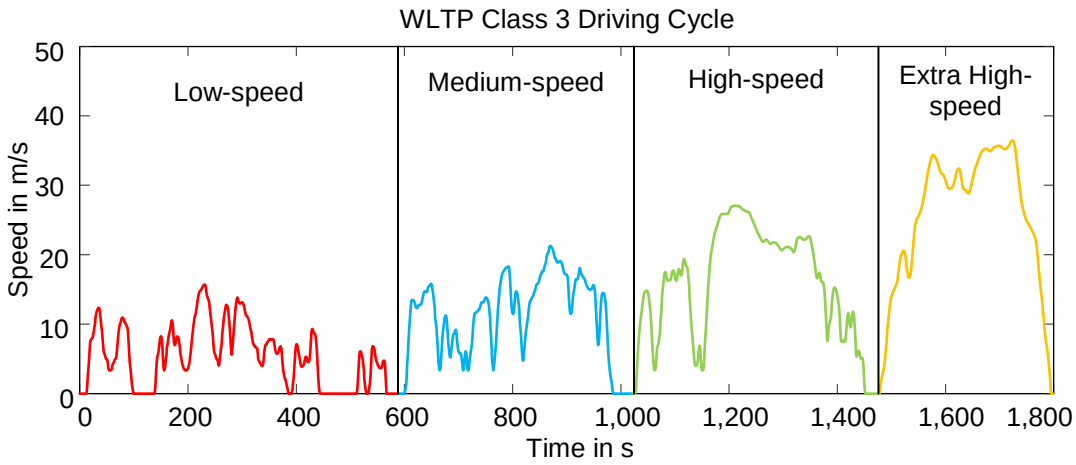

Figure 3.7: Speed vs time profile of WLTP C3

The vehicle model has to convert the speed profile into the electrical power requirements. To do so, it is separated into two sub-models: the car body model and the motor model. Both are adapted from [68], where they are described in detail and validated. The body model is based on the *BMW i3* B-segment hatchback car with the 60 Ah battery, as it is a good example for an urban vehicle with many parameters publicly available [183]. This BEV is still considered one of the most efficient EV despite being on the market for many years [184]. Factors like the vehicle mass, transmission ratio and transmission losses are considered and taken from the vehicle datasheets. With this, the model determines the torque and rotational speed requirements for the electric machine, which is the input for the motor model. This model is also based on the motor of the same reference vehicle *BMW i3*, which has a permanent magnet synchronous machine (PSM) with a rated power of 125 kW installed. It determines the required voltage, current and power factor from the inverter to operate at the defined conditions.

To increase simulation speed, the vehicle model is pre-simulated and only the necessary outputs are saved. The requested power output is independent from the battery voltage and is saved directly in a lookup table. The voltage profile, which is topped at maximum battery voltage in the CHB model, is stored directly as well. For the phase shift data, however, the voltage is increased from 120 V to 235 V in 5 V steps and each corresponding output is saved individually in a lookup table.

CHB Inverter Model without Losses

For the state estimation approach, the model of the inverter is strongly simplified, because it is not the main focus of this subchapter to evaluate the inverter functionality. No losses or waiting times are implemented. Only one phase is considered, since the phase balancing method works on a different principle, but would use the same input for load shifting as within one phase, as described in Section 3.2.4. The output of the motor model delivers phase-to-phase root mean square (RMS) values instead of single-phase sine wave signals. The current is not directly available and calculated from the power profile and the voltage profile. In order to obtain the actual sine waves, the RMS values are multiplied by $\sqrt{2}/\sqrt{3}$ to obtain the peak value and phase shifted by $\theta/(2\pi f)$ with $cos\theta$ and f as the power factor and the sine frequency, respectively. The frequency normally is direct proportional to the vehicle speed, but in this simplification is set

constantly to 32 Hz, as it sets the pulse widths equal and has little effect on the lossless simulation. The value is selected as it is with the range of possible frequencies, but it is low enough to enable executable simulation times.

The resulting voltage signal is used as a reference and is compared with the triangular carriers in order to generate the PWM signal as shown in Figure 3.8. Only absolute values of the voltages are used, which reduces the carriers by half. The carriers are generated by a triangular signal generator, multiplied by the SM voltages, offset for the cascading, and ordered by one of the selected sorting mechanisms as discussed in Section 3.2.5. The PWM signal is used to switch the reference current on the respective SM.

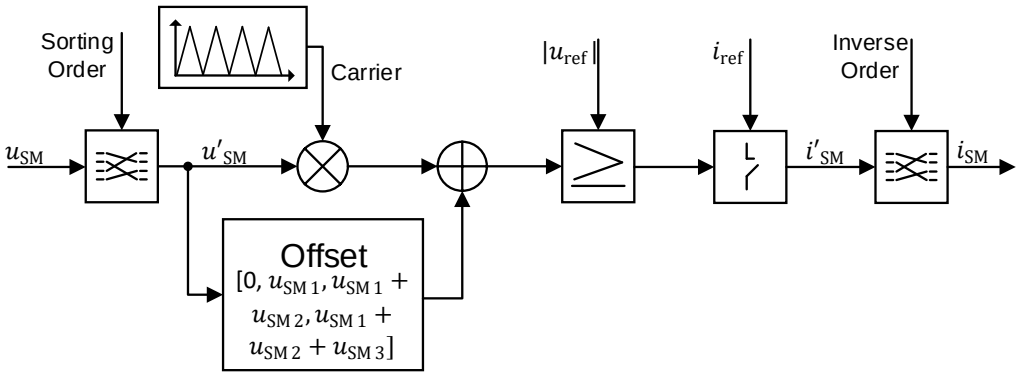

Figure 3.8: Structure of the CHB inverter model, adapted from [155]

Battery Model

To simulate the battery, several different methods are common. One is the electrochemical model based on the chemical processes happening in the cell. While these models are highly accurate, they are usually complex to simulate and are therefore too computationally intensive. Alternatives are empirical models, which are based on measurements from reference cells. Empirical models can be expressed with mathematical equations, which describe the electrochemical behavior and directly calculate required parameters, such as SOC and voltage. These models are fast to simulate, but lack in accuracy. A compromise of accuracy and simulation complexity are the equivalent circuit models (ECM), which use theoretical ideal electric circuit elements such as voltage sources, current sources, resistors, capacitors, etc. to model the battery. The parameters of the components are determined from experiments. The speed and accuracy of the simulation can be adapted with the number of theoretical elements included in the circuit, which is why it is selected for the state estimation approach.

The implemented battery model is based on an ECM with two RC circuits. The references are taken from the cylindrical *NCR18650PD* cell made by *Panasonic* with a minimum guaranteed cell capacity of 2.75 A h. The model was originally developed for lead acid batteries by Karl [185] and was further extended and parametrized by Ni [186] for Li-Ion batteries. The aging is excluded from this approach, where instead battery parameters for new and already aged cells are used to evaluate the SOC estimators as sorting mechanisms. It is a current controlled model, where the temperature is assumed constant at 35 °C, which is sufficient for a comparing evaluation.

To simulate a whole pack or in this case a SM instead of a single cell, different approaches are possible. In a discrete model, the actual circuit of the SM is rebuilt with the individual cell models. While this gives the most accurate results, especially considering the variances, it is also intense

to compute, because the reference cell has a rather small capacity and therefore there are thousands of cells in the pack. Another option is to have a direct model of the whole SM, which is parametrized using a reference module. For this dissertation, this is not possible, as there is no physical reference module available to derive the required parameters. Therefore, a scaled model is used, which linearly scales the parameters from a single cell to a hypothetical cell in the size of a whole SM. This ensures suitable simulation efforts with an accuracy that is sufficient for a comparison of the state estimators.

For the further model description, equations are used to calculate the parameters of the SM. While the equations are universally, for numeric examples a configuration of four SM per phase is used. This is because this configuration is identified as the most suitable one in Section 4.4.1 and therefore it is used as a reference configuration. The approach to extrapolate the results for different configurations is explained in Section 3.3.3.

The specifications of the overall battery pack are matched to that of the reference vehicle. It is rated with a nominal voltage of $u_{\mathrm{pack,nom}} = 360\,\mathrm{V}$ and a capacity of $c_{\mathrm{pack}} = 60\,\mathrm{A\,h}$, which results in a nominal pack energy of 21.6 kW h. The selected modeled cell is rated with a nominal voltage of $u_{\mathrm{cell,nom}} = 3.6\,\mathrm{V}$. Since each H-bridge can switch the polarity, the voltage reference point is half of the pack voltage. The total number of series connected cells per phase can be calculated as shown in Eq. (3.11):

$$m = \left\lceil \frac{u_{\mathrm{pack,nom}}}{2u_{\mathrm{cell,nom}}} \right\rceil. \tag{3.11}$$

Therefore, each phase leg of the CHB battery has to provide 180 V, which corresponds 50 cells in series per leg. The amounts of SM per phase leg now can vary between 1 and 50 depending on the size of the SM, and is selected as four as explained earlier. The amount of cells in series per SM can be calculated as shown in Eq. (3.12):

$$m_{\mathrm{SM}} = \left\lceil \frac{u_{\mathrm{pack,nom}}}{2Nu_{\mathrm{cell,nom}}} \right\rceil, \tag{3.12}$$

with N being the amount of SM per phase leg. In the mentioned example of four SM, it results in 13 cells in series in all 12 SM with a nominal module voltage of 46.8 V. The number of parallel cells per module n_{SM} is calculated in a way that the overall pack energy is equal to the reference vehicle, and is calculated as shown in Eq. (3.13):

$$n_{\mathrm{SM}} = \left\lceil \frac{2E_{\mathrm{pack}}}{3c_{\mathrm{cell}}u_{\mathrm{pack,nom}}} \right\rceil. \tag{3.13}$$

With a minimum cell capacity of 2.75 A h for the modeled cell, this results in 15 cells in parallel in each SM. Due to the ceiling functions, the derived pack has a higher capacity than the pack of the reference vehicle. However, if a DOD of 0.85 is assumed with an end of discharge voltage of 3 V and an end of charge voltage of 4 V, the CHB pack can store 19.1 kW h compared to the 18.8 kW h of the *BMW i3*.

To parametrize a scaled model of a SM, the variations have to be included as well. The inversion method is used to generate the parameters for each individual cell for each SM using distributions from literature mentioned in Section 3.1.3 [133, Ch. 2]. These cells are then randomly combined to SM. A $n\mathrm{p}ms$ configuration is used for the sub modules to avoid an increased number of BMS, as each string requires an own unit. There is no matching used, since it is not clear,

to which extend a battery pack assembler has the ability to perform that. With matched cells within a SM, an even greater utilization would be possible, as the homogeneity within the SM could be increased. No defect cells or outliers are included either, as the real rate and the ability to avoid them during manufacturing is not clear as well. To define an approximation of the scaled capacity of the SM, the smallest parallel branch has to be found, as it will limit the usable capacity as shown in Eq. (3.14):

$$c_{\mathrm{SM}} = \min_{l=1\ldots m} \sum_{j=1}^{n} c_{\mathrm{cell},l,j} \,. \tag{3.14}$$

Each SM is considered to have its own BMS, which monitors the states and stops the discharging of the module once its smallest parallel string is considered empty. It is also considered that the BMS passively balances the SOC within the SM at the end of each charging cycle, as it is realized in current conventional packs. The real minimum capacity value for a parallel string would be even lower due to self-balancing currents between cells in parallel, their resulting coulombic efficiency losses, the balancing losses, and additionally SOC variations as indicated with Eq. (3.1). However, the effects on the SM capacity are considered too insignificant to be included. To define the total inner resistance of the scaled SM, the individual resistances are combined according to their interconnection, as shown in Eq. (3.15):

$$r_{\mathrm{SM}} = \sum_{l=1}^{m} \frac{1}{\sum_{j=1}^{n} \frac{1}{r_{\mathrm{cell},j,l}}} \,. \tag{3.15}$$

For the remaining parameters of the ECM model, there are no variations available and therefore they are the same for each SM. With this equations and the evaluation of existing battery tolerances from Subchapter 3.1, two battery variation sets are generated: a new and an aged version. These two sets are then used in the battery model to simulate the pack behavior including the individual SM.

State Estimators

The selected three different state estimators are implemented in the simulation environment and used for a battery cycle simulation, so that they can be compared to a theoretical sorting. A short description shall be given here about the implementation of each.

Closed-Circuit Voltage Comparison

The CCV method measures the SM voltages directly and compares them to generate the current priority list. The voltage measurement is conducted during the zero crossing of the motor current to minimize the influences of the over-voltages. To reduce the distortion impacts on the OCV estimation further, an infinite impulse response (IIR) single pole digital low-pass filter is used, as shown in Eq. (3.16):

$$u_{\mathrm{SM}} = u_{\mathrm{SM,sense}} + e^{-\frac{T_{\mathrm{s}}}{\tau}} \left(u_{\mathrm{SM}-1} - u_{\mathrm{SM,sense}} \right), \tag{3.16}$$

where u_{SM} is the filtered voltage of the SM, $u_{\mathrm{SM,sense}}$ is the measured sensor input, T_{s} is the sample time and τ is the desired smoothing time constant [187, pp. 322–326]. The time constant is selected as 0.5 s. After each measurement, the new priority list is calculated and after the next

zero-crossing of the motor voltage applied to the SM. Since the performance of the CCV method was found insufficient during times where all four SM are active, the CCV method was modified in a way that theoretical sorting was used during these periods.

Pseudo-OCV

The implementation of the Pseudo-OCV method follows the principles of the CCV method with the difference that there is a waiting period, before the measurement is conducted. For the implementation, only one SM is measured, even if more SM are inactive at that time. Once the waiting period is over, the measured voltage is used to generate an updated priority list. The selection of the next measured SM follows the priority list as well, where the SM with the lowest priority is selected, unless it was not active in the previous cycle, as its states would not have changed in that case. If all SM have been active during one waiting period, the measurement is discarded, and theoretical sorting is used instead to avoid further unbalancing. The waiting time is a variable of interest, which is changed in order to find an optimum. It has to be sufficiently long to get measurements representing the OCV better, but a duration too long would result in the measurement being interrupted too often.

Luenberger Observer

The selected algorithm for this dissertation is based on [172], which requires the measurement of voltage and current for each SM as an input. As a first step, coulomb counting is conducted by integrating the current to obtain an open-loop prediction of the SM SOC with a sampling rate of 100 ms. The obtained SOC values are converted to OCV values using a SOC-OCV relationship function, which in this case is implemented as an interpolation of values from a lookup table. An ECM calculates the over-voltages with the measured current as an input, which are added to the calculated OCV. With the SM voltage calculated in this way and the real SM voltage, an error can be calculated, which is used to obtain the modeled SOC estimation using the coulomb counted SOC, as it is shown in Eq. (3.17):

$$SOC_{\mathrm{SM}} = SOC_{\mathrm{SM|SM-1}} + k_{\mathrm{B}}\left(u_{\mathrm{SM}} - \left(OCV_{\mathrm{SM}} + u_{\mathrm{ECMOP,SM}}\right)\right), \tag{3.17}$$

where k_{B} is the voltage correction gain and u_{ECMOP} is the calculated over potential of the ECM. A k_{B} = 0 results in a pure coulomb-counting SOC estimation including the before mentioned drifts. High values for k_{B} result in fast response to fluctuations, but include a lot noise to the final estimation. Therefore, a parameter tuning for the best results achieving k_{B} has to be conducted. An overview of the signal flow can be seen in Figure 3.9. The values of the SM SOC are directly used to generate the priority list.

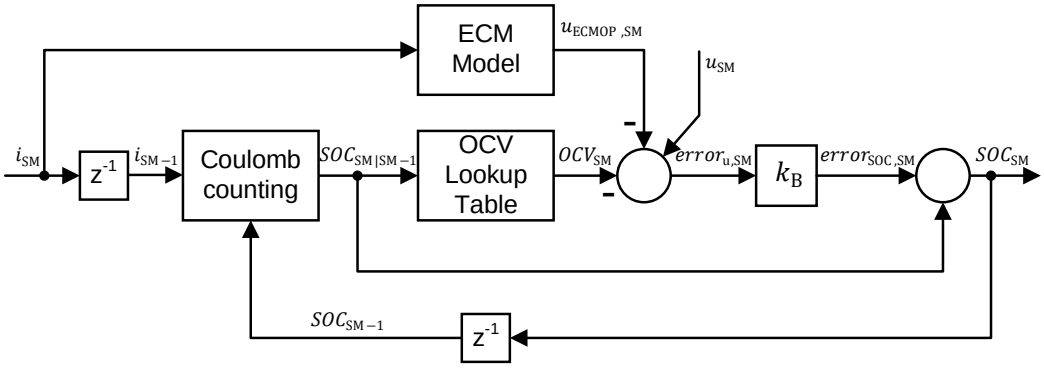

Figure 3.9: Signal flow diagram of the used Luenberger observer, adapted from [155]

A critical point of this simulation implementation is that the ECM with the same principle is used for the simulation of the cell as well as for the Luenberger observer. Therefore, the model has unrealistic high accuracies when applied to the simulation, which biases the result and opposes a comparison with the other methods. To compensate this, the parametrization of the Luenberger observer ECM is done with a different dataset, which still comes from the same battery cell type [60]. Only one RC circuit is used for the Luenberger observer ECM, which reduces the complexity and therefore the computational effort, if implemented in a commercial vehicle. Moreover, to make the simulation even more realistic, a sampling block is introduced for the measurement inputs. In this block, the voltage and the current are low-pass filtered with a time constant of 0.5 s and quantized with an interval of 10 mV and 0.5 A, respectively. Additionally, white Gaussian noise is added to the inputs to simulate imperfect measurements. However, this aspect still has to be considered critically when comparing the selected state estimators.

3.3.3 Simulation of State Estimators

To conduct the simulation, the battery pack is discharged with repeated driving cycles until it is considered fully discharged by the DOD definitions, which is selected to be 10 % SOC. Since the driving cycles are repeatedly used, it would be possible for harmonic patterns between fixed rotating schemes and driving cycles to occur. Therefore, the priority list randomly reinitializes after every 5 minutes of simulated driving.

Additionally, charging is simulated to be able to depict a whole cycle, as it would indicate the initial conditions for dis-/charging. Charging is done by a constant RMS voltage and current instead of driving cycles. Since the charging current still follows the PWM switching, this method is comparable to pulse charging. A DC charging would be possible as well, but would require additional hardware in form of an AC/DC converter like conventional charging stations, while the proposed AC charging is possible directly from the grid. Therefore, a charging power of 7.4 kW is selected, as this corresponds the three-phase 400 V grid charging possibility of the reference vehicle. The stopping condition for charging is 95 % SOC.

The simulation is implemented in *MATLAB Simulink*. To reduce the simulation time, the inverter frequency is reduced to 32 Hz instead of a variable frequency of between 0 Hz and 1 kHz. The carrier frequency is set to 3.2 kHz and the simulation step-size to 15.625 µs, which ensures ten sample points for each slope of the triangle signal. This simplification allows acceptable simulation durations, and has shorter steps compared to the time constants of relevant battery parameters. Since the results of the different methods are directly compared, the accuracy is sufficient.

The simulations are conducted with four SM per phase, representing a 9-level CHB inverter. As a reference for the comparison, a CHB inverter with a theoretical rotational sorting without any load shifting is used. The result, which is used to compare the different state estimators, is the ability to which extend it is possible to discharge/charge all the modules until their empty state. This can be determined with the remaining imbalance of charge. With this, first, the different state estimators are optimized individually by determining their best parameters, which result in the smallest imbalances. Subsequently, the methods are compared to each other and the best overall state estimator is identified.

With the preferred state estimation method found, it is then also possible to extrapolate the decrease in imbalance for other CHB inverter configurations with a different amount of SM/levels, where new-scaled SM battery parameters are calculated. According to the relative remaining

charge, the equalization potential and therefore the accessible potential of increased battery utilization can be determined. These improvements of imbalances are used in the next subchapter as an optimization input.

As a conclusion, in this subchapter, the problem of estimating the states and imbalances during vehicle operation is investigated. This is an important consideration for active battery interconnections, because only known differences can be equalized. However, it is in general not a straightforward task to estimate the states, and for the balancing, it is even more challenging due to the small variations. In this subchapter, first some potential methods known from literature are presented and evaluated regarding their suitability. The three most suitable ones are identified and then a simulation environment is described, which can be used to optimize each method and then compare them to each other to find the best fitting estimator. The results indicate the actually accessible potential of the battery, which is a required input for the configuration optimization in the following subchapter.

3.4 Optimization of the Inverter Configuration

Optimization is required to define the best configuration of the CHB inverter. This is because a too high modularization would cause additional losses due to the series connection of the submodules. However, a too small number of levels would not enable significant improvement of the limited capacity due to tolerances, as in this case still too many cells are connected in series in each SM, where the smallest cell defines the usable capacity. An additional concern is the cost of the hardware, as the amount of required components increases linearly with the number of SM. Therefore, an optimal efficient inverter might not be economically feasible. In the presented method, different configurations are systematically simulated. The cost of each configuration is assessed as well and included in the optimization. The results are sorted to identify the configuration with the highest efficiency and lowest costs.

The structure of this work package is clustered in an initial state of the art part followed by a description of the simulation model. Each part of this model is explained with a stronger focus on the costs and switch model. In the end, the evaluation is described, which defines the most efficient and economical configuration.

The content of this subchapter was developed with assistance of Ahmad [188], who contributed an initial implementation of the model including a first gathering of suitable switches. Parts of the implementation and their results are also found in a concurrent publication [189].

3.4.1 Initial Considerations for the Configuration Optimization

While the overall approach of CHB inverter is already described in literature, as mentioned in Subchapter 2.5, not too many configuration considerations can be found. Often, the only configuration consideration is depending on the actual use case, especially for grid connections, where a smooth output is required. The smallest CHB converter found only utilizes three levels [184], which results in three SM. On the other extreme, publications present CHB inverter with eleven [101], [190], twenty-one [191], [192] or even twenty-three levels [99], [193], which results in up to 33 SM. The most common configuration is the seven level/nine SM CHB inverter [31], [160], [194]–[198], which is also used in the concurrent dissertation by Chang [32]. Most publications mention that the configuration is adjustable, but indicate in their results that they worked with a

specific selection without mentioning a reason for their choice. Only one publication was found comparing different amounts of levels [199]. It concluded that a seven level/nine SM CHB inverter is the most efficient and correlated increased losses with a higher number of SM. However, the configuration within the SM was static and did not consider the system costs.

The power electronic circuit configuration within one SM mainly depends on the selected MOSFET switches. First, the selected switch has to be able to handle the applied voltage. The more levels there are in the CHB inverter, the lower the voltage per module, which results in a reduced blocking voltage requirement of the switch. Lower voltage rated switches tend to be less expensive and more efficient due to their decreased on-state resistance and switching losses. The current is independent from the amount of levels, but defined by the vehicle, motor, and driving profile. The maximum allowed current for a circuit is mainly limited by the thermal capabilities of the switch. To increase the current, either bigger switches with a higher possible current can be used, or switches can be connected in parallel to share the current. In other work, mostly a configuration is arbitrarily defined, and then a seemingly suitable switch is selected. This was also the approach in the concurrent dissertation [32].

The costs are an important input for a configuration optimization, as the most efficient solution might cause too high hardware costs, which counter-balance the possible gains from the higher efficiency and utilization. No quantitative cost considerations have been found for CHB inverters. The concurrent thesis considered the costs, but only to be able to compare the selected configuration with a conventional inverter, and not as a configuration optimization [32].

3.4.2 Approach

To be able to compare different configurations, a simulation model is developed, which can compare the efficiency in a sufficient accurate manner. The used inverter model from Section 3.3.2 is not capable of that, since it does not include efficiencies. Therefore, by reusing the vehicle model, the longitudinal simulation model of an EV is implemented, where all the involved components of a conventional electric powertrain are modelled to be able to assess the energy conversion efficiency. The required input parameters are defined to represent a specific commercially available EV as a reference to generate real world applicable results and to conduct validations. This conventional reference vehicle is then simulated to determine the overall energy consumption and efficiency. The costs for relevant parts, which would not be required in a CHB powertrain vehicle anymore, are approximated.

In the next step, this model is adapted for a CHB powertrain, where the different inverter configurations can be changed. Again, the costs for the relevant parts are approximated, and a more detailed model of the most critical components, the switches, is implemented. This allows a direct comparison between the conventional inverter and CHB inverter vehicle concerning efficiency and costs. The comparison is conducted in three different ways: either without any cost consideration to find the overall most efficient configuration, with different price ranges for the switches, or with a theoretical optimal switch. This theoretical optimal switch is an electrical component, which is not directly available on the market and for which the electrical parameters are fitted exactly to the requirements. This can be interesting, since commercially available switches always have their parameters defined with discrete levels, which sometimes might just be below the requirements for the selected configuration and therefore the next bigger one has to be selected. This could influence the costs or efficiency disproportionally.

The implemented simulation model mainly consists of three major components: the vehicle model, the inverter model, and the cost model. The vehicle model takes a driving cycle as an input and calculates the power requirement, the motor voltage, and the power factor. These inputs together with the switch parameters from the switch database are used in the variable inverter model, where different configurations can be simulated. The actual used energy for a driving cycle and the losses are forwarded from the inverter model to the cost model. Together with the selected switch and the configuration, which includes information about the possible utilization, the cost model can calculate a cost depending on which cost consideration is selected. The costs of the different configurations are sorted to create a ranking.

Wherever possible, existing sub-models or parts of simulations from previous research have been used to simplify the implementation and validation. This ensures that the results are comparable. A block diagram with the forwarded variables can be seen in Figure 3.10. The details of the relevant models are explained in the following sections.

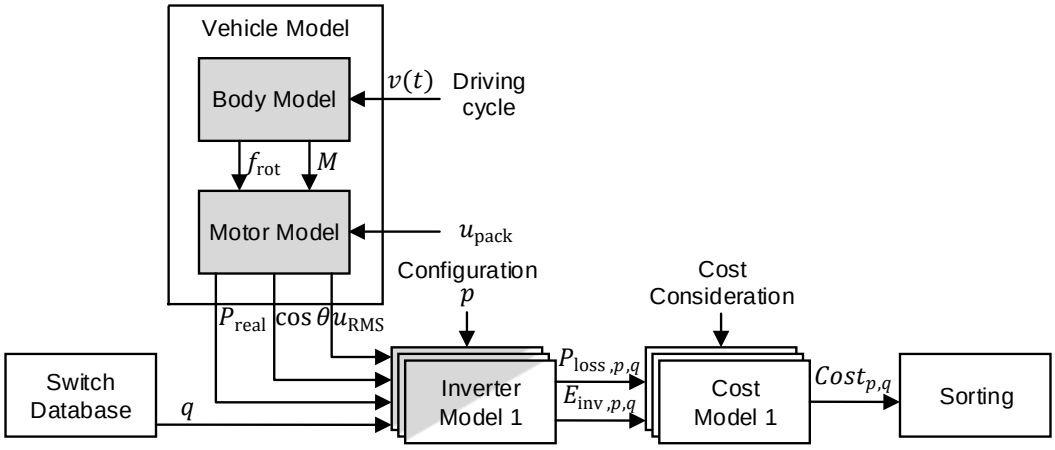

Figure 3.10: Block diagram of the simulation model indicating the sub-models and variables. Gray sub-models are based on existing models. Arrows indicate information direction.

3.4.3 Vehicle Model and Switch Database

The vehicle model consists of two main parts, the body model and the motor model, and is identical to the one used in Section 3.3.2. The same driving cycle and reference vehicle is used to ensure comparability. The other required inputs for modeling the CHB inverter are the switch parameters. For that, a database of in total 63 different MOSFET is created. The selection represents an overview of current automotive and consumer electric switches with a wide range of blocking voltages, conduction/switching losses, costs, and manufacturers. Only silicon based, discrete MOSFET switches are considered mainly because the relevant parameters are available as indicated in the concurrent dissertation [32]. Datasheets are gathered and the values of the switch parameters, which are explained in the following section, are extracted. The database consists of a detailed overview of switches from *Infineon*, complimented by examples from other manufacturers. Therefore, switches from *Infineon* are overrepresented in this database. *Infineon* was selected for this, as their published information seemed the most comprehensive. Two of the obtained parameters, the maximum current and voltage, represent absolute maximum values, where the component would be under large stress and therefore could show earlier fatigue, if operated at these values. A higher value would even destroy the component. Therefore, a derating is introduced. This is selected as 0.8 for the maximum blocking voltage and 0.75 for the

maximum current, following the IPC9592 standard [200, p. 55]. The switch database also includes the different possible switch costs, which are explained in Section 3.4.5.

3.4.4 Switch Parameters for CHB Inverter Model with Losses

With the outputs of the vehicle model and the switch database, the energy flows in the inverter can be directly calculated. The only relevant component is the actual switch in its selected configuration. Each switch is causing conduction losses and switching losses. The calculation is based on the principle described in [201], where twelve parameters, which are normally either directly available or derivable from the datasheet, are used to calculate the two losses including the consideration of the anti-paralleled diode and the reverse conduction. These twelve parameters are drain-source voltage V_{DS}, drain current I_{D}, temperature coefficient α, drain-source on resistance $R_{\mathrm{DS(on)}}$, dynamic resistance of the anti-paralleled diode R_{D}, diode on-state zero-current voltage U_{D0}, recovered charge of the anti-paralleled diode Q_{rr}, gate-drain capacitance $C_{\mathrm{GD1}} = C_{\mathrm{GD}}(U_{\mathrm{DD}})$, gate-drain capacitance $C_{\mathrm{GD2}} = C_{\mathrm{GD}}\left(R_{\mathrm{DS(on)}} I_{\mathrm{on}}\right)$, plateau voltage U_{P}, current rise-time during turn-on t_{ri}, and current fall-time during turn-off t_{fi}. A simple thermal model is included as well with a constant heatsink temperature of 30 °C to take a cooling of the inverter into account. A detailed description of the single switch simulation can be found in [32].

The individual switch simulation is then included in an inverter simulation, where all three phases are considered. The configuration depends on the selected battery parameters. With a rated battery voltage of 360 V and a rated cell voltage of 3.6 V, anything between 3 to 101 levels (corresponding to from 1 to 50 modules per phase) is possible and considered in the simulation. The maximum current is defined to be 400 A, same as in the reference vehicle. Because the maximum number of paralleled connections is not limited by the configuration, it is manually limited to 30 to reduce the simulation time, as it is also considered impractical to have too many paralleled switches.

As the parameters of the switches are retrievable from the datasheets, a simulation of all possible configurations is directly possible. The parameters of the theoretical optimal switch, however, have to be defined for each configuration individually. As there is no correlation of the twelve parameters known, first, a sensitivity analysis of the used switch model is conducted to identify those parameters, which have a significant impact on the efficiency. The maximum voltage V_{DS} and current I_{D} are directly defined by the number of series- and parallel-connected switches, and are therefore excluded from the sensitivity analysis. The remaining ten parameters are individually multiplied with a sensitivity factor starting from 0 until 2 in 0.2 steps. The base configuration used for the sensitivity analysis is the *IPT020N10N3* MOSFET from *Infineon* with three modules per phase and two parallel switches each, which is an optimum configuration within its cost category.

The result of the sensitivity analysis is shown in Figure 3.11. It is visible that the all the parameters, apart from the diode on-state zero-current voltage for small values, have a linear influence on the efficiency. A threshold of 10 % slope is defined as a relevance criterion. With that, only $R_{\mathrm{DS(on)}}$ (46.3 % slope), t_{ri} (15.9 % slope), and C_{GD2} (19.2 % slope) have a significant influence and therefore have to be considered for the theoretical optimal switch, while the other parameters remain fixed. To find the correlations of these three parameters with the maximum voltage and current, all possible combinations of the parameters for all switches in the database were investigated for interrelationships.

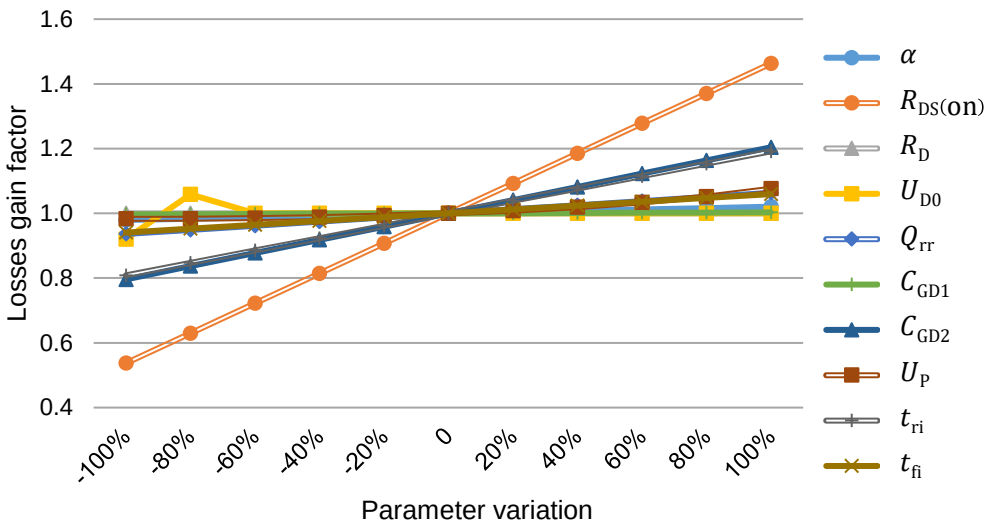

Figure 3.11: Sensitivity analysis of switch parameters and their influence on the efficiency. Adapted from [189]

The efficiency is mostly influenced by the drain-source on resistance $R_{DS(on)}$, where the losses are increased by almost 1.5, if the parameter is doubled. This is the case, because this resistance is almost solely responsible for the conduction loss. The resistance is influenced by a multitude of different conditions and compromises during the design of the switch, which cannot be directly modelled here. However, a medium linear relation with the drain-source voltage V_{DS} was found within the switch database. This can be explained with a higher breakdown voltage, which needs thicker semiconducting layers resulting in an increased resistance [67]. The coefficient of determination for this relation is in a medium range with 50.39 %, as shown in Figure 3.12.

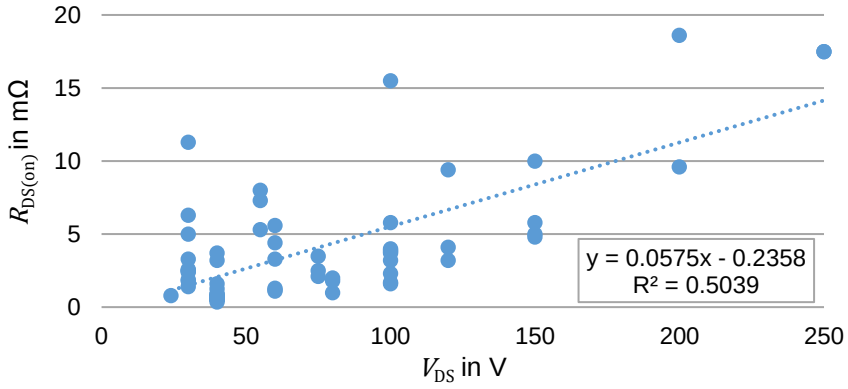

Figure 3.12: Relation between the voltage V_{DS} and the resistance $R_{DS(on)}$ of the selected switches. Adapted from [189]

The switching loss, in contrary to the conduction loss, is mainly caused by the gate-drain capacitance C_{GD2} and the current rise-time t_{ri}. In each switching cycle, a certain amount of energy is lost due to capacitive charging effects in the switch. Therefore, the switching loss majorly depends on the switching frequency. For the CHB inverter in this research a switching frequency of 20 kHz was selected as a compromise between switching losses and harmonic distortions. The switching losses depend on multiple design parameters [67], which are not directly available in the datasheets. Yet, for both parameters, linear approximations are possible with the drain current I_D. For the gate-drain capacitance C_{GD2} the approximation is shown in Figure 3.13 and

results in a medium coefficient of determination of 46.0 %. A few outlier are visible, which indicate that there are individual reasons, why parameters of specific switch models have a bad correlation to the linear approximation.

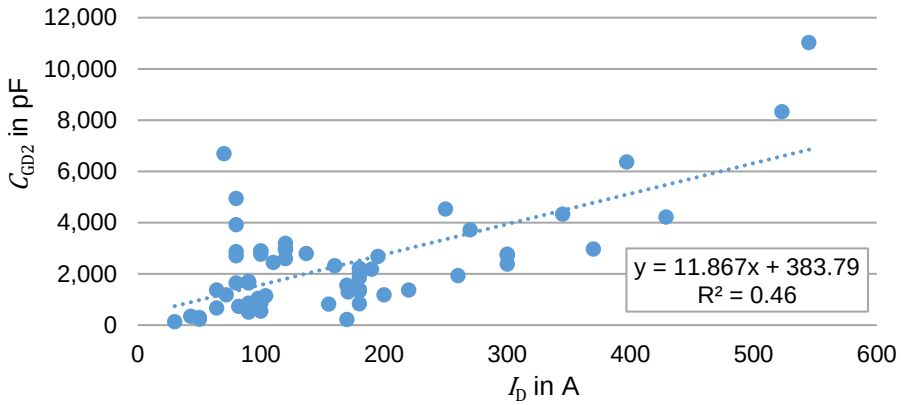

Figure 3.13: Relation between the current I_D and the capacitance C_{GD2} of the selected switches. Adapted from [189]

The current rise-time shows a rather low coefficient of determination of 29.21 %, as shown in Figure 3.14. Also no obvious outliers are visible, which indicates a general weak relation between the two parameters. However, this is still the strongest correlation found amongst all available parameters. On top of that, the sensitivity analysis indicates a rather weak influence of this parameter just above the threshold, which is why this approximation is still considered for the determination of the theoretical optimal switch.

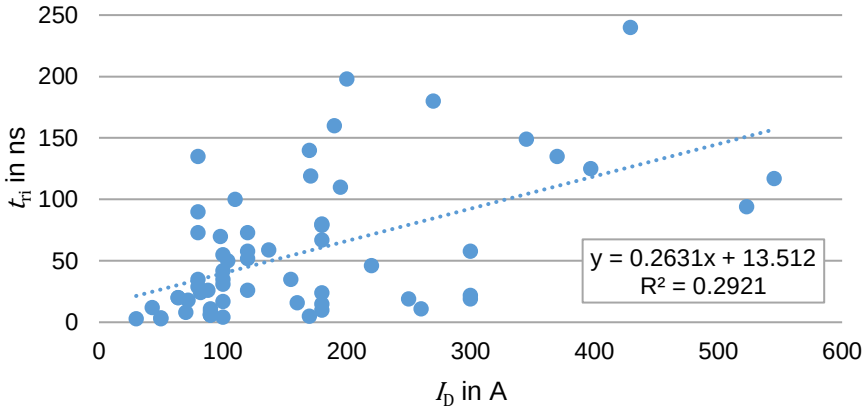

Figure 3.14: Relation between the current I_D and the capacitance C_{GD2} of the selected switches. Adapted from [189]

3.4.5 Cost Model

The costs are an important factor to consider for an optimization, if the system should be considered for a commercial implementation. First, the system has to bring a monetary benefit compared to the conventional electric powertrain system. This is already considered and shown in the concurrent dissertation, where a common, but arbitrary configuration was used [32]. For the configuration optimization, a compromise of high efficiency and economical advantage is required. The inclusion of costs in the evaluation is not trivial, as the prices of components are

not directly available. Especially original equipment manufacturer (OEM) can have special conditions due to the high purchasing volume. Prices, which are available, may include other influencing factors, for example the demand, supply, promotions, etc., which do not allow a direct comparison.

For the cost model used in this dissertation it is not the intention to determine the final cost or even price of the overall hardware and use this for the optimization. There are several additional uncertainties, for example the additional components, PCB manufacturing, enclosure, handling, etc., which could influence the accuracy of such a cost evaluation significantly. Therefore, the selected approach focuses on a comparative approach with the conventional inverter from the reference vehicle. This approach is selected, because it is considered that the overall effort to produce the powertrain will be the same with just a few components replaced. Therefore, by defining the costs for the removed and newly added components, a cost difference can be determined, which is then an input for the optimization. Additionally, not just the hardware changes are considered, as this just influences the initial purchasing price of the vehicle. Since there is a higher efficiency and utilization possible, additional savings are generated during the life cycle, which have to be included in the optimization as well. Even if the hardware costs initially increase, the lifetime savings still could compensate this and lead to a lower TCO.

The prices are identified and added to the database directly or modeled with input from the database. All prices are converted to USD as a common base currency, using the exchange rates stated in [5]. The biggest attention is put on the actual switches, since they are considered the major cost contributor of a powertrain [202], [203] and additionally they are the major elements to be replaced in a CHB inverter. Since their accurate costs cannot be confidently determined, five different approaches are used to get different cost categories, which help to get a better understanding and comparability.

“High” Cost Model

The “high” cost model uses component distributor prices. These are considered to be in the higher possible price range, since small quantities are sold with significant additional efforts on logistics and marketing. Prices can be heavily influenced by supply and demand and additional reasons. To get an overview among different distributors, a comparing service was used [204]. The price for the quantity of 1,000 pieces is used, since not all components have a further price reduction for 10,000 pieces. The highest price is selected amongst the different supplier, unless it is an outlier compared to the other distributors. This is done to avoid any special promotions or stock clearances, and to avoid any extra high prices due to low stocks or any other individual factors.

“Low” Cost Model

For the opposite, the “low” cost model, the lowest possible prices found anywhere are used. There is no restriction or quantity requirements set and the prices can be as low as only a few USD cents for smaller switches. Only assumed clickbait offers, mostly recognizable by a price indication using the smallest denomination of the used currency or by similar indicators, were not considered. Most of these low price range prices are found on various far-east e-commerce platforms. The originality, availability, or new-status cannot be confirmed for these components. Therefore, the prices have to be considered with care, but indicate a low range. It is possible that big OEM can get even lower prices than the ones indicated in the “low” cost model, but since

there is no confirmation possible, especially not for all selected switches from the database, this is not considered for the cost modeling. It is also possible that the prices are unrealistically low if they for example are sold below market value due to an insolvency or other reasons.

"Die Size" Cost Model

Both previously mentioned models might include a high independency of costs and actual specifications. Therefore, a method is required, which brings their attributes in relation with their potential costs. A promising approach is available from Burkart *et al.* [202], who linked the costs of power electronic semiconductors to the surface area of the die plus the packaging costs, as it is shown in Eq. (3.18):

$$C_{\mathrm{SC}} = C_{\mathrm{die}} + C_{\mathrm{package}} = \left(\sum_n \sigma_{\mathrm{die}(n)} A_{\mathrm{die},n} \right) + C_{\mathrm{package}}, \tag{3.18}$$

where σ_{die} is the specific price per die area A_{die} depending on the die technology and C_{package} is the package price including die integration and bonding. Burkart *et al.* did not indicate a specific price factor for Si MOSFET, so instead the 600 V Si PIN diode value (2.46 EUR/cm^2) is used, since its semiconductor structure and manufacturing process are the closest. The package price C_{package} stated in [202] only has values for rather large modules. However, a power trend line depending on the package surface area with a coefficient of determination of 99.56 % can be noticed and is therefore used to extrapolate the packaging costs for smaller modules with the surface area from the datasheets. This model is named "die size" cost model.

A problem for this model is that normally the die dimensions are not stated in the datasheet, as it is an irrelevant parameter for normal applications. For 21 MOSFET switches from *Infineon* the die surface area was mentioned in the corresponding bare die datasheets. For seven more switches, which were considered most relevant, the surface area was measured from purchased and opened samples, as shown in Figure 3.15. However, it was not possible to acquire samples for all the switches in the database and therefore this model only can compare some of the selected switches.

Figure 3.15: Opened MOSFET from different manufacturers and with different electric parameters. Adapted from [189]

“Voltage-Current” Cost Model

To overcome the limitations of the “die size” cost model, a method was searched to link the costs with other, in the datasheet available, parameters. For that, the 28 switches, where the die size is known, were analyzed. The best fit with a coefficient of determination of 88.55 % and an absolute average error of 7.46 % was found between the product of the drain-to-source voltage V_{DS} multiplied with the drain current I_{D} and the die surface area, as shown in Figure 3.16.

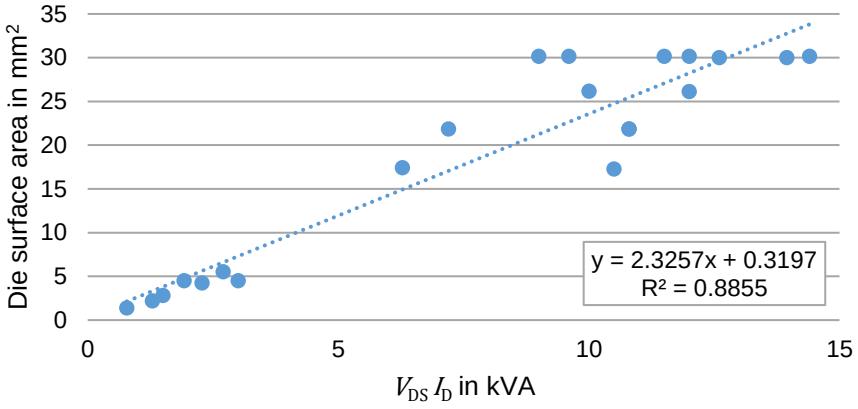

Figure 3.16: Relation between the Drain-to-Source Voltage V_{DS} multiplied with the Drain Current I_{D} and the die surface area. Adapted from [189]

Since both values are essential and therefore always available in the datasheet, it is possible to approximate the die area, which can then be used to calculate the switch cost according to [202] as mentioned in the previous subsection. The packaging costs are calculated in the same way as in the “die size” cost model. This model is named “voltage-current” cost model.

“Theoretical Optimal Switch” Cost Model

Beside of the cost models for the switches of the database, a model is required for the theoretical optimal switch. Since such a switch does not exist, no price data can be collected and a cost model is required, which brings the cost in relation to the actual parameters. The most straightforward approach is to use the relation presented for the “voltage-current” cost model, where a relation between the product of drain current and drain source voltage, and the die size is indicated. It is assumed that the other parameters of the switch do not influence the cost significantly. With the die size and Eq. (3.18), a cost for the semiconductor of the switch can be determined. The packaging costs cannot be derived from the switch database, as no trends are visible. This is because the packaging rather follows manufacturing concerns, soldering/mounting requirements, and cooling necessities than the electrical parameters. No relation is also indicated in Figure 3.15, where identical packages have different die sizes. Therefore, the packaging for the theoretical optimal switch is defined to be bigger than the die, so that the semiconductor is safely capsuled. Within the switch database with available die sizes, package-to-die ratios of 3 % to 44 % with an average of 20 % can be found. The highest value of 44 % is considered for the theoretical optimal switch, as it indicates its feasibility for a commercial switch and follows the idea of an optimal fitted component. Additionally, the switch from the database with this ratio is rated with V_{DS} = 250 V, which indicates that the voltage rating is not limiting such a package ratio. Higher ratios of 80 % using a *DirectFET* packaging [205] and even up to 100 % using a chip

scale packaging (CSP) [206] would be possible as well. However, they are not considered, because this would make the results not directly comparable to the other cost models based on the switch database, as no switch within it is using such a technology. The presented approach is labelled as “theoretical optimal switch” cost model.

The possible switch costs models are summarized in Figure 3.17 to give an overview over the possible cost ranges. All values besides of the “theoretical optimal switch” cost model are from the database. For the “theoretical optimal switch” cost model, the costs are gathered from all considered configurations, as the values in general can adapt to any values depending on the configuration of the CHB inverter.

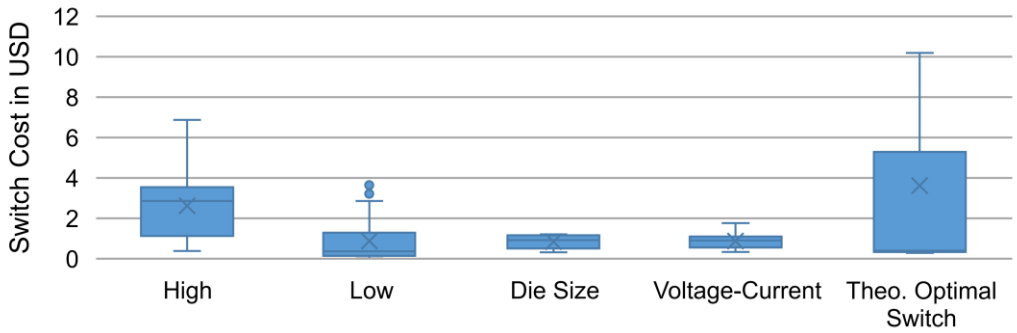

Figure 3.17: Summary of possible switch costs depending on the switch cost model

Other Components

Some other components beside of the switches would be different in a CHB inverter compared to a conventional IGBT inverter. They are considered as well and described here individually. Online distributor price comparisons are used similar to the “high cost” model with the difference that here overall lowest prices independent from any quantity requirements are selected excluding unrealistic false advertisement and rounded down to two decimal places [204]. To ensure the comparability, the same components and costs are used for both this work and the concurrent dissertation [32].

A challenge for CHB inverters is that each SM is connected in series. Therefore, no reference ground is possible, as this would short-circuit the SM. To solve this, each SM needs its own isolated power supply. This can be implemented with separated isolated DC/DC converters. The ±15 V DC power supply *MEA1D0515DC* from *Murata* is selected and a cost of USD 4.5 is estimated. Each SM needs one of them. Furthermore, the MOSFET switches need a driver, which can source and sink the controlling current to enable a fast switching, which reduces the switching losses. The *1ED020I12-F2* from *Infineon* is selected with a cost estimation of USD 2. Each SM needs four of them.

The controlling effort is assumed to be increased, since a high speed, isolated communication is required between the modules. This is especially necessary for the required alignment of the signals shown in Section 3.2.5. To be on the safe side, an additional cost of USD 150 is assumed to implement such enhanced communication.

Despite the high efficiency of the MOSFET switches, there is still a cooling system considered. A liquid cooling system is assumed for both the conventional and the novel inverter, so that the costs are equaled out. However, since the power electronics are more distributed in the CHB

inverter, an additional USD 0.45 is assumed for each SM [202]. This is a worst case scenario for the CHB and could be improved with integrated design of the module cooling [32, Ch. 8.3.2].

With the implementation of the CHB inverter, several components of the conventional powertrain are not necessary anymore. The most costly components are the IGBT switches. With the “die size” cost model based on [202] and the die size found in [207], the costs can be derived as USD 296.61. In addition, the IGBT switches require a driver to enable fast switching. The same drivers as for the MOSFET are considered, but with a reduced and fixed quantity of six units. Other components, which are not required in the CHB inverter anymore, are the input filter capacitors. The size is given for the reference vehicle [207] and can be calculated with the model stated in [202]. It results in a cost of USD 30.30.

The last components, which are different with the new powertrain, are the contactors for the battery pack in the reference vehicle. These contactors are a safety requirement, since the battery voltage is higher than the defined DC safety voltage of 60 V [58]. Therefore, each pole of the pack is equipped with a HV contactor, so that the pack can be potential-free once it is disabled either for standby or due to emergency reasons. Within the pack, however, the HV is still prevalent and still poses a safety risk especially for accident situations, where the integrity of the pack is damaged. With a CHB inverter, these contactors are not considered as required anymore. Firstly, this is because the batteries within the individual SM are potential free, once the switches are disabled, which is intrinsic the case once the controller is switched off. The MOSFET therefore work in a comparable way as dual solid-state contactors for each SM. Secondly, for most SM configurations, the SM voltage is below 60 V and therefore considered safe to handle anyways. Consequently, the CHB inverter can be considered safer while the hardware cost for the contactors can be omitted. This cost is assumed as USD 37 for each contactor.

Finally, the manufacturing overhead needs to be considered for both the removed and added costs. This is for the logistics and actual handling of the manufacturing and comes as a multiplying factor for the costs. For this work it is taken as 1.25 for power electronics converter production according to [203].

In total, the cost difference between the conventional IGBT inverter and the novel CHB inverter can be calculated with Eq. (3.19):

$$\Delta C_{\mathrm{components}} = \Sigma C_{\mathrm{IGBT}} + C_{\mathrm{contactors}} - \Sigma C_{\mathrm{CHB}}, \tag{3.19}$$

where ΣC_{IGBT} is the sum of all relevant costs of the IGBT inverter, $C_{\mathrm{contactors}}$ is the costs for both contactors and ΣC_{CHB} is the sum of all relevant costs for a CHB inverter including the switches. ΣC_{IGBT} is taken with USD 666.5 in this dissertation, and ΣC_{CHB} depends on the configuration and is calculated newly in each iteration.

Battery Costs

Beside of the different component costs of the inverter, there is an additional factor for the overall initial vehicle costs, if the powertrain is adapted from a conventional form to the proposed CHB inverter. Because of the higher efficiency and increased utilization of a CHB inverter driven vehicle, more of the energy stored in the battery is used for propulsion and therefore the car can drive further with the same battery capacity. Such a non-monetary benefit makes the powertrains hard to compare. Therefore, it is assumed that the range remains the same, which allows for a smaller battery pack with a more efficient and higher utilized powertrain. This reduced capacity

has a direct cost associated and therefore reduces the initial costs, which is used as an optimization factor. A smaller battery would have additional benefits such as reduced weight and volume and improved environmental impact, but they are not considered here, as they are not simply convertible into monetary benefits. Especially the battery weight would have an iterative benefit for the efficiency of the vehicle. However, as the results will show, it has an impact of around 1 % on the overall vehicle weight and is therefore considered insignificant to be incorporated. Additionally, it has to be considered that such a capacity reduction might not be feasible, since the cells are only available in discrete sizes. However, it allows a comparative optimization. The cost difference ΔC_{pack} can be calculated with Eq. (3.20):

$$\Delta C_{\mathrm{pack}} = \left((E_{\mathrm{Loss,IGBT}} - E_{\mathrm{Loss,CHB}}) R + \frac{ap_{\mathrm{c}} c_{\mathrm{pack}} u_{\mathrm{pack,nom}}}{1 + ap_{\mathrm{c}}} \right) C_{\mathrm{relBat}}, \tag{3.20}$$

where E_{Loss} is the average energy loss for the respective inverters, R is the range requirement, ap_{c} is the accessible potential capacity derived with the model from Section 3.3.3 and C_{relBat} is the cost per kWh for the battery on pack level. The loss of the IGBT inverter of the reference vehicle is calculated with IGBT inverter model as 1.22 kWh/100 km with the WLTP driving cycle. The loss of the CHB inverter depends on the CHB configuration. The range of the reference vehicle affects this cost calculation linearly, and is freely adaptable. It indicates that for vehicles with larger batteries, a different configuration can be a better option, since a larger saving on the battery costs is possible. For the calculations of the results (Subchapter 4.4), a range of 300 km is used as it is the official declaration of the reference vehicle [208] and such a magnitude of range is also supported by the desired daily range of the customers, even though the actual demand is lower [17]. The accessible potential capacity is the additional charge that can be utilized depending on the maximum usable potential p_{c} and the utilization factor, which depends on the quality of the state estimator and the control strategy, as it is shown in Subchapter 4.3. The battery cost is considered with USD 164.28 per kWh for Lithium based 18650 battery packs cells [5, Sec. 2017].

Energy Costs

An additional monetary difference besides of the initial costs are the changed energy costs due to the altered efficiency. Over the lifetime of the vehicle, the total accumulated costs for energy are therefore different. Such a total cost of ownership (TCO) consideration can enable a configuration with a higher initial cost, but with a lower operational cost that compensates the increased initial cost, if the increased efficiency compensates the more complex configuration. The running cost difference can be calculated with the average energy consumption difference multiplied with the costs for electricity and the estimated lifetime driven distance as shown in Eq. (3.21):

$$\Delta C_{\mathrm{Energy}} = \left(E_{\mathrm{Consum,IGBT}} - E_{\mathrm{Consum,CHB}} \right) D C_{\mathrm{relEnergy}}, \tag{3.21}$$

where E_{Consum} is the average energy consumption for the respective inverters, D the total distance driven over the lifetime and $C_{\mathrm{relEnergy}}$ the cost for the electric energy. The vehicle energy consumption can be simulated with the model, where the IGBT inverter is calculated with 13.26 kWh/100 km for the reference vehicle in the WLTP driving cycle and the CHB inverter again depends on the configuration. The total distance driven over the lifetime defines the range until the vehicle is damaged and aged at a stage, where it is not worth to repair it anymore. For BEV, often the battery is the limiting factor since here the aging is the fastest and a replacement might not be economical [5]. The value depends on several external factors, such as climate,

charging/driving behaviour, etc., so only an approximation is possible. The reference vehicle comes with a warranty of 100,000 miles (=160,934.4 km) [209], which can be considered a minimum value. However, it is not realistic, as multiple commercial BEV already have proven a higher possible mileage. Current research suggest that even up to 1 million miles of total lifetime can be possible [209]. For the reference vehicle, *Samsung SDI* 94 Ah cells are used [210]. In its datasheet a cycle life of at least 3,200, but up to 4,600 cycles is stated to reach an EOL of 80 % [211]. The lower value of 3,200 cycles is used for this dissertation, which results in a total driven distance of 960,000 km until end of life of the battery. The cost for the electric energy depends on external factors, for example availability of resources, political influence, incentives, etc., and therefore can vary a lot amongst different countries and regions. For this dissertation, the Germany 2015 price of USD 0.26 per kWh is selected [5]. It represents a rather high price compared to other countries, but as a high developed country without much access to own natural resources and a high share of renewable energy, the price is considered to include low incentives and can be seen as a future indicator for energy costs in other countries as well.

3.4.6 Cost Evaluation

The three mentioned possible cost differences can be summarized to an overall possible saving as shown in Eq. (3.22):

$$C_{\mathrm{saving}} = \Delta C_{\mathrm{components}} + \Delta C_{\mathrm{pack}} + \Delta C_{\mathrm{Energy}}. \tag{3.22}$$

It has to be mentioned that some of the three cost differences can be negative, especially for the components, but still represent an optimum for the overall savings. The optimal configuration for the CHB inverter is found by sweeping the configuration parameters within their possible limits and calculating the individual overall savings. These savings are then sorted and the highest cost saving indicates the best configuration. With the set of 63 switches in the database, from one to 50 modules per phase and from one to 30 parallel MOSFET for each switch, 94,500 possible configurations are evaluated. These include the most commonly mentioned seven-level configuration from Section 3.4.1 with single MOSFET per switch as well as the selected configuration from the concurrent thesis [32] with six paralleled MOSFET. For the evaluation, the best 100 configurations are considered for each switch cost model. Taking only the best or just a few best configurations could result in selecting outliers, which are caused by a specific interaction of components or outliers in the cost models due to unrealistic switch price selections. The combinations considered also include scenarios, when the overall savings are negative or when the configuration results in an invalid combination.

The comparison to investigate the influence of the switch costs is conducted separately in three ways: either without cost consideration, with the best switch selected from the database, or with the theoretical optimal switch model. Alternatively, the range requirement and the energy costs are varied to highlight the sensitivity of the model towards these parameters.

As a conclusion, in this subchapter, the method is described which is used to find the optimal CHB inverter configuration. As optimization factors the efficiency and the costs of the system, both for initial and running costs, are considered. A switch database is created including switch costs following five different cost models. Additionally to the switches from the database, the theoretical optimal switch model is introduced, which requires a more thorough examination of the switch parameters to be able to simulate exactly fitting switches in each SM configuration and to derive its potential costs. For the overall powertrain, not the total cost, but just the cost

difference compared to a conventional electric powertrain is calculated to avoid having to derive hard to determine costs of components and manufacturing. Finally, it is described how the simulation can be conducted to simulate all possible configurations and sort the results to find the optimal ones. The results indicate the best possible configuration and quantifies the actual capacity gain of the battery, cost, and efficiency of the proposed system.

As an overall conclusion of the methodology, it can be stated that the proposed separation of problem into four subchapters enables a clear structuring of the required tasks, which outcomes in the end lead to identify the potential benefit and to evaluate the fulfilment of the stated working hypothesis. For that, first, with an extensive compilation of battery research, the magnitude of the cell variation problem can be outlined. In a next step, ways are shown how the CHB inverter can be controlled to access the unutilized capacities. To do so, a measurement of the states during operation is required, which is defined in the next step. Finally, the best configuration and therefore the magnitude of the improvement can be simulated. The detailed descriptions of the implementations for the simulations and tasks define the bottom of the V-Model used to describe the structure of this dissertation. This is therefore the end of the decomposition, where from now on a re-composition is required to be able to answer the questions of this research in an ascending way, starting with low-level details until in the end the overall research question can be answered.

4 Results

In this chapter, as a first low-level re-composition working package of the V-Model, the results of the four different Methodology Subchapters are presented. It does not strictly follow the four individual steps indicated in the previous chapter, since some results are gained from iterative loops and are the output of several combined methods. However, it is still based on the same logic.

First, statistical results of the battery tolerances obtained from the battery dataset are presented and summarized to highlight the maximum usable potential of increased battery utilization clearly. This data is also used to parametrize the simulated battery packs and SM. In the next part, results from the control strategy and state estimation optimization are shown to indicate, which approach for each task should be selected and which parameters indicate the best performance and therefore should be used to configure the subsequent simulations. With the optimized simulation system defined, the utilization simulation can be conducted, which results in the determination of the accessible potential for all investigated configurations. In the next subchapter, the results of the configuration optimization are presented, depending on the various inputs of different cost models, cost factors inclusion, and other variables. A finalizing subchapter is summarizing the gained results, shows the actual best configurations, and indicates to which extend the proposed active interconnection fulfills the working hypothesis.

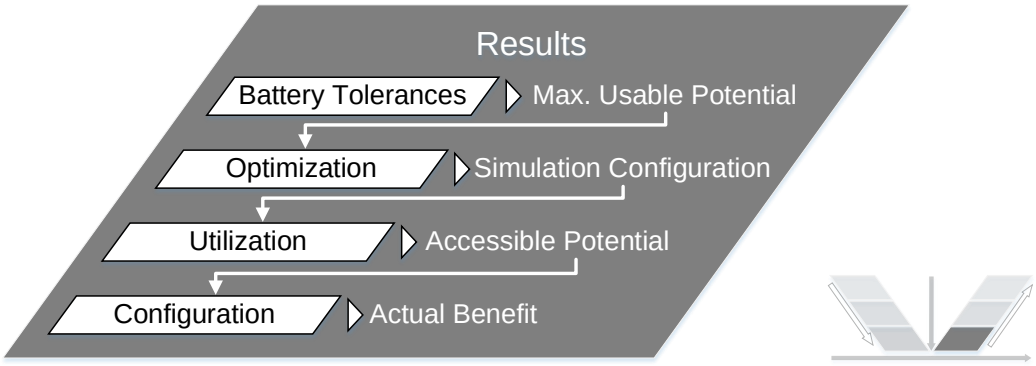

Figure 4.1: Structure of Chapter 4

4.1 Results of Battery Tolerances Potential

The first Results subchapter gives a statistical evaluation of the cell tolerance dataset created in Subchapter 3.1, which allows deriving several relevant aspects regarding the currently unused potential in conventional BEV. A special focus is put on the investigation of potential dependencies for different cell parameters, as this could give some recommendations regarding the selection of cells. Additionally, the results from analyzing the dataset are used to parametrize the reference cell, SM, and pack simulations, which are required for the subsequent simulations.

4.1.1 Capacity Tolerance

For the capacity, it was noted from the available data that state of inhomogeneity of the capacity SOI_c and relative spread sp_c are almost the same with an R-square value of 98 %. The coefficient of variance CV_c is correlating linearly with both SOI_c and maximum spread with an R-square value of 79 %. In addition, the maximum usable potential p_c has a linear correlation with the CV_c with an R-square value of 74 %. Therefore, it is considered that these parameters can be used interchangeably. Following observations are conducted with a focus on the maximum usable potential, as this value provides a direct input for the potentially increased utilization.

In total, an average CV_c of 1.22 % is found with 1.03 % on average for new cell sets and 1.91 % for aged cell sets, as shown in Figure 4.2a). The average relative spread is 5.61 % and the average SOI_c is 5.16 %. The maximum usable potential varies between minimum 0.27 %, maximum 9.85 %, and on average 2.87 % with a new average of 2.30 % and an aged average of 5.28 %.

There is no correlation noticeable between the variations and the year the data was generated, which is assumed to indicate the age of the cell technology approximately. There is no trend regarding the cell packaging compared to the capacity variations, either. In addition, the theory of a correlation between the nominal capacity and therefore the cell size and the coefficient of variation is also not valid within the dataset, as shown in Figure 4.2b). The packaging data is limited as there are only three prismatic and pouch data sets available. Regarding the different chemistries, some influence is seen on the CV_c, as shown in Figure 4.2c). However, the sample size is small for LCO and even smaller for LMO, and the LFP values are influenced by one strong outlier. For new cell sets, the mean capacity is up to 10 % lower than the nominal capacity and on average 1.1 % lower. Nevertheless, eight out of 19 data sets of new cells have a higher mean capacity then their nominal value.

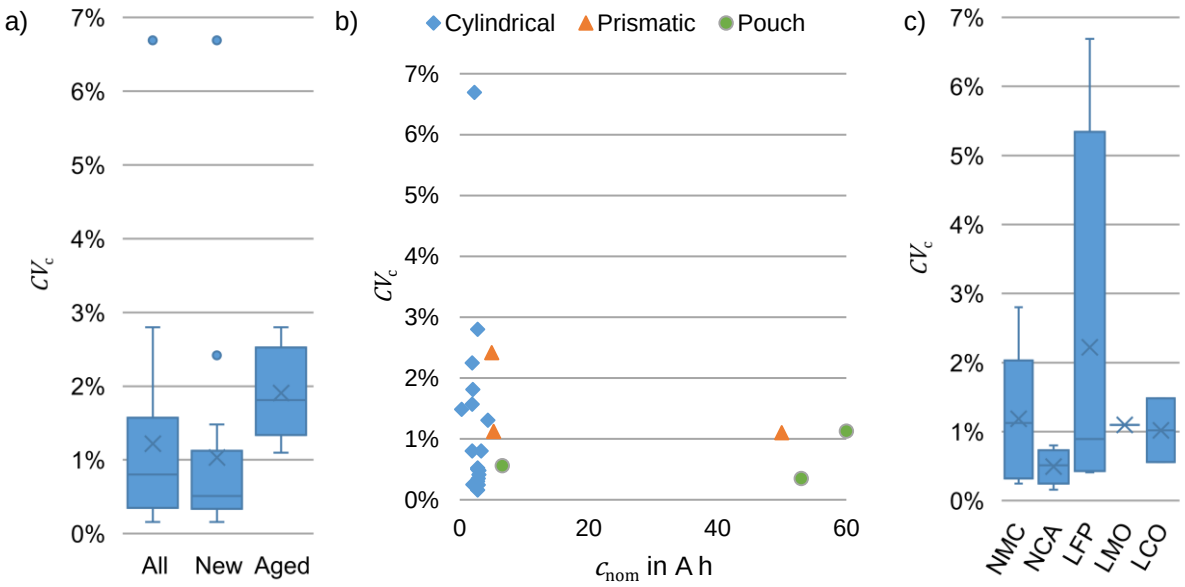

Figure 4.2: Statistical representation of a) CV_c distribution of all, new, and aged cell sets, b) relation of nominal capacity with CV_c, c) CV_c distribution depending on the cell chemistry

The skewness indicates a preselection of the new cells, as for eleven out of 17 sets the capacity distributions are right skewed. For aged cells, three out of four sets are considered left skewed, as their skewness is negative. This indicates that a few cells are aging disproportional faster than

others, causing the skewness to invert. Because of this, the maximum usable potential p_c is increasing with the age of the pack. It also highlights that a pack is aging faster than the individual cells due to a few outliers. A calendric aging during storage could explain the few left skewed "new" cell sets. There is no correlation between the skewness s_c and the CV_c. The kurtoses of the parameters show a similar behavior with 14 out of 17 new cell sets showing a k_c value below three, while for aged cell sets, two out of four are above three. This indicates the correctness of the theory that new cells are preselected with outliers removed, while for aged cells, new outliers become prevalent. Again, there is no correlation between the kurtosis k_c and the CV_c noticeable.

4.1.2 Internal Resistance Tolerance

For the internal resistance/impedance results, it first must be highlighted that the measurement methods vary even more than the capacity measurements. However, it is also evident that the tolerances of the resistance are much more severe compared to the capacity variations. The CV_r reaches from 0.7 % to 25.9 % with an average of 5.0 %, where the average of new cell sets is 5.3 % and of aged cell sets is 3.8 %, as shown in Figure 4.3a). It again can be seen that relative maximum spread, SOI_r and CV_r are correlating with high R-square values of above 90 % and therefore again these parameters can be used interchangeably. The average total relative spread is 18.9 % and the average total SOI_r is 18.8 %.

A weak correlation of 24.7 % between capacity variation CV_c and resistance variation CV_r can be seen in Figure 4.3b). This indicates that manufacturing tolerances affect both parameters, but not mandatorily with the same impact. The year of publication, which indicates the year of manufacturing for the cells, has no influence on the resistance variation. For packaging and chemistry analysis, the data is too limited, since not all data sets contain resistance data. The skewness s_r is for 13 out of 16 cell sets right skewed, again with the aged data too small to draw conclusions. It indicates random outliers from the manufacturing requirements, which seem to get worse over the cell life time as indicated by Schuster *et al.* [25]. The kurtosis data shows no trend and no correlation for the internal resistances.

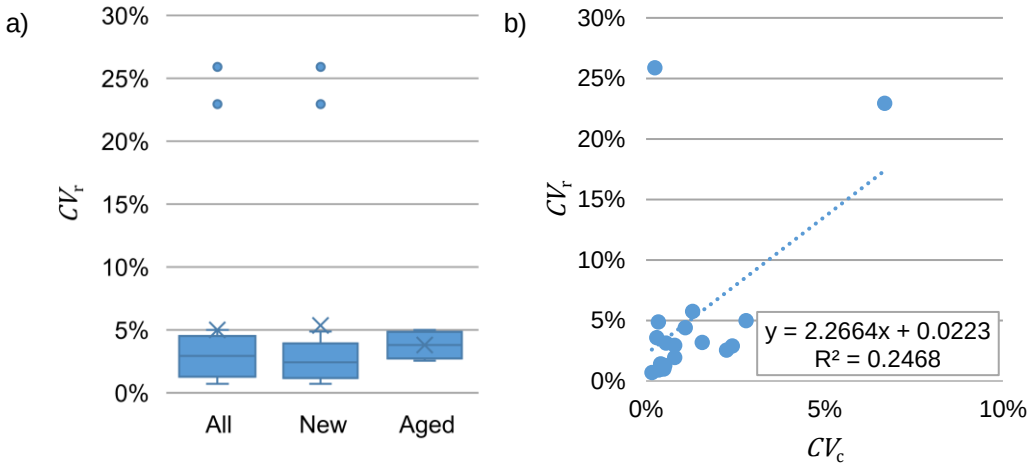

Figure 4.3: Statistical representation of a) CV_r distribution of all, new, and aged cells, b) correlation of CV_c with CV_r.

4.1.3 Summarizing Battery Tolerances

In general, a wide variation of tolerances is noticeable. Expected correlations between tolerances and other features of the cells are limited. A detailed overview of the attributes of all the key parameters with a separation of new and aged cells is shown in Appendix A, Table A.1.

An interesting and relevant aspect for this dissertation, the price of the different cells, is not taken into account in literature and therefore is not considered for this evaluation. It is assumed that lower priced cells without branding might have bigger tolerances. Even within a cell type, the manufacturers are conducting a preselection, which is highlighted by Baumhoefer *et al.* [30] with the usage of “C-grade” cells indicating there are at least three different quality levels available for that cell type. Such selections within a distribution, also visible with the right-skewness of new cells, additionally indicates that certain cells might be discarded if they do not fulfill the basic requirements. The costs of these rejects will increase the price of the sold batteries.

Another noticeable aspect is that in most examined data sets the mentioned sample size and the visible sample size are different. From the cells, which were evaluated by own measurements, it was noticed that certain individual cells indicate an unusable behavior. Some had far too small capacity/high resistance or a fast self-discharging nature. Even the effect that some cells were delivered deep discharged beyond the cutoff voltage was noticed. Such cells are removed from the pack manufacturing whenever possible and again the rejects increases the price. However, cell defects also can happen at any time during usage with effects from reduced available capacity until a total failure of the powertrain [212]. For all entries in the battery analysis, a rejection of 1.23 % is visible. Since these are the rejects from previously delivered or in packs assembled cells, it can be assumed that the overall rejection rate is even higher.

For some cell sets, a clear separation of batches is visible in the data, where groups of cells have similar properties. This increases the range of the values and is commonly tried to avoid by marking each cell individually with a (machine) readable tag. Pack manufacturers assemble battery packs by sorting the cells in certain orders using these markings combined with own additional measurements. Hereby parallel or serial matching can be applied, which both have negative effects. A preferred way is to match capacities in series to maximize the capacity utilization and to match resistances in parallel, which results in more evenly distributed currents [24].

It is shown that aging acts contrary to any efforts done during pack manufacturing to ensure a homogeneous pack, as the overall variations increase with time and usage without any clear dependency. So even by matching an initial pack and avoiding initial outliers, the parameter spread still increases over the battery lifetime.

In conclusion, the dataset shows that there is always a variation found, which is increasing during usage. It seems rather independent from cell size and used chemistry, but deteriorates over time. However, the order of magnitude of the variation is a single digit percentage. The maximum usable potential is on average only between 2.3 % and 5.3 % for new and aged cells and can be as low as 0.3 % for the best cells.

4.1.4 Cell Parametrization for the Simulation

For all the simulations, a parametrized reference CHB battery pack including realistic tolerances is required. It follows the model explained in Section 3.3.2, and the submodules are parametrized with values gathered for the dataset described in Section 3.1.3. Two sets of samples with different variations are generated: a new and an aged version.

The new cell parameter set is based on the publication of Campestrini *et al.* [135], as it is the same cell from which the ECM parameters are derived and it represents a branded, high quality cell used in automotive applications. It has to be mentioned that this is one of the best entries in the whole battery tolerances data set and therefore indicates a worst-case selection for the benefits of an increased battery utilization. However, it therefore depicts a realistic representation of the variations expected for automotive grade cells with highest requirements.

To enable a comparison and to highlight the utilization potential, first a set of individual cells is generated. No damaged cells are included, even though most sources from the battery dataset indicate their existence. However, their failure behavior is unknown and it is not clear how severe the deficiencies would be. Therefore, this effect is excluded. As the parameters of the cells are randomly generated following the statistical distribution, the set is generated 10,000 times and averaged to exclude random outlier for the reference CHB battery pack. The generated variations are shown in the Table 4.1 in the “New Cell” row and have a high similarity to the original data from Campestrini *et al.* However, they are not identical, as the sample size for the generation is much bigger than the original data sample size in the publication and the statistical features extracted from literature are just representing the values of their measurements. Based on the tolerances, the maximum usable potential of the individual cells can be calculated, which is slightly higher compared to the values from the source literature, but still one of the best compared to the whole tolerance data set.

In a next step, a conventional new pack is parametrized following the specifications of the reference vehicle and using the generated cells. To do so, 2,200 cells are randomly selected from the generated sample to form a battery pack. This pack follows a $100s22p$ configuration, and will be herein referred to as the self-generated conventional reference pack. This reference pack results in reduced variations compared to the individual cells. This is due to the connections of 22 cells in parallel, which evens out the tolerances within each parallel string. The detailed attributes of the self-generated reference pack are shown in Table 4.1 in the “New Pack” row. The maximum usable potential on pack level is reduced by around 79 % compared to the maximum usable potential of the individual cells, which roughly amounts to factor 5.

Table 4.1: Parameter attributes of reference pack with self-generated tolerances

Battery	Mean c	Min. c	Max. c	CV_c	SOI_c	sp_c	p_c
New Cell	2.88 A h	2.87 A h	2.89 A h	0.16 %	0.81 %	0.82 %	0.41 %
New Pack	63.36 A h	63.30 A h	63.42 A h	0.03 %	0.17 %	0.17 %	0.09 %
New 1*4 SM	43.17 A h	43.16 A h	43.18 A h	0.02 %	0.05 %	0.05 %	0.03 %
New 3*4 SM	43.17 A h	43.15 A h	43.18 A h	0.02 %	0.08 %	0.08 %	0.04 %
Aged Cell	1.86 A h	1.73 A h	1.99 A h	2.78 %	13.07 %	14.00 %	7.54 %
Aged Pack	40.96 A h	40.35 A h	41.58 A h	0.59 %	2.94 %	2.99 %	1.52 %
Aged 1*4 SM	27.59 A h	27.47 A h	27.70 A h	0.38 %	0.84 %	0.84 %	0.44 %
Aged 3*4 SM	27.59 A h	27.39 A h	27.76 A h	0.40 %	1.33 %	1.34 %	0.73 %

For the CHB inverter, the reference pack is formed in the same way. Variations observed on pack level depend on the configuration and in how many SM the pack is split. The attributes are therefore calculated for all possible configurations and the maximum usable potential as an example attribute is plotted in Figure 4.4. In this case, the tolerances indicate the maximum accessible potential between the SM. Within the SM, still unusable capacity remains due to variations and the static inner SM configuration. Two different calculations are made to highlight the difference of inter- and intra-phase utilization. Certain discontinuities are visible, which are caused by the ceiling function to calculate the number of cells in series per SM. The values of the scaled model parameters, which are picked for the four SM per phase configuration, as it is used to generate the following simulation model results, are shown in Table 4.2 and their attributes are indicated in Table 4.1, rows “New SM”, as well. The high number of decimal places hereby does not indicate spurious accuracy, since the numbers are generated from the distributions and the accuracy is required to highlight the small differences. A reduction of the maximum usable potential down to 6 % for intra-phase and 10 % for inter-phase utilization is visible, which roughly amounts to factor 10.

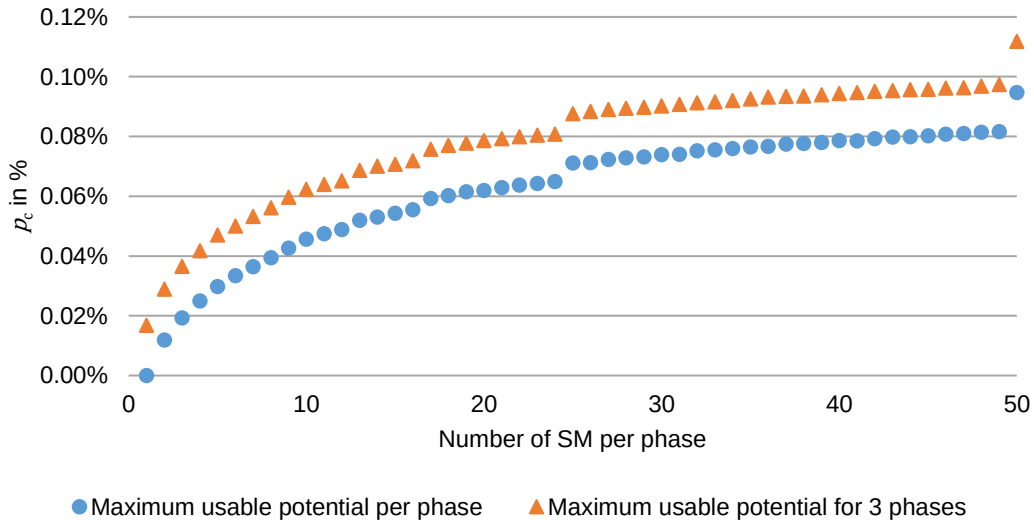

Figure 4.4: Maximum usable potential of the new, scaled battery cell model dependent on the number of SM per phase

For the aged cell parameter set, an identical approach is conducted to parametrize the reference packs. However, no ECM dataset or variation data is available for the selected reference cell. Therefore, an artificial cell is generated based on different sources. Some of the sources indicate a trend line of aged parameters compared to the number of cycles. In these cases, the value at an aging of 2,000 cycles is used [25]. The variation parameters of capacity and resistance are selected from the aged set of Devie *et al.* [124] in 2016, as the cell is similar to the reference cell. The mean value of the resistance is not directly usable since it is a different battery type. Therefore, the mean value of new cells is increased by 40 %, while keeping the coefficient of variation the same [213]. The same analysis as for the new cells is conducted, where first the tolerances between the cells are obtained, then within a conventional pack and lastly for all the possible CHB configurations. The results with a selection of four SM are included in Table 4.1 in the “Aged” rows and the exact values for further simulations are added to Table 4.2. They indicate an identical reduction of the initial high tolerances like for the new cells, once the cells are integrated in the pack or SM. However, due to the higher initial variations, higher maximum usable potential can be found in the packs. The factors of reductions remain the same as for the new cells.

Table 4.2: Defined parameter sets of SM for simulations

Parameter	SM 1	SM 2	SM 3	SM 4
$c_{\mathrm{SM,new}}$	43.1707 A h	43.1688 A h	43.1686 A h	43.1537 A h
$r_{\mathrm{SM,new}}$	18.7765 mΩ	18.7544 mΩ	18.7880 mΩ	18.8020 mΩ
$c_{\mathrm{SM,aged}}$	27.6297 A h	27.8052 A h	27.4216 A h	27.5337 A h
$r_{\mathrm{SM,aged}}$	26.1405 mΩ	26.2153 mΩ	25.9998 mΩ	26.2226 mΩ

For the remaining ECM parameters of the cells, no distribution could be found, and therefore they are equal in all SM. A factor of 1.2 is applied on the aged cell data to mimic the aging [213]. In addition, the OCV underlies some shift due to aging. An aging model was used to get the shifted relation [214].

It can be concluded that a CHB inverter may already enable a higher utilization just by the nature of the circuit, which is visible through the smaller maximum usable potential for the CHB packs compared to the conventional packs. On top of that, the remaining inequality can be made accessible by an active control of the individual SM, which is shown in the next subchapters. Nevertheless, it can be seen, that the maximum usable potential within the CHB inverter is even smaller than the already small potentials for the individual cells. The value is smaller than 0.05 % for new cells and still only less than 0.8 % for aged cells. Therefore, any active interconnection only can bring a benefit, if the circuit does not add any additional costs or losses. The control must allow regulating small amounts of energy. Moreover, the measurement of the differences must be more accurate than the actual differences to allow access.

4.2 Partial Aspects Optimization Results

This subchapter describes some intermediate optimization results from both the Control Strategy and the Module State Estimation Subchapters of the Methodology Chapter. Those results are necessary inputs to conduct the final simulations. First, intermediate results of the control strategy are presented, which focus on the aspect of the theoretical sorting. Subsequently, the state estimators are optimized individually and the results are compared to find the most suitable state estimator. The last part of this subchapter describes the charging to be able to simulate whole cycles with therefore realistic starting conditions.

4.2.1 Theoretical Sorting Results

Different rotating schemes where explored for the phase disposition PWM, when no specific sorting is applied. This is the case for the reference system, which is used as a baseline for comparison with the other sorting mechanisms. A rotating scheme is also required for the different sorting mechanisms, because there are driving scenarios, where the balancing sorting cannot be applied, but due to the nature of phase disposition PWM, a rotation must be included to avoid further external unbalancing.

Various different fixed and additional random rotation patterns were simulated. Random re-initializations where performed every 5 min of simulated driving to avoid interference of the repetitive driving cycles. The simulations were conducted with the new and the aged SM set.

Both were initialized with equal SOC, as perfectly balanced modules are assumed at the beginning. The simulation is continued until the first SM reaches its defined empty state. The investigated value for this simulation is the $\Delta SOC_{\max}$, which represents the maximum divergence between any of the SM SOC.

It was found that the rotation sequence (1-2-3-4, 1-3-2-4, etc.) does not have an impact on the $\Delta SOC_{\max}$, as long as it follows a repeating pattern and includes all SM. Only if a random pattern is applied, the results are different. As it can be seen in Figure 4.5a), which shows the $\Delta SOC_{\max}$ for the new SM, the first SM reaches its empty state after 14,171 s or 7.9 consecutive driving cycles. The variations between the SM thereby cause a maximum SOC difference of 0.035 % and 0.285 % for rotating and random sorting, respectively. It is visible that the rotating scheme performs overall much better. This is because the random scheme might select an inadequate order, which causes to increase the differences due to the phase disposition PWM.

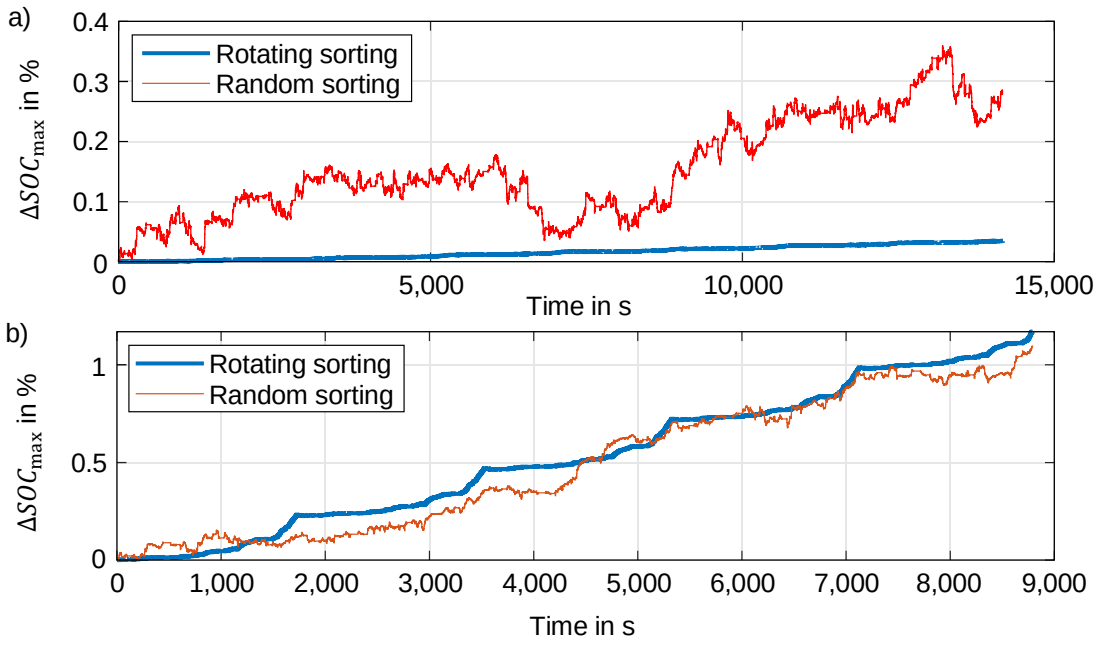

Figure 4.5: $\Delta SOC_{\max}$ plot over time during discharge until first SM is in empty state. Rotating sorting and random sorting applied for a) new modules and b) aged modules. Adapted from [155]

In Figure 4.5b), the results for the aged SM is shown. Due to the decreased capacities of the aged SM, the empty state for the first SM is reached much faster after 8,790 s or 4.9 consecutive driving cycles. The increased capacity variations also cause the maximum SOC difference to increase to 1.17 % and 1.09 % for rotating and random sorting, respectively. It can be seen that for aged modules the random sorting performs similar compared to the rotating sorting, especially towards the end of each driving cycle. However, as it is a random generation, variations in the result can be expected. Due to the indicated results, for the rest of this work, a rotating sorting scheme is used whenever a theoretical sorting is required, as the random sorting is outperformed for new SM and only equal for aged SM.

4.2.2 Pseudo-OCV Sorting Results

The Pseudo-OCV sorting significantly depends on the waiting time as described in Section 3.3.2. The in the literature given value of 3 s was based on considerations of the specific implementation [165], but since the waiting time has a negative impact on the overall pack behavior, a comparison of different values was conducted for this dissertation. Six different waiting times from 0.125 s to 4 s are simulated with the new and aged modules in the same way as in the previous section, and the $\Delta SOC_{\max}$ is observed to evaluate the different waiting times. An initial SOC spread of 3 % was set to investigate the converging capability.

An example of the results with a waiting time of 0.25 s is shown in Figure 4.6. Similar to the previous section, the discharging time for the aged modules is much shorter due to their reduced capacity. Two effects are visible: Firstly, the aged modules converge faster than the new SM. As their capacity is lower, their SOC can be equalized faster, as their relative load is higher. Secondly, after the SM reach an equilibrium, the difference is approximately four times higher for the aged SM compared to the new SM. This can be explained by increased over-voltages due to the increased impedance of aged cells and therefore slower kinetics, which cause a different fading behavior after a module is switched inactive. This results in a different optimal waiting time for the aged SM compared to the new SM.

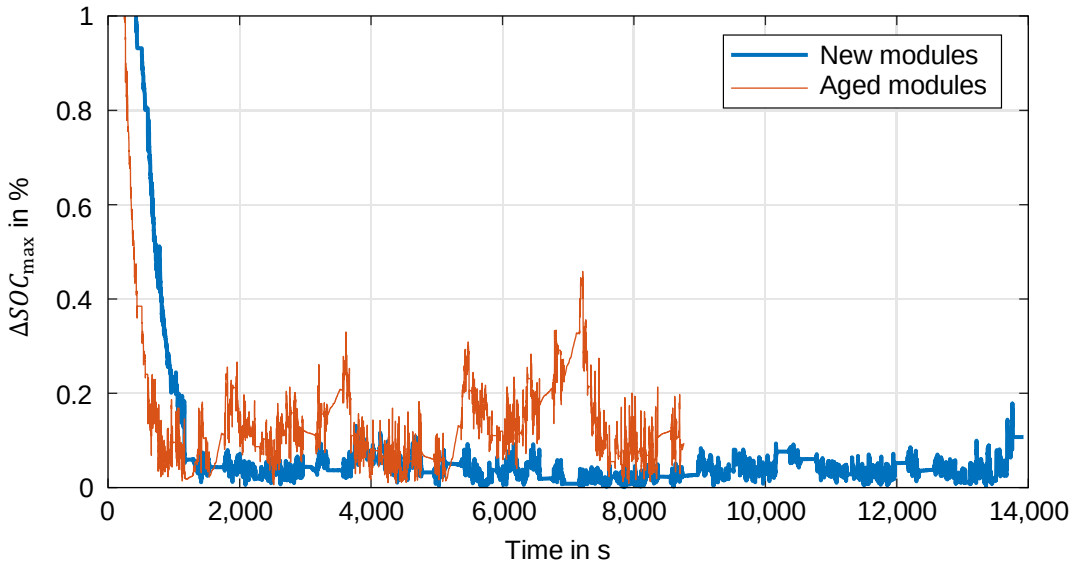

Figure 4.6: $\Delta SOC_{\max}$ plot over time during discharge until first SM is in empty state. Pseudo-OCV sorting applied with waiting time of 0.25 s for new and aged modules. Adapted from [155].

To identify the optimal waiting time, the average $\overline{\Delta SOC}_{\max}$ during the whole simulation is minimized. The average difference is chosen instead of the final $\Delta SOC_{\max}$, as it can be seen from Figure 4.6 that the actual value is fluctuating a lot depending on the stages of the driving cycle. As the simulation is continued until the first module reaches its empty state, this could happen at a time of low or high demand and therefore distort the result. In Figure 4.7 the results for all simulated waiting times are shown for new and aged SM as well as an average of both. The detailed results can be found in Appendix B, Table B.1. It is visible that for both SM, aged and new, an optimum waiting time can be found within the simulated range of waiting times, which is why no shorter or longer waiting times are considered.

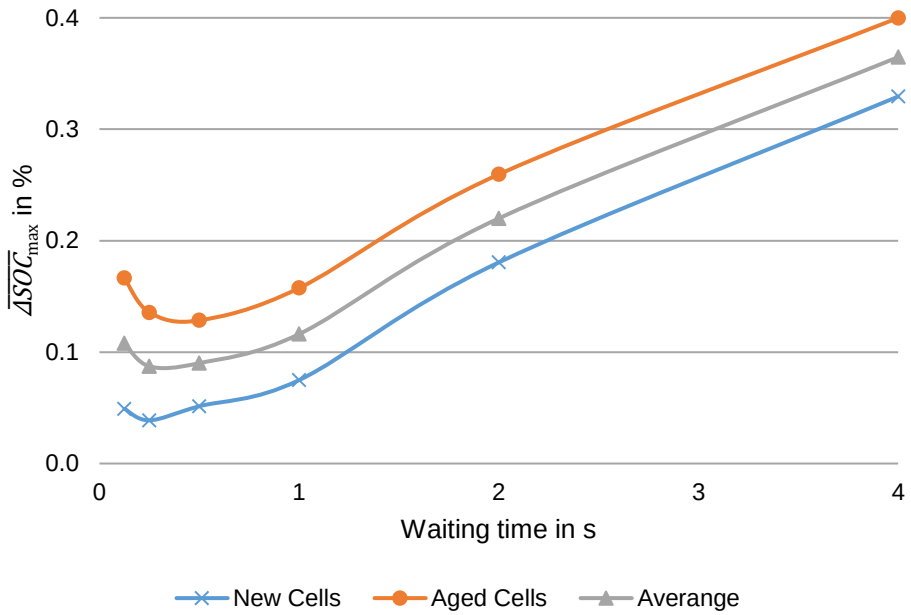

Figure 4.7: Average maximum SOC differences depending on different waiting times

The value of 0.25 s is used for all further simulations, as it represents a good compromise for accuracy for both modules, new and aged. It has to be considered that this determined waiting time might be different for different cell types or different SM configurations. However, the reached accuracy of Pseudo-OCV is assumed achievable also for other configurations and therefore is still used for the remaining work.

4.2.3 Luenberger Observer Results

Similar to the previous section, for the Luenberger observer the factor k_{B}, the voltage feedback correction gain, has to be optimized. The factor not only determines the possible accuracy, but also is responsible for the convergence speed and the noisiness of the observer's output. Different from the section before, the simulation was conducted with only one SM for two consecutive driving cycles, and the reference ΔSOC is the difference of the real SOC compared to the observer SOC in this section. This allows a better tuning of the observer gain factor for accurate SOC values, which hence results in better sorting and therefore utilization. The SM SOC was initialized with 95 %, whereas the Luenberger observer was initialized with 90 % to indicate the convergence from a value outside of the accuracy range. The driving cycle is repeated twice to be able to see the initial forced convergence as well as the behavior with the intrinsic misalignment. Five different parameters were tested from 0.0001 to 0.1 for new and aged SM.

For the new SM, the behavior is shown in Figure 4.8. The vertical line indicates the transition between the two driving cycles. It shows a certain offset error for all parameters, which is caused by the coulomb counting. It could be corrected, but it is not relevant for the sorting, since all SM would have the same offset, if the same Luenberger observer is used for all of them. Much more interesting for a proper utilization is the convergence behavior. Small observer gain factors indicate a too slow convergence from the initial error. In contrast, with larger k_{B}, the convergence is fast, but the output then fluctuates a lot. Especially towards the ends of both driving cycles, where the higher speed results in increased currents, for the largest simulated gain, the error gets even bigger than the initial set difference.

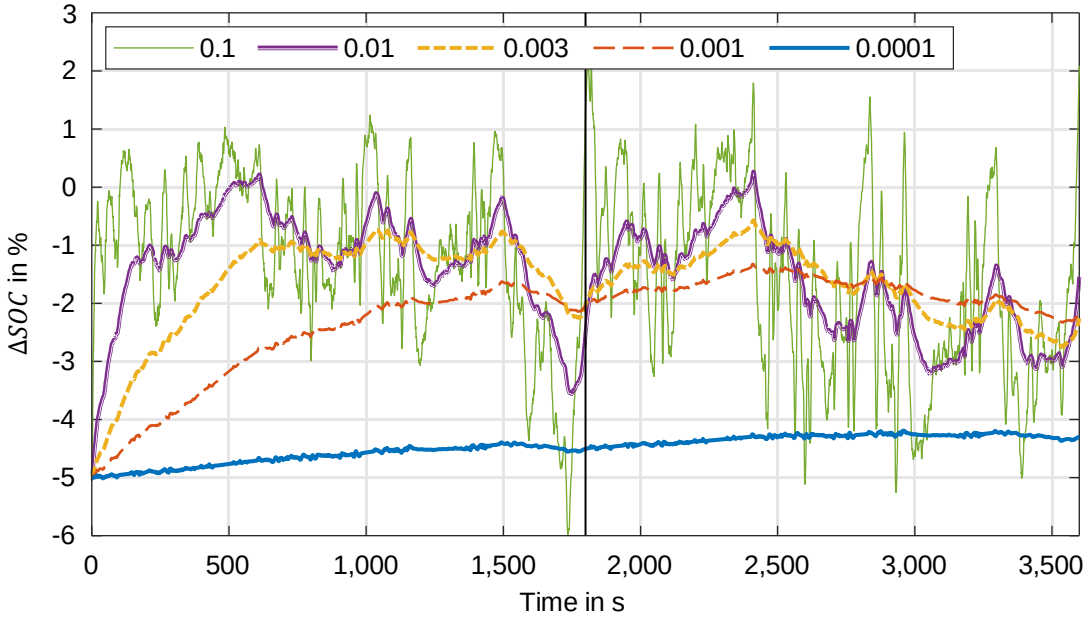

Figure 4.8: ΔSOC plot over time during discharge of single new SM for two driving cycles with different k_B. Adapted from [155].

The same simulation is repeated with an aged SM, which is shown in Figure 4.9. Since the Luenberger observer is not adapted to the aged cell parameters, the estimation errors are increased independent from the observer gain. Especially for low k_B, the Luenberger observer cannot compensate the drift of the coulomb counting, which in this case even causes the SOC to spread even further.

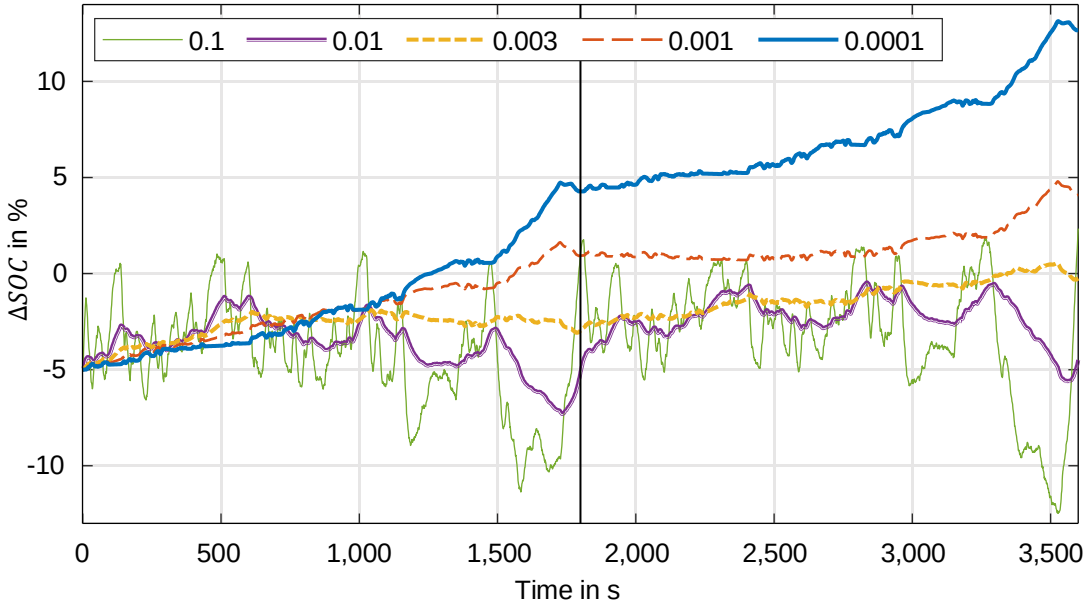

Figure 4.9: ΔSOC plot over time during discharge of single aged SM for two driving cycles with different k_B. Adapted from [155]

To define the optimum gain, an average ΔSOC is calculated. Only values after 1000 s are considered for this, since then all the outputs have converged. Since the values can be negative as well, the absolute value is considered, as shown in Figure 4.10. The detailed values can be found

in Appendix B, Table B.2. Both values of new and aged modules are averaged, which indicates an optimum for the gain factors between 0.001 and 0.003. For the remaining work, the factor k_B of 0.003 is selected, since it indicates the best compromise of accuracy and convergence speed by converging in less than 10 min. Using the Luenberger observer for a different CHB inverter configuration might require adapting the Luenberger observer itself, so that the included ECM is correctly parametrized. Nevertheless, the observer gain and the magnitude of the output is assumed the same, so that it will be used in the remaining thesis.

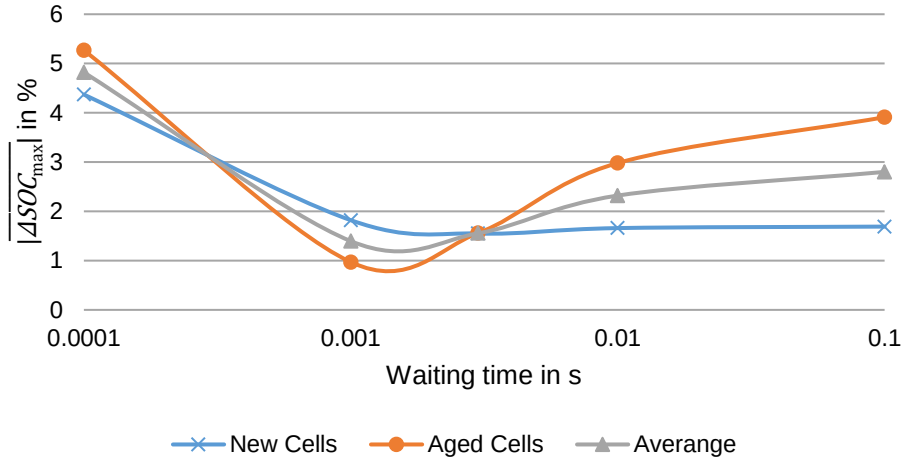

Figure 4.10: Average maximum SOC differences depending on different parameter k_B

4.2.4 State Estimator Comparison

Having defined the optimum configuration for all the state estimators, a comparison between them is possible to identify the overall best solution. This is conducted in the same way as in the previous sections, where the four defined modules are discharged with driving cycles until the first SM reaches its empty state and the maximum SOC difference between the SM is tracked. An initial SOC spread of 3 % is set to be able to compare the speed of convergence.

The comparison is done separately for new and aged modules and both results are shown in Figure 4.11. Overall, it can be seen that the aged cells converge faster than the new cells. This can be explained with the reduced capacity and therefore increased load. It is noticeable that Pseudo-OCV converges the fastest, where a stable state can be reached in around 15 min for new cells and around 13 min for aged. CCV requires a bit longer (approximately 30 min for new and 17 min for aged) and the Luenberger observer method needs the longest with almost 50 min for new modules and more than 20 min for aged. The averaged maximum SOC differences are summarized in Figure 4.12.

The overall average indicates the Luenberger observer as a sorting criterion with the best potential to equalize the SM. However, the second best is Pseudo-OCV, whose result only differs by 34 % and therefore is in a similar magnitude. Additionally, Pseudo-OCV shows the fastest convergence and comes with a simple and therefore cost effective implementation as well, which can be scaled with no extra costs. In principle, just a timer, the anyways-necessary voltage measurement, and a comparing unit are required. In contradiction, Luenberger observer requires more computational power to perform the arithmetic ECM operations and a memory unit for the lookup table for each SM. Another consideration is a possible overestimation of the Luenberger observer accuracy in the simulation because the in principal same ECM is used for both the

Luenberger observer and the actual SM model. Therefore, Pseudo-OCV state estimation as a sorting criterion is considered the most suitable solution for the indicated problem and used for the remaining work.

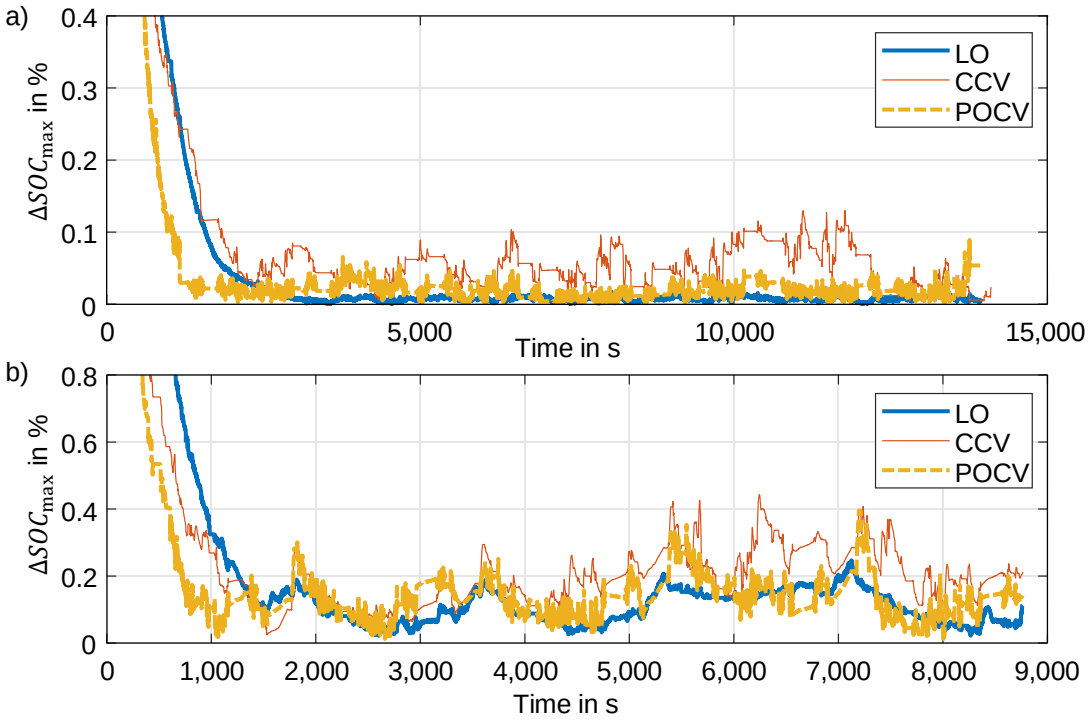

Figure 4.11: Comparison of different state estimators as balancing inputs for a) new SM and b) aged SM. Adapted from [155]

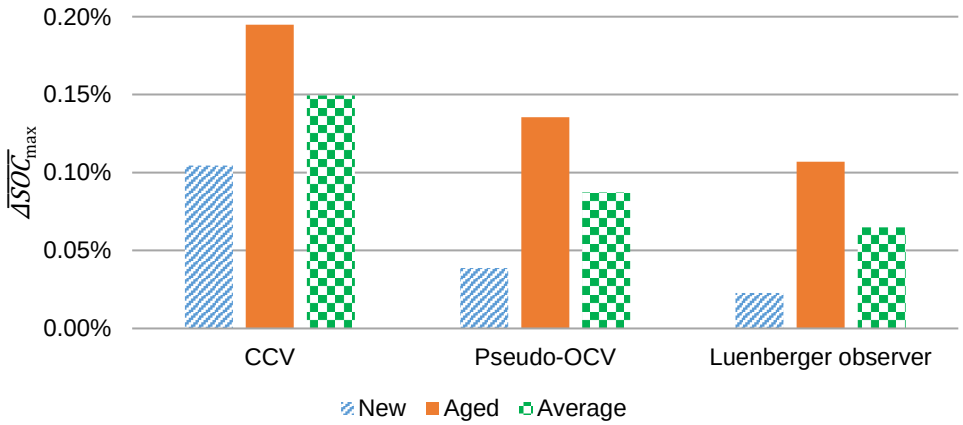

Figure 4.12: Comparison of average maximum SOC differences between different state estimators

4.2.5 Remaining Imbalance after Charging

With the most suitable state estimator defined, the initial discharging condition remains as unknown. This information is necessary to be able to compare the system to a conventional powertrain under realistic conditions. In the previous sections, this initial condition, the SOC difference at the start, was defined manually to a large value to be able to compare the convergence, but the real value can only be derived by defining and simulating the charging profile as well.

To do so, AC charging from the three-phase 400 V grid is simulated. To adapt the voltage, a 2.2:1 transformer is assumed to match the voltages for the individual phases. This means that in the beginning of a charging process for an empty battery pack all SM are active to provide the required voltage. Therefore, the Pseudo-OCV method is not possible and theoretical sorting is applied, which keeps the current imbalance rather stable. After a certain time depending on the charging current, the SM reach a charge level and therefore a voltage, where not all SM are required anymore to follow the charging voltage. After this point, one module can be excluded and therefore the Pseudo-OCV sorting and balancing method can be applied. This enables the SOC differences to be minimized within the convergence time. This approach is implemented in the simulation and it shows a maximum SOC difference as depicted in Figure 4.13a) and Figure 4.13b) for new and aged cells, respectively.

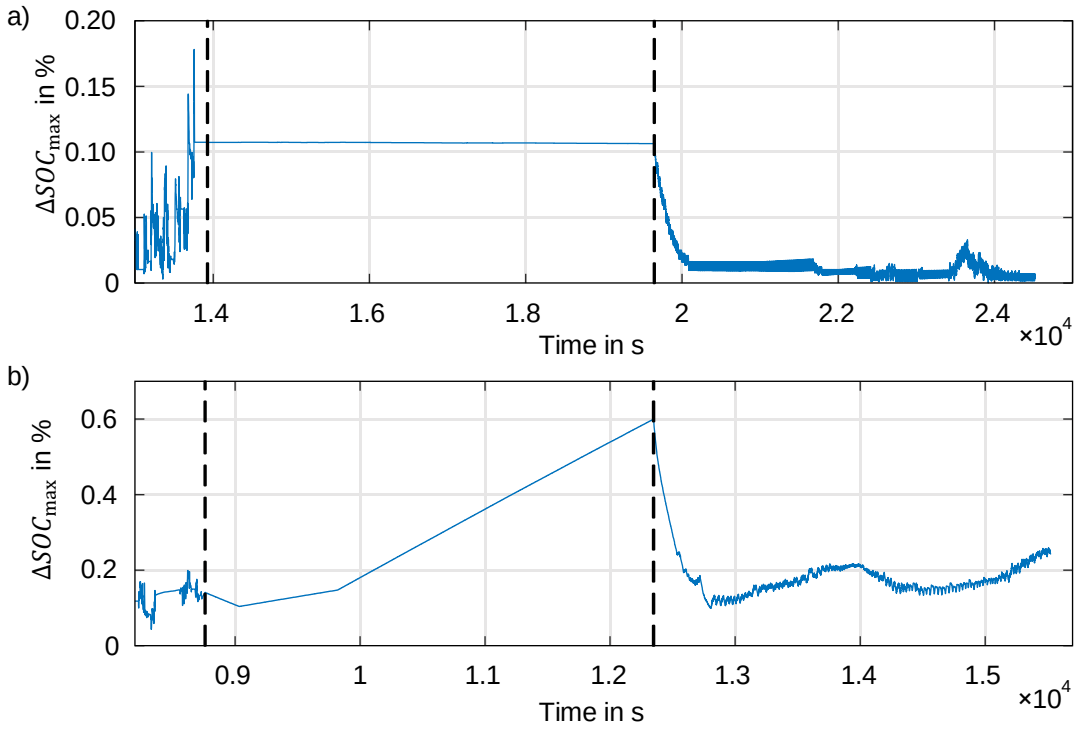

Figure 4.13: $\Delta SOC_{\max}$ plot over time during charge until first SM is in full state. Start of charge with theoretical sorting after a driving cycle discharge at first vertical line. Pseudo-OCV sorting applied at second vertical line for a) new and b) aged modules. Adapted from [155]

The charging starts directly after a discharging of all SM with driving cycles until the first SM reaches its empty state, which is defined with 10 % to limit the DOD. The start of charging is indicated with the first vertical line in the figures. For the aged SM it can be seen that the theoretical sorting is not able to keep the differences equal. Instead, the differences first get slightly better, after which they increase significantly. A similar behavior is noticeable for the new modules as well, just in a much smaller magnitude and therefore hardly visible. It can be explained by the specific order of the SM, when the charging starts. The SOC of SM with a smaller capacity are rising faster, as they see higher C-rates due equal currents. Depending on the initial SOC differences, this is causing the indicated behavior. Nevertheless, when the phase voltage reaches the level where not all SM are required to reach the charging voltage anymore, Pseudo-OCV balancing can be used, which start is indicated with the second vertical line. In this phase, the differences are balanced within minutes and reach their final maximum SOC spreads of

0.004 % and 0.25 % for new and aged modules, respectively. The exact final values of all SM are used in the following simulations as initial conditions for discharging.

The optimization of partial simulation aspects can be concluded with the following definitions for the simulation configuration: The rotation scheme for theoretical sorting is irrelevant as long as it is done in a repeating order and not randomly. The compared state estimators are optimized and compared, where the Luenberger Observer obtains the best results. However, it is closely followed by the Pseudo-OCV method, which is much easier to implement, faster to converge, and easier to scale. Therefore, Pseudo-OCV method is used, also because it is not confirmed that the high accuracy of the Luenberger Observer still can be achieved in a non-simulated environment. A full charging cycle is simulated with the selected balancing methods to obtain the initial SOC differences for the simulation of discharge cycle. With this aspects defined, the possible increase of utilization can be simulated.

4.3 Increased Utilization Results

In this subchapter, the accessible potential, and therefore a utilization factor for the SM is obtained by simulation. First, the real increased utilization for the simulated configuration of four SM is determined. The resulting accessible potential is then brought in relation with the maximum usable potential of the SM in form of a utilization factor, which can be used to extrapolate the increased utilization for different CHB configurations.

4.3.1 Improved CHB Battery Utilization

The utilization of the optimized CHB system is compared to a conventional battery pack/VSI for new and aged SM. To enable a direct comparison, the conventional battery pack is simulated consisting of SM as well, but with fixed interconnections. The initial conditions are defined as perfectly balanced batteries for the VSI and the end of charge conditions mentioned in Section 4.2.5 for the CHB system. They are then discharged with the same driving cycles. The end of the simulation is defined with the first paralleled cells and therefore SM reaching their empty state, even though the CHB inverter driven vehicle actually still could continue its journey with reduced power by bypassing the empty SM. The number of interest is the real SOC from the simulation for all the individual modules.

As visible in Figure 4.14, in all cases the spread caused by the variations results in the situation, where the SM with the lowest SOC triggers the simulation to end. Due to the higher spread of the VSI system, this end is happening earlier with a higher remaining energy in the other SM. In case of the new SM, as shown in Figure 4.14a), the final spread is similar, since the initial spread is kept rather equal during the discharge, while the VSI system is slowly diverging. It causes the CHB simulation to run for 1.09 s longer due to the increased energy utilization in this lossless simulation. This duration converts in an accessible potential of 0.008 % for a single phase. Calculated for the three-phase system, an accessible potential of 0.013 % is visible, which means the maximum usable potential is accessed with a utilization factor of 30.9 %.

For the aged SM shown in Figure 4.14b), due to the aged cell parameters, an increased SOC spread of more than 1 % for the modules used in the VSI system is visible. The spread for the aged CHB SM is increased as well due to the other aged parameters, but because of the narrower distribution, the pack can be used for 13.84 s longer compared to the conventional system.

This can be converted in an accessible potential of 0.16 %, which results in an accessible potential of 0.26 % for the three-phase system. Here, a utilization factor of 35.8 % of the maximum usable potential can be seen.

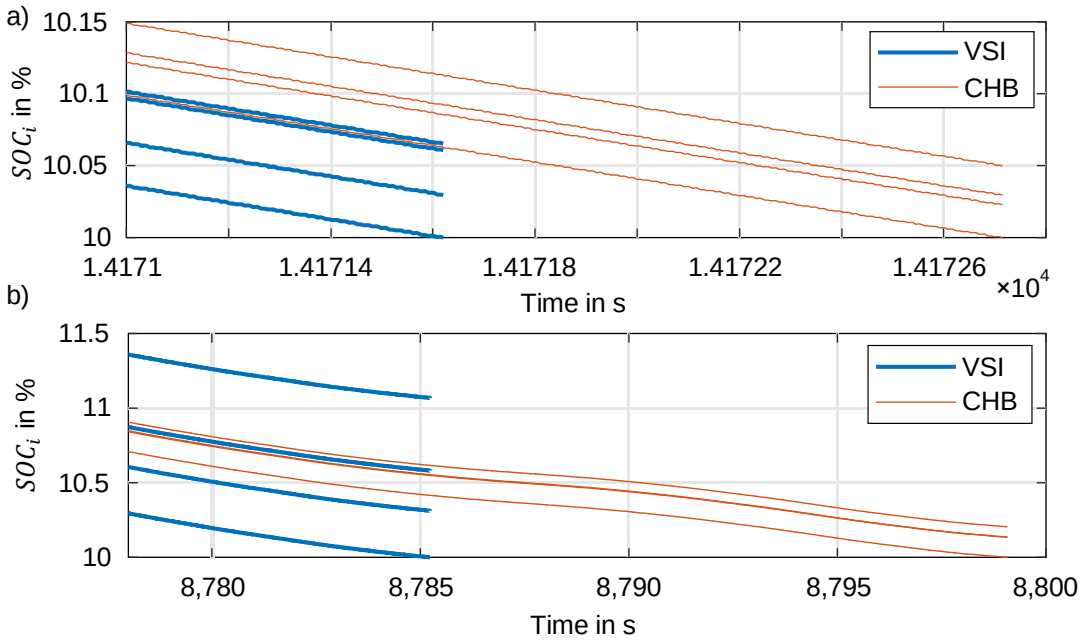

Figure 4.14: SOC_i plot over time during discharge of both CHB and VSI powertrain until first SM is in empty state for a) new and b) aged modules. Adapted from [155]

4.3.2 Utilization Extrapolation for other Configurations

The simulated increased utilization and therefore accessible potential is only calculated for the four SM configuration to keep the simulation efforts manageable. Since the maximum usable potential is known for all considered reference CHB configurations (Figure 4.4), the ratio of the increased utilization can be extrapolated using the utilization factor to indicate the possible accessible potential for all configurations. This is an important input for finding the optimal configuration in the next subchapter, as an increased utilization reduces the battery size and therefore costs.

The extrapolation is based on the finding that the utilization factor is similar between new and aged modules, which have different variations in capacity and internal resistance. This can be explained by the other parameters, which are aging as well. Therefore, the sorting gets less accurate and the spread is larger compared to new cells resulting in a roughly equal utilization factor. It is therefore assumed that the accessible potential ap_c is directly correlating with the maximum usable potential p_c, and is independent on other cell parameters. To not overestimate the gain, the lower value of 30.9 % utilization of the maximum usable potential is taken and considered for all the three-phase configurations. The results are shown in Figure 4.15 for both new and aged modules in all possible configurations. Due to the visible discontinuity, no equation fit, but a lookup table is generated and used for the configuration optimization in the next subchapter.

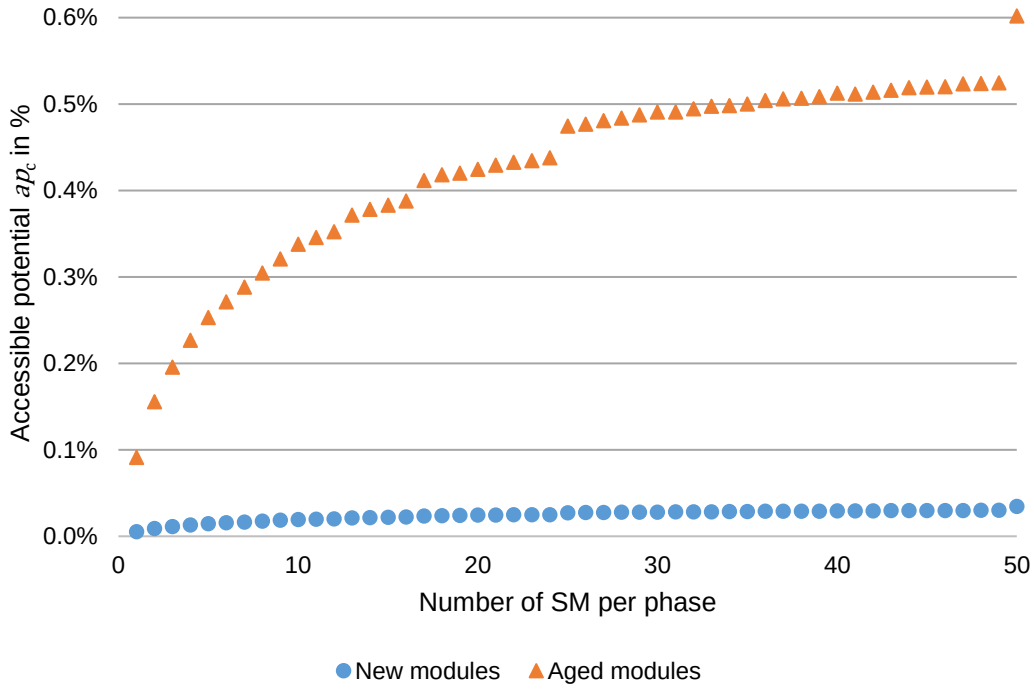

Figure 4.15: Accessible potential of new and aged three-phased CHB battery dependent on the number of SM per phase

As a conclusion, in this subchapter it is shown that the maximum usable potential of the SM can be made partially accessible with the mentioned optimized controlling and state estimations of the CHB modules. This utilization is simulated in detail for the four SM configuration and indicates a utilization factor of around 30 %. This factor can be used to extrapolate the accessible potential for all configurations. The result indicates the amount of battery capacity, which can be reduced in each individual configuration and therefore it shows the cost reduction potential of the battery pack. This is used as an input in the next subchapter to find the optimal configuration.

4.4 Results of the Configuration Optimization

With all the cost-influencing factors defined, now the results of the simulations regarding the best configuration, as explained in Section 3.4.6, can be given. This is conducted with a focus on four different categories: how many modules are selected, which switch constellation is preferred, which efficiency results from this configuration, and which costs are caused and reduced by the selected implementation. For each aspect, the results have to be differentiated regarding the underlying switch cost models, as they generate diverging configurations. The last section then gives a summary of the optimization results and defines the overall optimal configuration and its benefits. It also includes a table with the detailed results, so that they can be compared directly.

4.4.1 Number of Modules

The amount of SM per phase is a dominant question of this research, as a high number allows a better utilization, but increases the costs and losses due to the switches. In general it is found, that there are between two and eight modules possible for all switch cost models excluding the

model, where no costs are considered. In that case, a much higher number of 10 to 28 modules with an average of 17.79 is found. It therefore can be said that for efficiency and utilization maximization, a medium number of SM is preferred. Is the number even further increased down to almost cell level per SM, efficiency losses are much higher than the gains from increased utilization. However, if the switch costs play a role, rather independent from their cost impact, solutions of around 4 SM per phase are preferred with the die size relating costs indicating slightly less SM (on average 3.62) and the research based and theoretical optimal switches slightly more (on average 4.13). Without the no cost model, it results in an average of 3.92, which leads to the conclusion, that four SM per phase and therefore 12 SM in total with a 9-level CHB configuration can be considered the best.

4.4.2 Switch constellation

The switch constellation firstly looks into the amount of switches in parallel. Again, the model with no cost consideration results in different parameters compared to the other cost models. High number of switches are preferred here ranging from 19 to the maximum number of 30. Would the simulation limit be set higher then 30, even larger number of parallel switches would be selected, as the conduction losses can be even further reduced. The average of 26.7 however indicates that the switching losses also increase with the amount of parallel switches, which leads to the conclusion, that there is a theoretical optimum, which is less then infinity. Since such a hypothetical result is not relevant for this dissertation, the results with considered switch costs are the relevant part. Here, across the switch cost models, numbers from 2 to 30 can be found with averages of between 7.16 and 15.12. The highest number of 30 is only found in a few cases in the low cost model and this might be caused by unrealistic low prices for some switches. A total average of 11.27 is found leading to the conclusion that a configuration of 11 switches in general works best.

Another question of the switch constellation is the type of switch selected. With no costs considered, the switch *BUK9J0R9-40H* made by *Nexperia* is the preferred choice for 88 out of 100 configurations, indicating this as a highly efficient switch. For high and low cost models, different preferences can be found based on the different prices associated with them. The die size based models both prefer the *IPD90N10S4L-06* from *Infineon* indicating a good price/efficiency ratio. For the theoretical optimal switch, the switch voltage V_{DS} and the maximum current I_{D} with their according de-rating are directly defined by the number of modules and parallel switches. They therefore match perfectly for each configuration. For the remaining switch parameters, a rather high conduction resistance of on average 3.89 mΩ with values from 2.11 mΩ to 7.08 mΩ can be found. Due to this, the switch prices are in lower ranks from USD 0.35 to USD 1.03 with an average of USD 0.50.

4.4.3 Efficiency

The efficiencies are in general substantial higher compared to conventional inverters, which is an outcome discussed in the concurrent thesis as well [32, p. 37]. The highest efficiencies can be found when the costs are not considered. A value of up to 99.80 % and on average still 99.78 % are simulated in this category and therefore define the benchmark. In comparison, the reference IGBT powertrain only reaches efficiencies of 93.65 % for the same driving cycle load in the same reference vehicle. This optimum configuration and its increased efficiency would reduce the required battery energy content up to 3.56 kWh.

With the cost consideration, the low cost model generates the highest results with an efficiency of on average 99.12 % and the high cost model the lowest with on average 98.98 %. Only the theoretical optimal switch is slightly lower with on average 98.69 %, which indicates that this model is not able to find better configurations then models with actual switches. The total average without the no cost category is found at 98.96 %. It shows an improvement of 5.31 % compared to the conventional inverter and reaches the maximum benchmark closely.

4.4.4 Cost

The results of the simulation indicate that the configuration without cost considerations would have high additional hardware costs of between USD 3,847 and up to USD 13,500 and therefore on average USD 6,806 more than the reference IGBT inverter due to the high number of parallel switches and number of SM. The savings of battery capacity reduction and reduced running costs without any hardware costs are rather independent from the configuration with an average of USD 3,477, which indicates the cost benchmark. It also means that even with the most efficient powertrain, such an implementation on average would cost the user USD 4,070 more during the lifetime compared to the reference vehicle. This highlights the necessity to include cost considerations for finding the optimum CHB inverter configuration.

For all the other cost models it is visible that the inverter itself on average is always more expensive compared to the conventional inverter. Even with the low cost switches, an additional cost of USD 205 is expected on average and this can range up to USD 630 on average for the high cost switches. Altogether, on average, increased hardware costs of USD 398 have to be expected. However, due to the decreased battery size and the saved running costs, between USD 2,474 (theoretical optimum switch) and USD 2,926 (low cost switch model) can be saved in a TCO comparison. The average value is USD 2,647, which is only USD 842 below the maximum benchmark of the most efficient configuration and this difference can be as low as USD 424 in the best case.

4.4.5 Summary of Configuration Optimization

In Table 4.3, a summary of the main results for the different switch cost models is given. The values are averaged excluding the maximum savings with no cost consideration, since these results are not feasible in an economic way and maybe even hard to integrate into the package. They therefore would distort the results. In Figure 4.16, the cost saving for the best 100 configurations of the different cost models are depicted. The data entry “No cost” shows the savings due to reduced battery capacity and decreased energy costs, but without any hardware costs. Otherwise, its values would all be in the negative range. Also included in Figure 4.16 is a total average and an average excluding the maximum savings to highlight the possibilities without the distortion from infeasible results. It can be seen that certain cost models, especially the high cost model and the voltage current model, have a few outliers, which indicates a certain combination of parameters achieve a unregularly high efficiency due to interacting factors. This outlier behavior also can be seen in a less obvious way for the other cost models, which is why the top 100 configurations where averaged to filter out this effect.

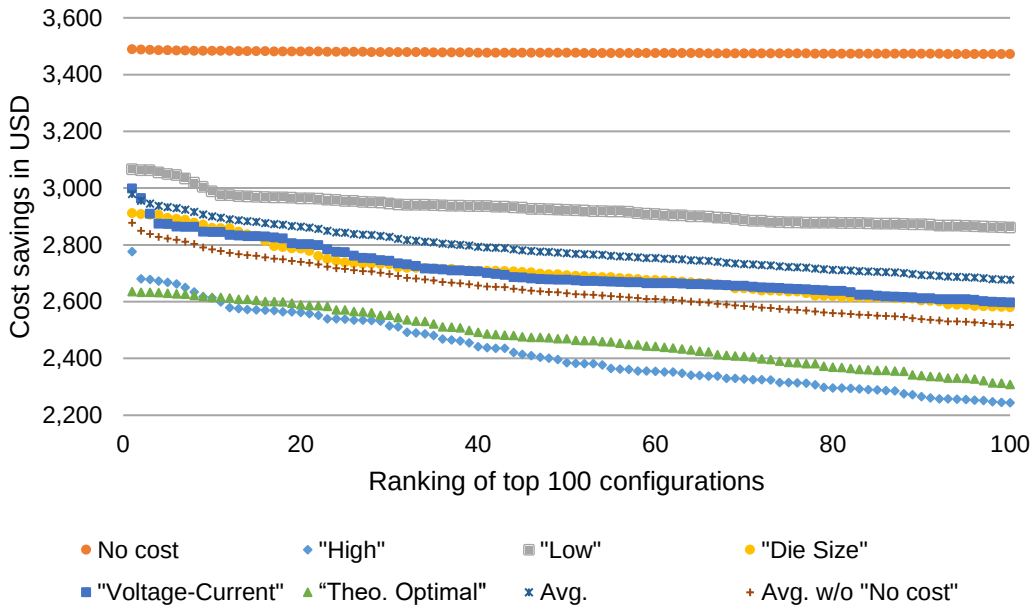

Figure 4.16: Cost savings in USD for the top 100 ranked results for the different switch cost models

Table 4.3: Summary of the main results for the different switch cost models

Cost Model	No Cost	“High”	„Low“	“Die Size”	“Voltage-Current”	“Theo. Optimal”	Avg. of Models
Min. Number of Modules	10	3	3	2	2	2	2.40
Max. Number of Modules	28	8	5	5	5	7	6.00
Avg. Number of Modules	17.79	4.08	4.12	3.62	3.62	4.18	3.92
Best Number of Modules	17	3	4	3	3	3	3.20
Most Number of Modules	13	3	5	3	3	3	3.40
Freq. of Most Module	12	43	44	54	48	25	42.80
Min. Num. of Parallel Sw.	19	2	2	2	2	4	2.40
Max. Num. of Parallel Sw.	30	30	30	24	20	26	26.00
Avg. Num. of Parallel Sw.	26.69	11.67	15.12	9.09	7.16	13.33	11.27
Most Num. of Parallel Sw.	30	7	7	6	6	10	7.20
Max. Efficiency in %	99.80	99.40	99.44	99.33	99.35	99.20	99.34
Avg. Efficiency in %	99.78	98.98	99.12	99.00	99.02	98.69	98.96
Avg. Inv. Cost Dif. in USD	-	630	205	361	366	426	398
Max. Cost Save. in USD	3,489	2,776	3,065	2,911	2,998	2,635	2,877
Avg. Cost Savings in USD	3,477	2,422	2,926	2,705	2,709	2,474	2,647

4.5 Overall Results

This subchapter is summarizing the results. With an increased utilization of the energy stored in automotive battery packs, first the magnitude of the problem was analyzed. Only small tolerances of a few percent where found for new cells. These tolerances increase over time with the aging of the cells. On an individual cell basis, this results on average in a currently unused potential of 2.30 % for new cells and 5.28 % for aged cells. However, this unused potential is reduced in a static pack like in the reference vehicle due to the parallel connection roughly by a factor of 5. In a CHB pack, this unused potential is split into the still unusable potential within the SM and the theoretical usable potential. Its value depends on the number of SM, where more SM are better. The maximum usable potential for a four SM/nine level CHB inverter is reduced from the initial value approximately by factor 10. To access this potential, a control strategy is required. A level shifted PWM is indicated as the most practical control strategy. It is theoretically able to utilize the full potential within a short time of several minutes, depending on the initial SOC differences. However, to do so, the sorting needs accurate information with respect to which module to prioritize. Current SOC estimators struggle with this task, as normally their accuracy is in a similar magnitude as the tolerances. On top of that, since each SM needs its own state estimator, the costs for these systems have to be considered as well. A cost effective method with a high relative accuracy (qualitative defining which SM has a higher charge without defining the quantitative result) is found with the Pseudo-OCV method. With optimized parameters, it is found that this method can access around 30 % of the maximum usable potential, which results in a utilization factor of 30 for the initial individual cell capacity tolerance. It therefore can be seen that the increased utilization has little impact on the overall battery behavior. Especially for rather consistent cells like the ones selected for the simulation with no defect cells, it results in minor, almost irrelevant gains in the per mille magnitude. Results that are slightly more significant can be expected if less homogeneous cells are used.

However, the CHB enables other benefits as well, which can be summed up to an overall monetary benefit. This becomes clear during an overall optimization of the configuration. Firstly, when the initial inverter costs are compared, the CHB inverter is on average USD 398 more expensive than a conventional inverter, even in its best configurations. However, there are some configurations, where the CHB inverter hardware can cost less than the reference inverter, especially when using the “low” cost model. A different perspective is indicated, when the efficiency gains with a CHB inverter are considered, and therefore the initial vehicle price is reduced by the costs for the decreased battery capacity. In this case, even with the “high cost” model, the first top 30 configurations indicate a cost saving compared to the reference vehicle and for less expensive cost models the initial vehicle costs can be even less. If now the running costs are considered as well, where energy cost savings are possible with the reduced energy requirements, a total average saving of USD 2,647 can be obtained with an on average reduced initial vehicle costs of USD 120.

As a summary, it can be concluded that a close to optimum CHB inverter configuration for the selected scenario would consist of four SM in each phase, where each switch comprises of 11 switches in parallel with each SM consisting of $13s15p$ battery cells. Such a configuration is shown in Figure 4.17.

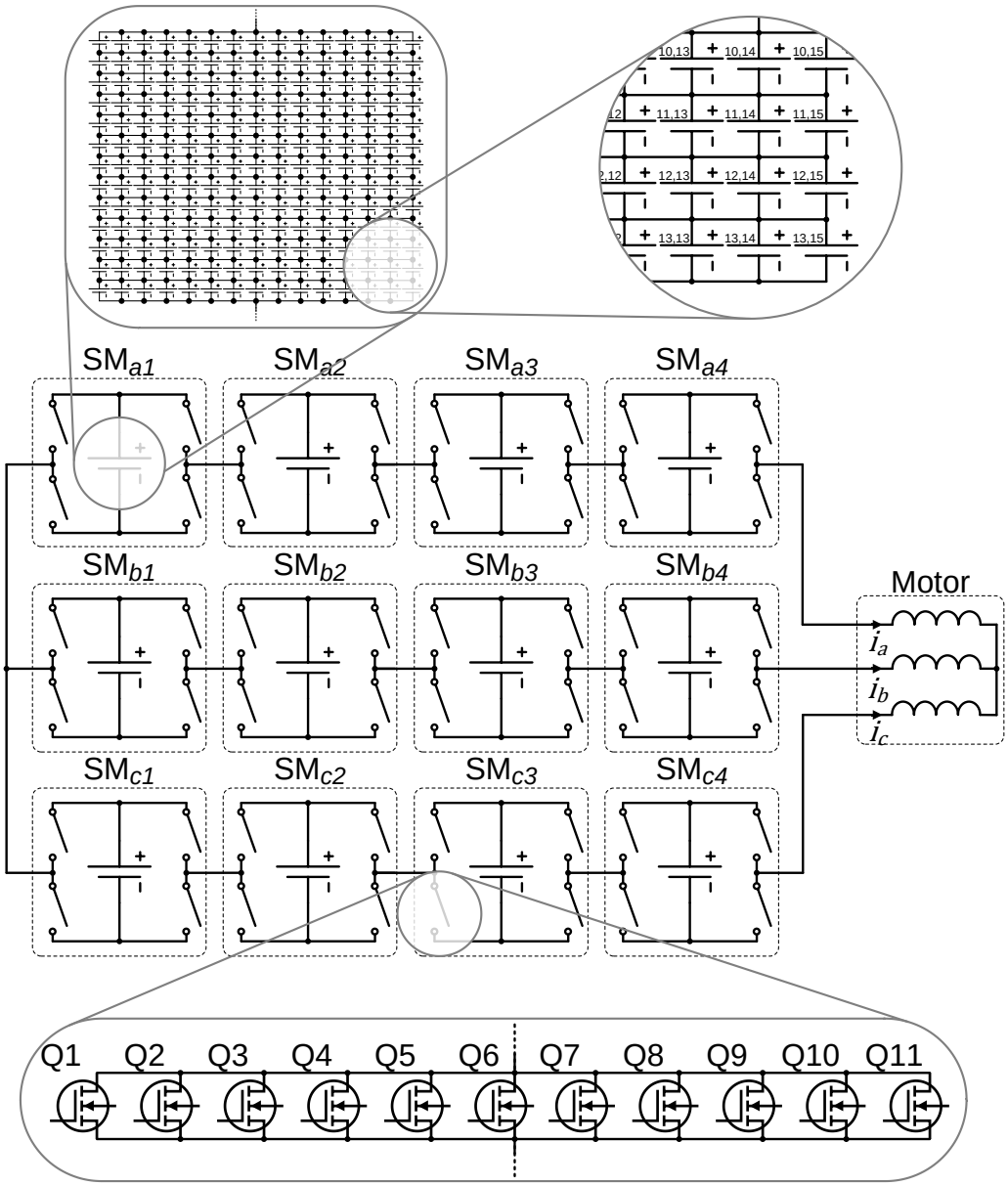

Figure 4.17: Simplified layout of the optimal CHB inverter configuration as a result of the conducted simulations using the defined scenario.

5 Discussion

The presented results in the previous chapter indicate the CHB inverter as a suitable solution to access the unused tolerances in a vehicle battery. With an optimized configuration, this will mainly increase the efficiency and additionally enable an increased battery utilization, even though this effect has limited impact on the overall benefit. Following the V-Model re-composition as shown in Figure 5.1, this chapter firstly aims to highlight the plausibility of the indicated results by critically discussing them. It thereby orientates the discussion of the results on the four steps indicated in the Methodology Subchapters. As a next step, recommendations on a commercial implementation are given, starting from cell level and then increasing the scope to module, pack, and eventually system level. In the end of this chapter, future challenges and limitations are discussed and an outlook is given.

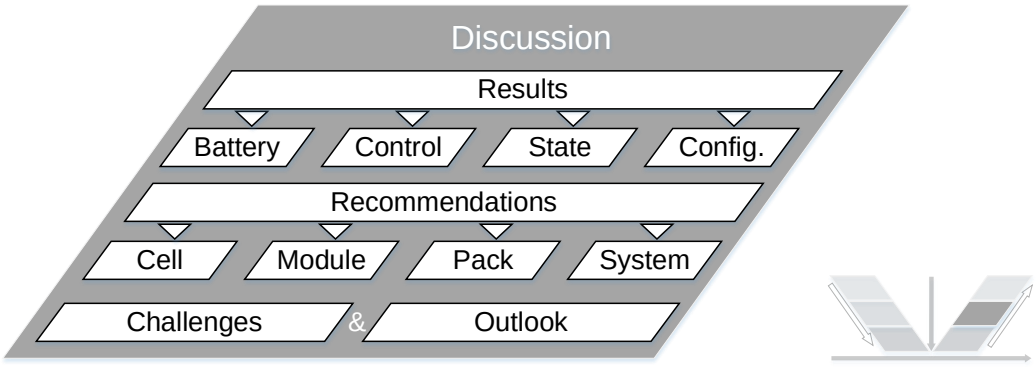

Figure 5.1: Structure of Chapter 5

5.1 Discussion of Results

The results presented in Chapter 4 are solely based on the methods introduced in Chapter 3 including the mentioned assumptions and simplifications. This subchapter highlights the dependencies of the results on the selected methods and indicates the sensitivities of selected parameters and interpretations.

5.1.1 Discussion of Battery Data

A big effort was made to compile the battery dataset of different cell variation data as extensive as possible by combining data collected from literature and own experiments. However, the dataset is still limited in its size. Collecting own data requires extensive experiments. The first challenge is the acquisition of a relevant amount of sample cells. While individual cells are available on the aftersales market, larger batches are difficult to procure. These aftermarket cells often originate from mixed batches and with unknown history/age. Especially the relevant cells from automotive battery manufacturers are hardly sold in the magnitude of a few hundred samples for research. A considered alternative is to buy automotive aftermarket replacement battery

packs and disassemble them. Apart from the issue of the already conducted matching, the biggest challenge would be the disassembly process, since, as explained in Section 3.1.3, the cells are normally welded together, and an un-welding adds additional stress on the cells. In addition, the aging status of such a pack is mostly unknown. Independent from the source, such an acquisition would require substantial funding, since a minimum sample size is required to be able to discuss the variations. This is especially the case for larger cell sizes, since the costs are linearly correlating with the capacity, but the requirements for the sample size remains the same. Even after the cells are available, the tests are time and equipment intensive, which again is a financial challenge.

All these reasons combined explain, why the literature about battery variations is so sparse. Other researchers are assumed to face similar challenges. On top of that, in the literature, different publications have unrelated research priorities, so the available data varies and the methods to acquire data are not identical, which makes them not ideal for comparison. Various sources have different experimental methods, especially in how they define a “full” and an “empty” cell with deviating end of charge and end of discharge voltages, other DOD and alternative charging/discharging modes (CC/CCCV). The commonly used CCCV charging and sometimes even discharging method, which is unrealistic in vehicle applications, is found to reduce the measured variations [24]. Finally, for most publications, no raw data is available, and therefore that data was extracted from the plots, which especially for the sources with large sample sizes of a few thousand cells reduces the accuracy.

The limited amount of data restricts the usage to evaluate certain correlations like packaging or cell size, if the sample size is too low. The available data shows no clear relations, but this could be different with more entries in the dataset. The main problem for all the cell data are the missing cost details that are needed to estimate the quality level. The cell quality and cost would be an interesting input for the optimization. It would indicate, to which extend it makes sense to use cells with worse tolerances but lower costs in a CHB inverter.

5.1.2 Discussion of the Control Strategy

The definition of the reference modules, which are used for simulations that implement the control strategy, indicates an important drawback. Even though there are initial tolerances with an apparent maximum usable potential for the individual cells, this is strongly reduced due to the configuration of the cells within the CHB inverter. This is mainly caused by the usage of cells with small individual capacity and therefore the requirement to connect them in parallel. This parallelization is causing two unwanted effects: firstly, the capacity of this parallel string is averaged from all the cells. Therefore, the variations between the different parallel strings are reduced, which causes the cell tolerances to be inaccessible even with a CHB inverter. The second aspect is the possible aggravation of the cell conditions in parallel connections mentioned in Section 3.1.1 [123], [130]. The small cells used to configure the reference SM were selected due to the availability of a well parametrized and validated model that suited the computational requirements. Another fact, which is not included in the definition of the reference SM, are the faulty cells. While such excluded cells were noticed for many entries in the battery tolerance dataset, the selected cell type did not directly indicate such behavior and the failure mechanisms are unclear. An inclusion would have increased the variations and therefore the maximum usable potential of the modules.

The control strategy was evaluated build on the premise to only implement the load shifting based on the modulation of the commanded voltages u_{as}^{*}, u_{bs}^{*}, and u_{cs}^{*}, but not of an alternation for those voltages. For the equal utilization, relatively less important topics of the control strategy, such as the THD minimization, have not been considered, since there is no conflict expected. In addition, the question of an optimal switching frequency was not evaluated due to the considered irrelevance for the utilization. However, it is important to optimize these topics as well, since they influence the efficiency, the reliability, and the compatibility with other components.

5.1.3 Discussion of State Estimation

A point of concern is that the selected state estimation method Pseudo-OCV only works on the prerequisite that there are times, where not all modules have to participate in the generation of the desired phase voltages and currents equally. It is shown that this assumption can be considered applicable for urban driving cycles, but shows limitations for longer high demand phases, such as continuous high speed driving on highways. It therefore works well for vehicles used in mixed or pure urban scenarios like passenger cars and public transportation. These are also the scenarios, where the current IGBT based inverters show their largest disadvantages. On the contrary, for vehicles like trucks or even more for ships, planes, or grid applications, long periods of equal and high power demand are required. Here, the SOC estimation using the Pseudo-OCV method may not be the preferred selection.

For charging, it is shown that until medium SOC, all modules are fully required to participate and therefore no balancing based on the Pseudo-OCV method is possible. Only if the battery is charged beyond that SOC level, the load balancing can function. Such a scenario again is applicable for passenger cars and similar vehicles, which are often fully charged during standing times, but not useful to the same extent for vehicles, which are repeatedly charged for short times and therefore constantly operated with a medium SOC.

Beside of the already strongly reduced maximum usable potential, a rather low utilization factor of the maximum usable potential of only around 30 % is noticeable. This is majorly caused by the miniscule accessible potential, which is in the same range than the accuracy of the state estimator. The increased accessible potential for aged cells is challenged by the increased inaccuracy of the state estimation due to the other deteriorated cell parameters. Another reason is that the utilization factor depends on the ΔSOC at the end of discharge. This value fluctuates during the discharge depending on the driving conditions, and the driving cycle stops during a random time step. The utilization factor therefore becomes a random value between the minimal and maximum range. Such a behavior is avoided as much as possible by averaging the value, but this still defines an unrealistic scenario, as typically the vehicle would not drive with regular demand pattern until the battery suddenly switches itself off. As the last part of a real driving cycle with an empty battery, a low-demand parking maneuver should be common, which would allow an increased equalization. However, this is not applicable for comparing in simulations, which is why the described approach is selected.

5.1.4 Discussion of Configuration Optimization

From the range of results for the configuration optimization, it can be seen that the configuration and even more the selection of the switches have significant impact on the efficiency of the CHB inverter. Even within one cost model, there are significant differences between the individual savings of different configurations. The main impact comes from the actual selection of the

switches, which can be seen in the no cost consideration, where the savings and efficiencies are stable over a wide range of configurations.

A further point to acknowledge is that the evaluation only considered the top 100 configurations. A smaller sample size could overemphasize the outliers. A bigger sample size on the contrary includes less efficient results and therefore it might underestimate the potential cost savings. If the ranking for a larger amount of results is inspected, it is seen that the top 50 to top 100 configurations show an increased improved result, while the remaining savings indicate a proportional decrease over the rankings. An example is shown in Figure 5.2 for the “low” cost model, where the overall and initial savings for the top 10,000 results are shown.

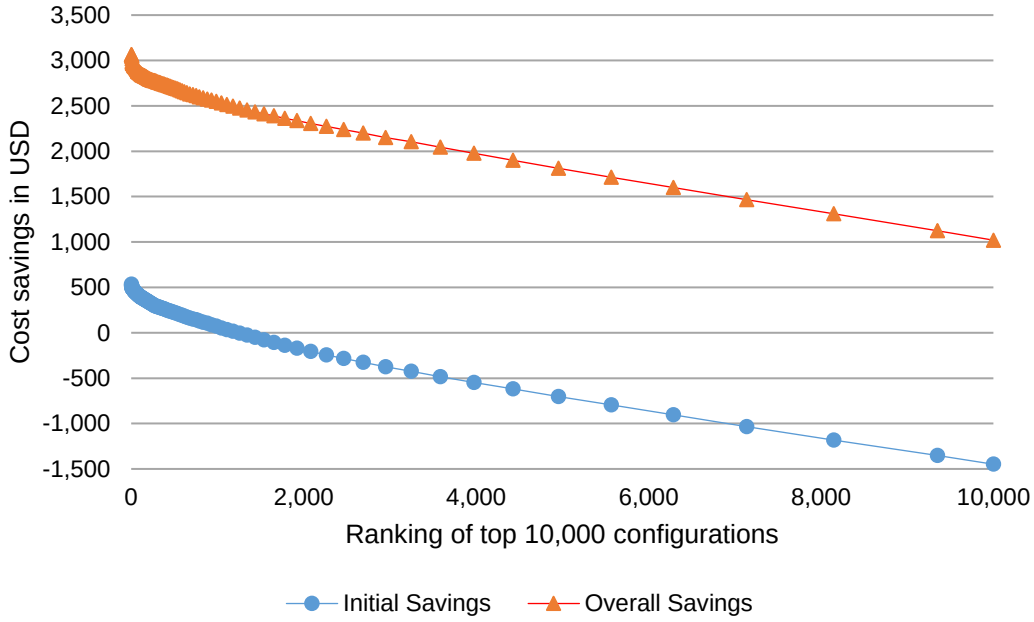

Figure 5.2: Cost savings in USD for the top 10,000 ranked results for low switch cost models

The results of the theoretical optimal switch show a rather low efficiency and rather high cost compared to the other cost models, even though it matches the requirements accurately. An initial explanation for the subpar fitness of the model are the multiple assumptions and approximations with mediocre coefficients of determination. However, it is visible that the other cost models show outlier results for their top 10 configurations, which is not the case for the “theoretical optimal switch” cost model. This can be explained with the hypothesis that with real switches, certain configurations reach an increased benefit due to interacting parameters, which is not possible for the generic “theoretical optimal switch” cost model. Therefore, it can be concluded that with the “theoretical optimal switch” cost model, the right magnitude for a specific input setting can be found, but for finding the real optimum configurations, real switch parameters are required.

Another considerable aspect is that due to the increased efficiency, a reduction of the battery capacity is calculated to convert the range gain into a monetary benefit for comparison. While such a reduction might not be possible due to the discrete parameters of the cells and cell configuration requirements, it allows an evaluation of the magnitude of the benefit. On overall average, a capacity reduction of 8.94 A h amongst all cost models can be seen with a range of 19.4 % between the lowest and highest possible reduction. Such a reduction could be converted into a weight reduction of 18.5 kg and a volume reduction of 9.2 dm^3 of the battery pack.

The results of the optimization of the configuration show a high sensitivity for several simulation input parameters. The most prominent shall be explained in the following paragraphs.

A sensitive parameter to calculate the cost savings are the energy costs, as they leverage the total savings in larger magnitudes and therefore influence the selected configuration. Within the energy cost consideration, two factors have to be assumed: the costs for electric energy and the total driven lifetime distance:

For the energy costs, a reference country with rather high energy costs was selected compared to other countries [5]. To indicate the impact of the energy costs, a sensitivity analysis was conducted. It includes the energy costs of other countries: the United States of America, Peoples Republic of China, Argentina, and hypothetical free electric energy. A linear correlation of the energy savings with the overall cost savings can be noticed. If the energy costs are changed by the factor ε, the total cost savings over lifetime are changing with the factors $0.84\,\varepsilon + 0.15$. Due to the changed savings, different configurations are preferred. However, they remain in comparable ranges. For example, with the energy cost of the US, which are 40 % lower, a reduction on the average number of modules of 4 % can be obtained. It is therefore assumed that the energy costs influence the cost savings, but not so much the configuration optimization.

For the second sensitive parameter of the energy cost calculation, the total driven lifetime distance, some might argue that the selected distance of 960,000 km is too high. This is a valid argument considering some current smaller passenger cars reach their EOL with less mileage, even though the amounts of cycles until EOL is a constant matter of improvement. For this factor, the sensitivity analysis concluded a direct correlation with a factor close to 1. It is therefore important to select a matching mileage to conduct the optimization.

The actual battery variations influence the optimal configuration only insignificantly, if they vary in the indicated ranges. For the concurrent publication of the configuration optimization, the models were simulated without cell tolerances and the increased utilization [189]. It can be seen that there is almost no difference in the results, especially since the costs are rounded to cent values. Also in the configurations, only minor deferrals can be seen. This majorly can be explained with the strongly reduced accessible potential for new cells, which only has a small contribution to the cost savings and therefore influences the optimization only on insignificant levels.

5.2 Recommendations on System Configuration and Commercial Application

This subchapter shall give some indications and recommendations with respect to how the presented CHB inverter as an active battery interconnection can be commercially implemented. It combines the findings of the results and discussions presented in the previous chapters. A definition of the overall energy storage as a system is given. For this purpose, the considerations are explained starting with the smallest element, the cell, and continuing on incrementing levels until the whole vehicle environment is considered.

5.2.1 Cell Level

The results of this dissertation indicate a recommendation of using larger cells independent from other vehicle relevant considerations in CHB inverter driven vehicles. Current counter arguments,

which are decreased reliability and the better averaging of the capacities in parallel strings with a high number of cells, are not relevant anymore for the CHB inverter. Regarding the reliability, the concurrent dissertation already has shown a decreased failure probability due to the used circuits and components [32]. Additionally, within this research, it is shown that not all modules are required to operate the vehicle, as they can be bypassed. Both arguments put together indicate an increased vehicle reliability. Regarding the other argument, the increased averaging of more cells in parallel strings, in a CHB inverter, larger differences between the SM actually increase the accessible potential and reduced parallel averaging is therefore beneficial. Within a SM, the cells should be as equal as possible to decrease the limitations by the conventional circuit and balancing, just as in a conventional battery pack. With less, bigger cells, the possibility of less variance is increased.

Packaging for larger cells prioritizes pouch and prismatic cells, because with them a higher pack density is achievable with larger cells. However, also cylindrical cell size in automotive use cases are indicating an increasing trend since larger cells have multiple benefits in general [215]. Beside of that, no packaging preference is visible. The argument is similar for the selected cell chemistry, as within the limited sample size, no preference is visible as well. The overall variations of the cells could be less strict, if that is beneficial for the cell costs, as long as no other aspect like safety is compromised.

The aging of the cells is not significantly influenced by the CHB inverter, even though there are high frequency discharge pulses. This is investigated in detail in a publication, where the author is a co-author [216] and also in the concurrent thesis [32].

A further battery manufacturing improvement and therefore reduction of the cell tolerances would not conflict with the concept of the CHB inverter. Its main benefit, even with current cells, comes from the increased efficiency, and not from the increased utilization.

5.2.2 Module Level

The results of the configuration optimization indicate that the modules should have 13 cells or alternatively 13 batches of parallel cells in series. This results in nominal voltage of 46.8 V and even during charging guarantees the voltage to be below the critical 60 V at any time. Therefore, no high voltage precautions are required when the vehicle is deactivated. No contactors are required either as the switches function as solid-state contactors. A normal battery pack module BMS can be used to balance the cells within the SM. An active balancing in the SM can increase the utilization further. This can function even more efficient due to the reduced series connections per SM and therefore downscaled charge transfer. The number of parallel cells depends on the capacity of them, where larger cells are assumed beneficial as mentioned in the previous section. An adapted theoretical maximum accessible potential depending on the number of parallel cells is visible as depicted in Figure 5.3., if the variations of the reference cell are just extrapolated on different cell sizes. It indicates a visible increase in the maximum usable potential, if less, bigger cells are connected in parallel, which supports the arguments in the previous discussion section.

A matching within the SM is still favorable, as it would decrease losses and aging between parallel strings and increase usable charge of the series connected batches. This matching is simpler compared to conventional packs. Less cells have to be matched, and the matching of modules is not critical anymore, as the CHB inverter control can adapt the individual loads.

For each of the four switches of the H-bridge 11 MOSFET should be connected in parallel, because switches with higher current ratings tend to have unproportioned higher costs. As an

alternative, switch modules can be used as well, where only the dies internally are connected in parallel. This could reduce the packaging costs and manufacturing/cooling efforts. The switch parameters of voltage V_{DS} and current I_{D} should only over fulfil the requirements as close as possible to minimize the costs. Other factors, which influence the efficiency, have to be optimized with the mentioned methods with regards to the costs.

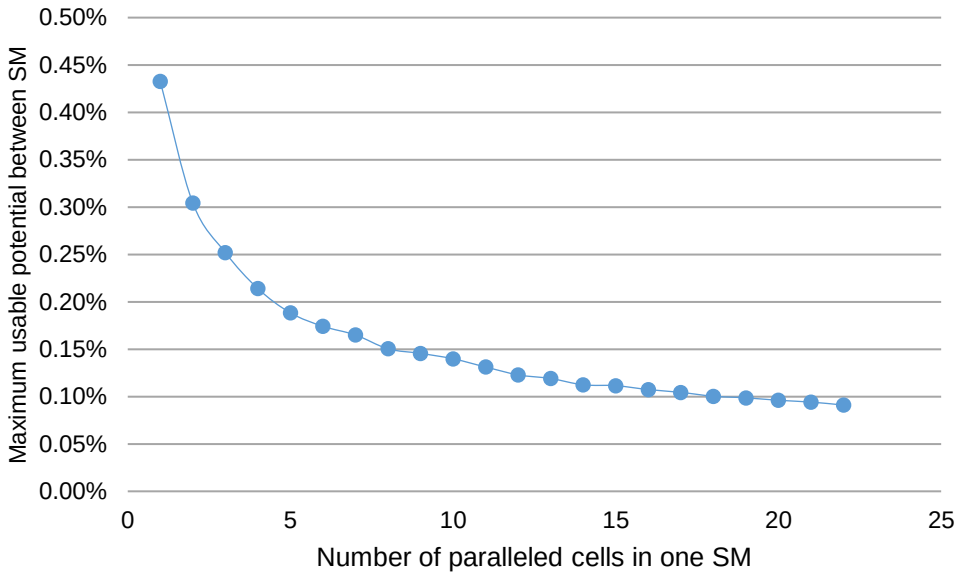

Figure 5.3: Maximum usable potential between the SM depending on the number of parallel cells in each SM

5.2.3 Pack Level

The result of the configuration optimization indicates that the whole pack ideally should consist of four modules per phase and therefore 12 SM in total. A higher number of SM would increase the accessible usable potential, but also would raise the costs disproportional due to the increased number of required components. An even further increased number of modules would also reduce the efficiency of the system.

A failing module can be easily excluded without limiting the vehicle functionality much. The faulty SM is completely detached with both negative and positive terminal disconnected. The switches have to bypass the SM, but even if one switch is damaged, due to the circuit of the H-bridge, the second pair works as a redundant bypass. In the proposed configuration, the failure of a single SM results in a reduction of 8.3 % of overall capacity and maximum available power, while the vehicle remains fully drivable.

The modularity requires a defined amount of modules where the vehicle can fulfill all the requirements and specifications. Damaged modules result in the previously discussed reduction in capacity and vehicle performance. On the contrary, it is no problem to add additional modules. These for example could be spare modules for high reliability applications. Adding spare modules also improves the Pseudo-OCV sorting method, since then a module is always available to be excluded, so that the SOC can be determined more accurately due to reduced overpotential. It has to be considered that adding additional modules would increase the overall usable capacity by the capacity of those modules. However, since they are connected in series, it would also increase the losses due to the increased circuit resistance.

Another relevant consideration is the communication between the modules. A master controller is required to control the individual SM, where the control strategy is implemented. The SM act as slaves communicating their individual states, for example SOC and other important parameters back to the master. Especially under the consideration of possible spare modules and a simple replacement of individual aged or faulty modules, a modular addressing of the modules is required. Communication between automotive components is still commonly done with the Controller Area Network bus (CAN bus), where several nodes exchange information with a multi-master serial bus protocol [217]. Each node is thereby addressed with a unique message ID. Each message ID must not be used multiple times to avoid conflicting information, and it is therefore normally permanently defined and programmed into the nodes. For the idea of identical and easy replaceable SM, the idea of a self-assignation of CAN bus identifiers was therefore implemented and published [218].

5.2.4 System Level

On a system level, a big consideration is the required charger. Normally, charging electronics are required to convert the three-phase voltage of the grid into DC voltage required by the battery. For lower charging powers, common electric vehicles include an integrated converter, so that the vehicle can be charged from a normal power outlet. For increased charging power, normally above 11 kW, such power electronics get too bulky to be integrated into the vehicle. Therefore, external chargers provide the required DC for the conventional battery. For the CHB battery, it already includes the required power electronics to provide and accept (recuperation) three-phased AC voltage. It is therefore possible to connect the CHB battery directly to the AC grid, just using the mentioned voltage transformer. Nevertheless, already existing DC charging stations still can be used to charge vehicles with a CHB battery, as the SM also can be switched in a forwarding mode, where they can be charged with DC conventionally. Therefore, an interoperability is ensured and no specific changes in the existing charging infrastructure are required.

Another system level relevant consideration is the second life application of the modules and packs. Since the CHB inverter is able to provide the required AC voltage, such recycled packs can be directly connected to the grid without the effort of setting up a new interface. Additionally, packs and modules from differently aged vehicles can be combined.

5.3 Further Challenges and Outlook

With all the benefits of a CHB inverter as an active battery interconnection explained and discussed, a few points should be mentioned, where the proposed system has restrictions and therefore requires more effort to find suitable solutions. In addition, an outlook of the research is given, where further investigation and optimization could build on the presented work.

5.3.1 Challenges for CHB Inverter Implementation

If a CHB Inverter is implemented in a vehicle, some technical solutions cannot be used the same way as they are currently integrated in BEV. The two most outstanding ones shall be mentioned here including some potential solutions, without investigating them deeper, as they are not part of this research.

Multiple Propulsion Motors

A currently increasing trend visible for several different BEV is the integration of several motors [219]. This dissertation focuses on a single motor implementation, but multiple current and future vehicle models feature two motors, one for each axle [220]. Due to the small space requirement of the electric powertrain compared to an ICE, the disadvantages of two motors are small, but it adds benefits to the vehicle, such as improved traction and optimized recuperation. High performance vehicles may even have four motors, so that each wheel can be controlled individually and therefore options like torque vectoring are possible [221]. In conventional EV with multi-motor configuration, a dedicated inverter is required for each motor, while the battery pack only has to ensure it can handle the maximum power demands of all motors.

With the configuration investigated in this dissertation, a multi motor control is not directly possible, since each motor needs its own control. However, there are theoretical modifications possible, which enable handling of one or more additional motors. The simplest way would be to include extra CHB inverters including their own battery SM for each motor. This could be done by limiting the SM size for each motor, so that the CHB inverter capacities add up to the same overall capacity similar to that of the single motor version. Two full sets of electronics would be needed, and on top of that, the overall amount of battery material might be increased due to the power requirements. Another approach could be to add an additional layer of H-bridges on each SM. Therefore, the batteries in the SM would be unaltered, but the amount of electronics would double. From a hardware perspective, this is comparable to multi-motor powertrains in current BEV where also two independent power electronic inverters must be used. It has to be mentioned that this method would require a careful investigation and synchronized control, as certain switch states may cause an internal SM short circuit [32]. A third alternative, which would need to be investigated carefully regarding its feasibility, is the option to drive two motors with one set of power electronics and still be able to control speed and torque individually [222].

High Voltage Auxiliaries Energy Supply

Another challenge is powering the remaining HV components in the vehicle besides the motor, which require energy from the battery. Especially the air conditioning compressor and the heating systems are critical, as they both consume high power and therefore they are normally implemented as HV components to keep the current low. Both can be implemented as three-phase consumers requiring inverters, so that the problem is direct comparable with the multi-motor configuration problem mentioned in the previous section. Therefore, the same solutions as mentioned there are possible. Additional hardware in form of converters is also required in current conventional BEV, so that no significant additional costs are expected. It only has to be considered that no off-the-shelf components would be suitable and new developments of the power electronics would be required. Alternatively, these components also can be implemented as low voltage (LV) auxiliary components, which are discussed in the next section.

Low Voltage Auxiliaries Energy Supply

A low voltage auxiliary energy supply is always required to provide electrical power for all the auxiliaries, for example sensors, actuators and control units. This is normally implemented as a 12 V DC supply for cars and 24 V for trucks and busses. In a conventional BEV, a central DC/DC converter, implemented as a buck converter, reduces the voltage and charges an low voltage

buffer battery from which all the units are supplied. This buffer battery also provides the activation energy to wake up the vehicle from a standby state.

As there is no HV link voltage from the battery pack available with a CHB inverter, the conventional implementation is not feasible anymore. A solution can be the in the previous section mentioned additional layer of hardware on all SM, where an independent AC voltage is generated and converted with an AC/DC converter. Another alternative is the usage of individual DC/DC converters directly on the SM terminals as presented in [223]. To reduce the costs and efforts, this approach does not need to be implemented for all SM. The unbalance caused by the additional load on this one module would be compensated by the CHB inverter with the investigated methods. However, this could cause the modules with the extra converters to age differently due to the different load. Yet another idea could be to charge the required buffer battery with a small AC/DC converter every time the vehicle is decelerating. The most feasible and efficient idea is still subject to be identified in further research.

5.3.2 Outlook

The presented research in this dissertation has a specific research question, for which the methods are defined and matching results are presented. However, while working on the topic, further interesting topics were discovered, which should be mentioned here as potential future work.

Reference Vehicle

The research is limited to the mentioned and introduced reference vehicle. Other vehicles, especially from different classes with different parameters, could produce divergent results, which could be compared against each other to generate further insights. This requires access to further detailed and validated vehicle data as an input for the models. Different vehicles could be other passenger vehicles, but also larger and smaller vehicles to see the differences, especially for the configuration optimization. Beside of the vehicle itself, also different battery configurations could be interesting. An either increased or decreased capacity would have an impact on the tolerances as well as the configuration. In a similar way, different pack voltages would lead to different results, as a different amount of cells would be connected in series and parallel. For higher charging powers, some newly introduced BEV use higher voltages of 800 V and the voltage might be even higher in the future [224]. This results in more cells in series, and therefore different tolerance results. A different voltage also might change the optimal CHB configuration, since it would generate different conduction losses in the switches due to reduced currents.

Mixing of different Modules

For this dissertation, the SM are quite similar apart from the cell variations, which influence the SM tolerances. However, the CHB inverter idea is not limited to that, as the potential is shown to balance different SOC and capacities. Therefore, the mix of aged and new modules could be an interesting further topic. This would for example enable the use case, where an EOL battery does not need to be replaced completely, but just a few new modules could be added to ensure sufficient range, which would reduce the battery replacement costs, if still needed in the future. Alternatively, even new vehicles could be sold with some reused modules, which could reduce the initial costs. The mixing of different SM also could include joining different types, for example, modules with an increased current capability mixed together with modules of a higher capacity.

Second life

The aspect of second life applications for CHB inverter batteries is mentioned in this work, but it can be investigated in detail to define an accurate use case. A reconfiguration could be considered, since the aged modules have different parameters, where a different number of SM per phase could be considered. A parallelization could be possible as well, if a high number of modules are connected to a bigger energy storage cluster. Additionally, an optimization for the configurations could be conducted, which combines the vehicle and second life use case. An improved second life use case could increase the resell value of the batteries and therefore be an additional incentive to purchase a BEV.

Charging

Charging directly from the AC grid is mentioned and simulated on the battery side. Further investigations and a more detailed definition of the charger could highlight the potential cost savings for the vehicle as well as the charging infrastructure. This cost saving for the whole system could be interesting for vehicle use cases such as public transportation and could be included in the configuration optimization.

Further Optimization with Prototype Implementation

The buildup of a vehicle sized prototype as a proof of concept and for further validation of the models was initially planned for this work. The planning and hardware implementation was finalized. The CHB battery was based on a prototype pack left over from a previous project [141]. Parts of this prototype implementation are also described in the concurrent dissertation [32]. Unfortunately, the available battery cells were too damaged due to deep self-discharging and aging, so results generated with this prototype were considered not reliable enough for this dissertation. A replacement of the cells was not possible due to financial and time restrictions. For future work however, such a prototype could define the actual implementation in a more detailed way and would allow especially for the state estimation an even better tuning of the parameter. This would be even more meaningful if combined with other points mentioned in this outlook.

6 Summary

Due to the further increased human population and the accompanying environmental degradation, a common effort is put on reducing emissions. A significant contribution is possible with more sustainable transportation. Battery electric vehicles have the potential to reduce air pollution and improve efficiency. Hence, they are regarded as an important step towards environmentally friendly mobility. However, their market penetration is relatively low due to their higher purchasing prices compared to conventional combustion engine vehicles. The battery is the most expensive part of an electric vehicle and therefore has a crucial leverage on the public adoption. Cells for automotive battery packs incorporate certain variations due to manufacturing tolerances, especially with regard to their capacity. Due to the way the cells are interconnected in the pack, cells with smaller capacity may limit the overall useable energy. Therefore, this study aims to evaluate an increased battery utilization using active cell interconnection in order to reduce costs and hence to increase the prevalence of BEV.

First, a literature review is conducted to evaluate different available battery interconnection solutions in research and commercial applications to minimize the impacts of the cell tolerances. After the evaluation of the benefits and disadvantages of each solution, the CHB inverter is identified as the most promising solution to increase the utilization of batteries without adding additional hardware and therefore increasing the costs. However, current literature does not state, which CHB configuration is the most suitable one and what are the possible accessible potentials of increased utilization from monetary and efficiency perspective.

The dissertation therefore develops a method using a CHB inverter to increase the utilization of the cell tolerances without increasing the costs of the vehicle for extra hardware. It evaluates what are the actual benefits in terms of costs with an optimized CHB configuration in a BEV.

To achieve this, first an overview of the actual cell tolerances is presented based on own experiments and literature. For this overview, a focus is put on any possible correlations of cell variation parameters, e.g., cell size/chemistry and capacity tolerances. This would allow proposing recommendations for the pack design and cell selection to increase the utilization. However, no systematic correlations between the different cell variation parameters are found, indicating that the main reason for increased variations seems to be a lower production quality and therefore decreased cell costs. An output of the tolerances overview are reference variations of automotive cells, which are used as an input in the remaining work packages.

In the next step, a control strategy is developed, which is necessary to control the CHB modules in a way they individually contribute power to the load depending on their current available potential. PWM is used, as it is the most common way to control switches in a converter. With a modified phase disposition PWM, where the modules are sorted according to their current SOC, a balancing and full utilization between the modules within a phase is possible. Between the phases, the neutral point shift method enables a continuous drivable condition for the vehicle with proportional discharge, even if whole modules are excluded.

The following work package considers the requirement to estimate the module states accurately enough to be able to sort and control them accordingly. Hereby, not the absolute SOC value is required with high accuracy, but an accurate sorting according to their relative states. Multiple different state estimators available from literature are reviewed and summarized. Three state estimators indicate a good compromise of being able to conduct the sorting, yet being affordable due to simple implementations. To be able to parametrize and compare these methods, a simulation tool is used with reference modules based on the results from the cell variation review. For each method, the best parameters are found for the specific use case, and then these optimal method results are compared against each other. It is shown that the Pseudo-OCV method makes the different module SOC converge the fastest and then keep them comparably equal. Its implementation is cost effective, as it only relies on simple voltage measurements, waiting periods and value comparisons. However, even with the optimized method, only about 30 % of the maximum theoretical potential is accessible with the presented methods, whereas the remaining potential is left unutilized.

The final step requires the optimization of the CHB inverter configuration with respect to the number of modules, switch model, and parallel switch configurations. Those configurations are compared to each other regarding their efficiency, and additionally their system costs, since the most efficient solution might not be economical feasible. To find this best configuration, an electric vehicle simulation is used as a reference platform for the comparison. The costs are included with different cost models for the switches, as their real costs are not directly available. It is found that on average, the best TCO benefit is achieved with a configuration of four modules per phase and therefore 12 SM in total, where each switch comprises of 11 parallel MOSFET and with each SM comprising of $13s15p$ battery cells. In this case, the hardware cost for the inverter is slightly more expensive than for a conventional inverter. However, due to the savings of the reduced battery capacity, the initial vehicles cost is already lower. Combined with the increased efficiency and therefore resulting energy cost savings, this leads to a smaller TCO of the vehicle. The investigated reference vehicle shows an initial vehicle cost reduction of USD 120 and a TCO saving of USD 2,647. The increased utilization only plays a minor role in the cost savings, as the parallel connection of cells reduces the accessible tolerances, and the utilization factor is small due to challenges in balancing the small variations.

As an overall conclusion, it is shown that the CHB inverter has the capability to access some of the unused capacity caused by the cell tolerances in an automotive battery pack. However, as the tolerances within new and rather homogeneous cells are minuscule and only partially accessible, this benefit is negligible. Nonetheless, even if the tolerances would be infinitesimal small, the CHB inverter with its increased efficiency still would bring the mentioned monetary benefit for the whole vehicle, initially and over the lifetime. Since it has the potential to reduce the costs and enables possible other benefits, such as increased reliability and the ability to replace modules, an implementation is still recommendable. Additionally, it would enable the usage of cells with greater variations and therefore potentially reduced battery costs. The lower initial costs and decreased TCO due to increased efficiency facilitates the adoption of electric vehicles. It therefore can further increase the market penetration of EV. With this improved prevalence and other concurrent factors, such as less polluting production of vehicle components and cleaner energy sources, a contribution to reduce the impact of mobility on the environment is possible.

List of Figures

List of Tabels

Bibliography

[1] N. Wang, L. Tang, and H. Pan, “A global comparison and assessment of incentive policy on electric vehicle promotion,” *Sustain. Cities Soc.*, vol. 44, pp. 597–603, Jan. 2019.

[2] G. Santos, “Road transport and CO 2 emissions: What are the challenges?,” *Transp. Policy*, vol. 59, pp. 71–74, Oct. 2017.

[3] P. Gong *et al.*, “Urbanisation and health in China,” *Lancet*, vol. 379, no. 9818, pp. 843–852, Mar. 2012.

[4] M. Lienkamp and T. Poeck, *Status Elektromobilität 2018 - Ausblick Geschäftsmodelle und Strategien*. Munich, Germany: Researchgate, 2018.

[5] R. Kochhan, S. Fuchs, B. Reuter, P. Burda, S. Matz, and M. Lienkamp, “An Overview of Costs for Vehicle Components , Fuels and Greenhouse Gas Emissions,” *Researchgate*, pp. 1–19, 2017.

[6] S. J. Curran, R. M. Wagner, R. L. Graves, M. Keller, and J. B. Green, “Well-to-wheel analysis of direct and indirect use of natural gas in passenger vehicles,” *Energy*, vol. 75, pp. 194–203, Oct. 2014.

[7] “Air Pollution Control Technology Fact Sheet.” United States Environmental Protection Agency: Office of Research and Development, Washington, D.C., pp. 1–6, 2002.

[8] “BP Statistical Review of World Energy 2019,” vol. 68. British Petroleum Company, Edinburgh, pp. 1–64, 2019.

[9] M. K. Yoong *et al.*, “Studies of regenerative braking in electric vehicle,” in *2010 IEEE Conference on Sustainable Utilization and Development in Engineering and Technology*, 2010, pp. 40–45.

[10] J. Kester, L. Noel, G. Zarazua de Rubens, and B. K. Sovacool, “Promoting Vehicle to Grid (V2G) in the Nordic region: Expert advice on policy mechanisms for accelerated diffusion,” *Energy Policy*, vol. 116, pp. 422–432, 2018.

[11] X. Zhang, X. Bai, and H. Zhong, “Electric vehicle adoption in license plate-controlled big cities: Evidence from Beijing,” *J. Clean. Prod.*, vol. 202, pp. 191–196, Nov. 2018.

[12] A. Jenn, K. Springel, and A. R. Gopal, “Effectiveness of electric vehicle incentives in the United States,” *Energy Policy*, vol. 119, pp. 349–356, Aug. 2018.

[13] C. Brand and J. Anable, “‘Disruption’ and ‘continuity’ in transport energy systems : the case of the ban on new conventional fossil fuel vehicles,” in *European Council for an Energy Efficient Economy (ECEEE) Summer Study 2019 Proceedings*, 2019, pp. 1117–1127.

[14] P. Slowik, N. Pavlekno, and N. Lutsey, “Assessment of next-generation electric vehicle technologies,” Washington, 2016.

[15] H. Jiang and F. Lu, “To Be Friends, Not Competitors: A Story Different from Tesla Driving the Chinese Automobile Industry,” *Manag. Organ. Rev.*, vol. 14, no. 3, pp. 491–499, Sep. 2018.

[16] “List of Electric Vehicles,” *EV-Rater*, 2019. [Online]. Available: https://evrater.com/evs. [Accessed: 23-Jul-2019].

[17] T. F. Golob and J. Gould, “Projecting use of electric vehicles from household vehicle trials,” *Transp. Res. Part B Methodol.*, vol. 32, no. 7, pp. 441–454, Sep. 1998.

[18] “Average New-Car Prices Up 3% Year-Over-Year for June 2019,” *Kelley Blue Book*, 2019. [Online]. Available: https://mediaroom.kbb.com/2019-07-02-Average-New-Car-Prices-Up-3-Year-Over-Year-for-June-2019-According-to-Kelley-Blue-Book. [Accessed: 23-Jul-2019].

[19] G. Berckmans, M. Messagie, J. Smekens, N. Omar, L. Vanhaverbeke, and J. Van Mierlo, “Cost Projection of State of the Art Lithium-Ion Batteries for Electric Vehicles Up to 2030,” *Energies*, vol. 10, no. 9, p. 1314, Sep. 2017.

[20] G. Hill, O. Heidrich, F. Creutzig, and P. Blythe, “The role of electric vehicles in near-term mitigation pathways and achieving the UK’s carbon budget,” *Appl. Energy*, vol. 251, p. 113111, Oct. 2019.

[21] M. Wietschel, M. Kühnbach, and D. Rüdiger, “Die aktuelle Treibhausgas- emissionsbilanz von Elektrofahrzeugen in Deutschland,” Karlsruhe, No. S 02/2019, 2019.

[22] C.-S. N. Shiau, C. Samaras, R. Hauffe, and J. J. Michalek, “Impact of battery weight and charging patterns on the economic and environmental benefits of plug-in hybrid vehicles,” *Energy Policy*, vol. 37, no. 7, pp. 2653–2663, Jul. 2009.

[23] M. Dubarry, N. Vuillaume, and B. Y. Liaw, “From Li-ion single cell model to battery pack simulation,” in *2008 IEEE International Conference on Control Applications*, 2008, no. 808, pp. 708–713.

[24] K. Rumpf, M. Naumann, and A. Jossen, “Experimental investigation of parametric cell-to-cell variation and correlation based on 1100 commercial lithium-ion cells,” *J. Energy Storage*, vol. 14, pp. 224–243, Dec. 2017.

[25] S. F. Schuster, M. J. Brand, P. Berg, M. Gleissenberger, and A. Jossen, “Lithium-ion cell-to-cell variation during battery electric vehicle operation,” *J. Power Sources*, vol. 297, pp. 242–251, Nov. 2015.

[26] L. Lu, X. Han, J. Li, J. Hua, and M. Ouyang, “A review on the key issues for lithium-ion battery management in electric vehicles,” *J. Power Sources*, vol. 226, pp. 272–288, Mar. 2013.

[27] S. M. Lukic, Jian Cao, R. C. Bansal, F. Rodriguez, and A. Emadi, “Energy Storage Systems for Automotive Applications,” *IEEE Trans. Ind. Electron.*, vol. 55, no. 6, pp. 2258–2267, Jun. 2008.

[28] L. Zhou, Y. Zheng, M. Ouyang, and L. Lu, “A study on parameter variation effects on battery packs for electric vehicles,” *J. Power Sources*, vol. 364, pp. 242–252, Oct. 2017.

[29] M. Baumann, L. Wildfeuer, S. Rohr, and M. Lienkamp, “Parameter variations within Li-Ion battery packs – Theoretical investigations and experimental quantification,” *J. Energy Storage*, vol. 18, pp. 295–307, Aug. 2018.

[30] T. Baumhöfer, M. Brühl, S. Rothgang, and D. U. Sauer, “Production caused variation in capacity aging trend and correlation to initial cell performance,” *J. Power Sources*, vol. 247, pp. 332–338, Feb. 2014.

[31] F. Chang, F. Roemer, M. Baumann, and M. Lienkamp, “Modelling and Evaluation of Battery Packs with Different Numbers of Paralleled Cells,” *World Electr. Veh. J.*, vol. 9, no. 1, p. 8, Jun. 2018.

[32] F. Chang, “Improving the Partial Load Efficiency of Electric Powertrains by Silicon MOSFET Multilevel Inverters,” Ph.D. dissertation, Technical University of Munich, 2019.

[33] P. Rook, “Controlling software projects,” *Softw. Eng. J.*, vol. 1, no. 1, p. 7, 1986.

[34] W. Dieterle, “Mechatronic systems: Automotive applications and modern design methodologies,” *Annu. Rev. Control*, vol. 29, no. 2, pp. 273–277, Jan. 2005.

[35] Intergovernmental Panel on Climate Change, *Climate Change 2014 - Mitigation of Climate Change*. Cambridge: Cambridge University Press, 2014.

[36] C. C. Chan, “The State of the Art of Electric, Hybrid, and Fuel Cell Vehicles,” *Proc. IEEE*, vol. 95, no. 4, pp. 704–718, Apr. 2007.

[37] J. de Santiago *et al.*, “Electrical Motor Drivelines in Commercial All-Electric Vehicles: A Review,” *IEEE Trans. Veh. Technol.*, vol. 61, no. 2, pp. 475–484, Feb. 2012.

[38] F. Chang, O. Ilina, O. Hegazi, L. Voss, and M. Lienkamp, “Adopting MOSFET multilevel inverters to improve the partial load efficiency of electric vehicles,” in *2017 19th European Conference on Power Electronics and Applications (EPE’17 ECCE Europe)*, 2017, p. P.1-P.13.

[39] T. Barlow, S. Latham, I. Mccrae, and P. Boulter, “A reference book of driving cycles for use in the measurement of road vehicle emissions,” Berkshire, 2009.

[40] A. Jossen and W. Weydanz, *Moderne Akkumulatoren richtig einsetzen*. Muenchen, Germany: Reichardt Verlag, 2006.

[41] H. Budde-Meiwes *et al.*, “A review of current automotive battery technology and future prospects,” *Proc. Inst. Mech. Eng. Part D J. Automob. Eng.*, vol. 227, no. 5, pp. 761–776, May 2013.

[42] J. W. Choi and D. Aurbach, “Promise and reality of post-lithium-ion batteries with high energy densities,” *Nat. Rev. Mater.*, vol. 1, no. 4, p. 16013, Apr. 2016.

[43] T. Horiba, “Lithium-Ion Battery Systems,” *Proc. IEEE*, vol. 102, no. 6, pp. 939–950, Jun. 2014.

[44] G. E. Blomgren, “The Development and Future of Lithium Ion Batteries,” *J. Electrochem. Soc.*, vol. 164, no. 1, pp. A5019–A5025, Dec. 2017.

[45] L. H. Saw, Y. Ye, and A. A. O. Tay, “Integration issues of lithium-ion battery into electric vehicles battery pack,” *J. Clean. Prod.*, vol. 113, pp. 1032–1045, Feb. 2016.

[46] K. Qian *et al.*, “Abuse tolerance behavior of layered oxide-based Li-ion battery during overcharge and over-discharge,” *RSC Adv.*, vol. 6, no. 80, pp. 76897–76904, 2016.

[47] M. Brand *et al.*, “Electrical safety of commercial Li-ion cells based on NMC and NCA technology compared to LFP technology,” in *2013 World Electric Vehicle Symposium and Exhibition (EVS27)*, 2013, vol. 6, no. 3, pp. 1–9.

[48] C. Julien, A. Mauger, K. Zaghib, and H. Groult, “Comparative Issues of Cathode Materials for Li-Ion Batteries,” *Inorganics*, vol. 2, no. 1, pp. 132–154, Mar. 2014.

[49] A. Kirchev, “Battery Management and Battery Diagnostics,” in *Electrochemical Energy Storage for Renewable Sources and Grid Balancing*, Elsevier, 2015, pp. 411–435.

[50] *Electric Vehicle Battery Test Procedures Manual*, no. 2. United States Advanced Battery Consortium, 1996.

[51] M. A. Hannan, M. S. H. Lipu, A. Hussain, and A. Mohamed, “A review of lithium-ion battery state of charge estimation and management system in electric vehicle applications:

Challenges and recommendations," *Renew. Sustain. Energy Rev.*, vol. 78, pp. 834–854, Oct. 2017.

[52] R. Schröder, M. Aydemir, and G. Seliger, "Comparatively Assessing different Shapes of Lithium-ion Battery Cells," *Procedia Manuf.*, vol. 8, pp. 104–111, 2017.

[53] F. Larsson, "Lithium-ion Battery Safety-Assessment by Abuse Testing, Fluoride Gas Emissions and Fire Propagation," Ph.D. dissertation, Chalmers University of Technology, 2017.

[54] "Technical specification - Winston LFP1000AHC cell." GWL Power, Prague.

[55] M. M. Kerler, "Eine Methode zur Bestimmung der optimalen Zellgröße für Elektrofahrzeuge," Ph.D. dissertation, Technical University of Munich, 2018.

[56] M. Dubarry, N. Vuillaume, and B. Y. Liaw, "Origins and accommodation of cell variations in Li-ion battery pack modeling," *Int. J. Energy Res.*, vol. 34, no. 2, pp. 216–231, Feb. 2010.

[57] S. Rothgang, T. Baumhöfer, and D. U. Sauer, "Necessity and Methods to Improve Battery Lifetime on System Level," in *EVS28*, 2015, pp. 1–9.

[58] *Addendum 99: Regulation No. 100*, vol. 2, no. 99. United Nations: World Forum for Harmonization of Vehicle Regulations, 2013, pp. 1–82.

[59] G. L. Plett and M. J. Klein, "Simulating battery packs comprising parallel cell modules and series cell modules," in *24th International Battery, Hybrid and Fuel Cell Electric Vehicle Symposium and Exhibition 2009, EVS 24*, 2009, vol. 1, no. 1, pp. 146–162.

[60] P. Keil, "Aging of Lithium-Ion Batteries in Electric Vehicles," Ph.D. dissertation, Technical University of Munich, 2017.

[61] J. Schmalstieg, S. Käbitz, M. Ecker, and D. U. Sauer, "A holistic aging model for Li(NiMnCo)O2 based 18650 lithium-ion batteries," *J. Power Sources*, vol. 257, pp. 325–334, Jul. 2014.

[62] M. Dubarry *et al.*, "Identifying battery aging mechanisms in large format Li ion cells," *J. Power Sources*, vol. 196, no. 7, pp. 3420–3425, Apr. 2011.

[63] P. Keil *et al.*, "Calendar Aging of Lithium-Ion Batteries," *J. Electrochem. Soc.*, vol. 163, no. 9, pp. A1872–A1880, Jul. 2016.

[64] E. Martinez-Laserna *et al.*, "Battery second life: Hype, hope or reality? A critical review of the state of the art," *Renew. Sustain. Energy Rev.*, vol. 93, pp. 701–718, Oct. 2018.

[65] S. Rohr *et al.*, "Quantifying Uncertainties in Reusing Lithium-Ion Batteries from Electric Vehicles," *Procedia Manuf.*, vol. 8, pp. 603–610, 2017.

[66] B. Wu and M. Narimani, *High-Power Converters and AC Drives*. Hoboken, NJ, USA: John Wiley & Sons, Inc., 2017.

[67] J. Lutz, H. Schlangenotto, U. Scheuermann, and R. De Doncker, *Semiconductor Power Devices*. Berlin, Heidelberg: Springer Berlin Heidelberg, 2011.

[68] F. Chang, O. Ilina, M. Lienkamp, and L. Voss, "Improving the Overall Efficiency of Automotive Inverters Using a Multilevel Converter Composed of Low Voltage Si mosfets," *IEEE Trans. Power Electron.*, vol. 34, no. 4, pp. 3586–3602, Apr. 2019.

[69] L. M. Tolbert, F. Z. Peng, and T. G. Habetler, "Multilevel inverters for electric vehicle applications," in *Power Electronics in Transportation (Cat. No.98TH8349)*, 1998, pp. 79–84.

[70] Z. Fang, D. Jiang, and Y. Zhang, “Study of the characteristics and suppression of EMI of inverter with SiC and Si devices,” *Chinese J. Electr. Eng.*, vol. 4, no. 3, pp. 37–46, Sep. 2018.

[71] Haizhong Ye, Y. Yang, and A. Emadi, “Traction inverters in hybrid electric vehicles,” in *2012 IEEE Transportation Electrification Conference and Expo (ITEC)*, 2012, pp. 1–6.

[72] M. Daowd, N. Omar, P. Van Den Bossche, and J. Van Mierlo, “Passive and active battery balancing comparison based on MATLAB simulation,” in *2011 IEEE Vehicle Power and Propulsion Conference*, 2011, pp. 1–7.

[73] J. Cao, N. Schofield, and A. Emadi, “Battery balancing methods: A comprehensive review,” in *2008 IEEE Vehicle Power and Propulsion Conference*, 2008, pp. 1–6.

[74] M. J. Isaacson, R. P. Hollandsworth, P. J. Giampaoli, F. A. Linkowsky, A. Salim, and V. L. Teofilo, “Advanced lithium ion battery charger,” in *Fifteenth Annual Battery Conference on Applications and Advances (Cat. No.00TH8490)*, 2000, pp. 193–198.

[75] S. Steinhorst, M. Lukasiewycz, S. Narayanaswamy, M. Kauer, and S. Chakraborty, “Smart Cells for Embedded Battery Management,” in *2014 IEEE International Conference on Cyber-Physical Systems, Networks, and Applications*, 2014, pp. 59–64.

[76] M. Preindl, C. Danielson, and F. Borrelli, “Performance evaluation of battery balancing hardware,” in *2013 European Control Conference (ECC)*, 2013, pp. 4065–4070.

[77] Hong-Sun Park, Chong-Eun Kim, Chol-Ho Kim, Gun-Woo Moon, and Joong-Hui Lee, “A Modularized Charge Equalizer for an HEV Lithium-Ion Battery String,” *IEEE Trans. Ind. Electron.*, vol. 56, no. 5, pp. 1464–1476, May 2009.

[78] P. Wacker, “Effizienzsteigerung im Antriebsstrang von Elektrofahrzeugen mittels aktiver Batteriepackverschaltung,” Ph.D. dissertation, Technical University of Munich, 2018.

[79] Y. Zheng, X. Han, L. Lu, J. Li, and M. Ouyang, “Lithium ion battery pack power fade fault identification based on Shannon entropy in electric vehicles,” *J. Power Sources*, vol. 223, pp. 136–146, Feb. 2013.

[80] Y. Li and Y. Han, “Used-battery management with integrated battery building block system,” in *2015 IEEE Applied Power Electronics Conference and Exposition (APEC)*, 2015, pp. 3177–3182.

[81] Y. Li and Y. Han, “Power electronics integration on battery cells,” in *2014 IEEE Applied Power Electronics Conference and Exposition - APEC 2014*, 2014, vol. 2, pp. 3318–3322.

[82] T. Zimmermann, P. Keil, M. Hofmann, M. F. Horsche, S. Pichlmaier, and A. Jossen, “Review of system topologies for hybrid electrical energy storage systems,” *J. Energy Storage*, vol. 8, pp. 78–90, Nov. 2016.

[83] N. Bouchhima, M. Schnierle, S. Schulte, and K. P. Birke, “Optimal energy management strategy for self-reconfigurable batteries,” *Energy*, vol. 122, pp. 560–569, Mar. 2017.

[84] Y. Li and Y. Han, “A Module-Integrated Distributed Battery Energy Storage and Management System,” *IEEE Trans. Power Electron.*, vol. 31, no. 12, pp. 1–1, 2016.

[85] Z. Li, O. Onar, A. Khaligh, and E. Schaltz, “Design and Control of a Multiple Input DC/DC Converter for Battery/Ultra-capacitor Based Electric Vehicle Power System,” in *2009 Twenty-Fourth Annual IEEE Applied Power Electronics Conference and Exposition*, 2009, pp. 591–596.

[86] S. Thomas, M. Stieneker, and R. W. De Doncker, “Development of a Modular High-Power Converter System for Battery Energy Storage Systems,” *EPE J.*, vol. 23, no. 1, pp. 34–40, Mar. 2013.

[87] F. Ju, Q. Zhang, W. Deng, and J. Li, “REVIEW OF STRUCTURES AND CONTROL OF BATTERY-SUPERCAPACITOR HYBRID ENERGY STORAGE SYSTEM FOR ELECTRIC VEHICLES,” in *Advances in Battery Manufacturing, Service, and Management Systems*, Hoboken, NJ, USA: John Wiley & Sons, Inc., 2016, pp. 303–318.

[88] S. Steinhorst *et al.*, “Distributed reconfigurable Battery System Management Architectures,” in *2016 21st Asia and South Pacific Design Automation Conference (ASP-DAC)*, 2016, pp. 429–434.

[89] T. Kim, W. Qiao, and L. Qu, “Self-reconfigurable multicell batteries,” in *2011 IEEE Energy Conversion Congress and Exposition*, 2011, pp. 3549–3555.

[90] H. Kim and K. G. Shin, “DESA: Dependable, Efficient, Scalable Architecture for Management of Large-Scale Batteries,” *IEEE Trans. Ind. Informatics*, vol. 8, no. 2, pp. 406–417, May 2012.

[91] F. Helling, S. Gotz, and T. Weyh, “A battery modular multilevel management system (BM3) for electric vehicles and stationary energy storage systems,” in *2014 16th European Conference on Power Electronics and Applications*, 2014, pp. 1–10.

[92] H. Kim and K. G. Shin, “On Dynamic Reconfiguration of a Large-Scale Battery System,” in *2009 15th IEEE Real-Time and Embedded Technology and Applications Symposium*, 2009, pp. 87–96.

[93] S. Ci, N. Lin, and D. Wu, “Reconfigurable Battery Techniques and Systems: A Survey,” *IEEE Access*, vol. 4, pp. 1175–1189, 2016.

[94] L. He, E. Kim, and K. G. Shin, “A Case Study on Improving Capacity Delivery of Battery Packs via Reconfiguration,” *ACM Trans. Cyber-Physical Syst.*, vol. 1, no. 2, pp. 1–23, Feb. 2017.

[95] M. Momayyezan, B. Hredzak, and V. G. Agelidis, “Integrated Reconfigurable Converter Topology for High-Voltage Battery Systems,” *IEEE Trans. Power Electron.*, vol. 31, no. 3, pp. 1968–1979, Mar. 2016.

[96] T. Morstyn, M. Momayyezan, B. Hredzak, and V. G. Agelidis, “Distributed Control for State-of-Charge Balancing Between the Modules of a Reconfigurable Battery Energy Storage System,” *IEEE Trans. Power Electron.*, vol. 31, no. 11, pp. 7986–7995, Nov. 2016.

[97] R. H. Baker and L. H. Bannister, “Electric power converter,” U.S. Patent 3 867 643, 14-Jan-1975.

[98] Jih-Sheng Lai and Fang Zheng Peng, “Multilevel converters-a new breed of power converters,” *IEEE Trans. Ind. Appl.*, vol. 32, no. 3, pp. 509–517, 1996.

[99] A. Majed, Z. Salam, and A. M. Amjad, “Harmonics elimination PWM based direct control for 23-level multilevel distribution STATCOM using differential evolution algorithm,” *Electr. Power Syst. Res.*, vol. 152, pp. 48–60, Nov. 2017.

[100] I. Colak, E. Kabalci, and R. Bayindir, “Review of multilevel voltage source inverter topologies and control schemes,” *Energy Convers. Manag.*, vol. 52, no. 2, pp. 1114–1128, Feb. 2011.

[101] L. M. Tolbert, Fang Zheng Peng, and T. G. Habetler, “Multilevel converters for large electric drives,” *IEEE Trans. Ind. Appl.*, vol. 35, no. 1, pp. 36–44, 1999.

[102] L. Maharjan, T. Yamagishi, H. Akagi, and J. Asakura, “Fault-tolerant control for a battery energy storage system based on a cascade PWM converter,” in *2009 IEEE 6th International Power Electronics and Motion Control Conference*, 2009, vol. 24, no. 6, pp. 945–950.

[103] M. Quraan, “Modular Multilevel Converter With Embedded Battery Cells for Traction Drives,” Ph.D. dissertation, University of Birmingham, 2016.

[104] J. Rodriguez *et al.*, “Multilevel Converters: An Enabling Technology for High-Power Applications,” *Proc. IEEE*, vol. 97, no. 11, pp. 1786–1817, Nov. 2009.

[105] A. Nabae, I. Takahashi, and H. Akagi, “A New Neutral-Point-Clamped PWM Inverter,” *IEEE Trans. Ind. Appl.*, vol. IA-17, no. 5, pp. 518–523, Sep. 1981.

[106] K. K. Gupta, A. Ranjan, P. Bhatnagar, L. K. Sahu, and S. Jain, “Multilevel Inverter Topologies With Reduced Device Count: A Review,” *IEEE Trans. Power Electron.*, vol. 31, no. 1, pp. 135–151, Jan. 2016.

[107] T. A. Meynard and H. Foch, “Multi-level conversion: high voltage choppers and voltage-source inverters,” in *PESC `92 Record. 23rd Annual IEEE Power Electronics Specialists Conference*, 1992, pp. 397–403.

[108] M. Quraan, T. Yeo, and P. Tricoli, “Design and Control of Modular Multilevel Converters for Battery Electric Vehicles,” *IEEE Trans. Power Electron.*, vol. 31, no. 1, pp. 507–517, Jan. 2016.

[109] N. Li, F. Gao, T. Yang, L. Zhang, Q. Zhang, and G. Ding, “An integrated electric vehicle power conversion system using modular multilevel converter,” in *2015 IEEE Energy Conversion Congress and Exposition (ECCE)*, 2015, pp. 5044–5051.

[110] L. M. Cunico, G. Lambert, R. P. Dacol, S. V. G. Oliveira, and Y. R. de Novaes, “Parameters design for modular multilevel converter (MMC),” in *2013 Brazilian Power Electronics Conference*, 2013, vol. 2, pp. 264–270.

[111] Qingrui Tu, Zheng Xu, and Lie Xu, “Reduced Switching-Frequency Modulation and Circulating Current Suppression for Modular Multilevel Converters,” *IEEE Trans. Power Deliv.*, vol. 26, no. 3, pp. 2009–2017, Jul. 2011.

[112] F. Altaf and B. Egardt, “Comparative Analysis of Unipolar and Bipolar Control of Modular Battery for Thermal and State-of-Charge Balancing,” *IEEE Trans. Veh. Technol.*, vol. 66, no. 4, pp. 2927–2941, Apr. 2017.

[113] A. Marzoughi, R. Burgos, D. Boroyevich, and Y. Xue, “Design and Comparison of Cascaded H-Bridge, Modular Multilevel Converter, and 5-L Active Neutral Point Clamped Topologies for Motor Drive Applications,” *IEEE Trans. Ind. Appl.*, vol. 54, no. 2, pp. 1404–1413, Mar. 2018.

[114] Y. Okazaki *et al.*, “Experimental Comparisons Between Modular Multilevel DSCC Inverters and TSBC Converters for Medium-Voltage Motor Drives,” *IEEE Trans. Power Electron.*, vol. 32, no. 3, pp. 1805–1817, Mar. 2017.

[115] G. S. Shehu, A. B. Kunya, I. H. Shanono, and T. Yalcinoz, “A Review of Multilevel Inverter Topology and Control Techniques,” *J. Autom. Control Eng.*, vol. 4, no. 3, pp. 233–241, 2016.

[116] F. Helling, J. Gluck, A. Singer, and T. Weyh, “Modular multilevel battery (M2B) for electric vehicles,” in *2016 18th European Conference on Power Electronics and Applications (EPE’16 ECCE Europe)*, 2016, pp. 1–9.

[117] F. Helling, J. Glück, A. Singer, H.-J. Pfisterer, and T. Weyh, “The AC battery – A novel approach for integrating batteries into AC systems,” *Int. J. Electr. Power Energy Syst.*, vol. 104, pp. 150–158, Jan. 2019.

[118] A. Singer, F. Helling, T. Weyh, J. Jungbauer, and H.-J. Pfisterer, “Modular multilevel parallel converter based split battery system (M2B) for stationary storage applications,” in *2017 19th European Conference on Power Electronics and Applications (EPE’17 ECCE*

Europe), 2017, p. P.1-P.10.

[119] F. Chen, W. Qiao, and L. Qu, “A modular and reconfigurable battery system,” in *2017 IEEE Applied Power Electronics Conference and Exposition (APEC)*, 2017, pp. 2131–2135.

[120] M. Ebadpour, M. B. B. Sharifian, and S. H. Hosseini, “A New Structure of Multilevel Inverter with Reduced Number of Switches for Electric Vehicle Applications,” *Energy Power Eng.*, vol. 03, no. 02, pp. 198–205, 2011.

[121] S. M. Goetz, A. V. Peterchev, and T. Weyh, “Modular Multilevel Converter With Series and Parallel Module Connectivity: Topology and Control,” *IEEE Trans. Power Electron.*, vol. 30, no. 1, pp. 203–215, Jan. 2015.

[122] Z. Zheng, K. Wang, L. Xu, and Y. Li, “A Hybrid Cascaded Multilevel Converter for Battery Energy Management Applied in Electric Vehicles,” *IEEE Trans. Power Electron.*, vol. 29, no. 7, pp. 3537–3546, Jul. 2014.

[123] R. Gogoana, M. B. Pinson, M. Z. Bazant, and S. E. Sarma, “Internal resistance matching for parallel-connected lithium-ion cells and impacts on battery pack cycle life,” *J. Power Sources*, vol. 252, pp. 8–13, Apr. 2014.

[124] A. Devie and M. Dubarry, “Durability and Reliability of Electric Vehicle Batteries under Electric Utility Grid Operations. Part 1: Cell-to-Cell Variations and Preliminary Testing,” *Batteries*, vol. 2, no. 3, p. 28, Sep. 2016.

[125] K. Rumpf, A. Rheinfeld, M. Schindler, J. Keil, T. Schua, and A. Jossen, “Influence of Cell-to-Cell Variations on the Inhomogeneity of Lithium-Ion Battery Modules,” *J. Electrochem. Soc.*, vol. 165, no. 11, pp. A2587–A2607, Aug. 2018.

[126] M. J. Brand, E. I. Kolp, P. Berg, T. Bach, P. Schmidt, and A. Jossen, “Electrical resistances of soldered battery cell connections,” *J. Energy Storage*, vol. 12, pp. 45–54, Aug. 2017.

[127] T. Wang, K. J. Tseng, J. Zhao, and Z. Wei, “Thermal investigation of lithium-ion battery module with different cell arrangement structures and forced air-cooling strategies,” *Appl. Energy*, vol. 134, pp. 229–238, Dec. 2014.

[128] N. Yang, X. Zhang, B. Shang, and G. Li, “Unbalanced discharging and aging due to temperature differences among the cells in a lithium-ion battery pack with parallel combination,” *J. Power Sources*, vol. 306, pp. 733–741, Feb. 2016.

[129] I. Zilberman, J. Schmitt, S. Ludwig, M. Naumann, and A. Jossen, “Simulation of voltage imbalance in large lithium-ion battery packs influenced by cell-to-cell variations and balancing systems,” *J. Energy Storage*, vol. 32, no. August, p. 101828, Dec. 2020.

[130] X. Gong, R. Xiong, and C. C. Mi, “Study of the characteristics of battery packs in electric vehicles with parallel-connected lithium-ion battery cells,” in *2014 IEEE Applied Power Electronics Conference and Exposition - APEC 2014*, 2014, vol. 51, no. 2, pp. 3218–3224.

[131] T. Bruen and J. Marco, “Modelling and experimental evaluation of parallel connected lithium ion cells for an electric vehicle battery system,” *J. Power Sources*, vol. 310, pp. 91–101, Apr. 2016.

[132] C. Pastor-Fernández, T. Bruen, W. D. Widanage, M. A. Gama-Valdez, and J. Marco, “A Study of Cell-to-Cell Interactions and Degradation in Parallel Strings: Implications for the Battery Management System,” *J. Power Sources*, vol. 329, pp. 574–585, Oct. 2016.

[133] L. Devroye, *Non-Uniform Random Variate Generation*. New York, NY: Springer New York, 1986.

[134] S. Paul, C. Diegelmann, H. Kabza, and W. Tillmetz, “Analysis of ageing inhomogeneities

in lithium-ion battery systems," *J. Power Sources*, vol. 239, pp. 642–650, Oct. 2013.

[135] C. Campestrini, P. Keil, S. F. Schuster, and A. Jossen, "Ageing of lithium-ion battery modules with dissipative balancing compared with single-cell ageing," *J. Energy Storage*, vol. 6, pp. 142–152, May 2016.

[136] S. Rothgang, T. Baumhofer, and D. U. Sauer, "Diversion of Aging of Battery Cells in Automotive Systems," in *2014 IEEE Vehicle Power and Propulsion Conference (VPPC)*, 2014, pp. 1–6.

[137] F. An, L. Chen, J. Huang, J. Zhang, and P. Li, "Rate dependence of cell-to-cell variations of lithium-ion cells," *Sci. Rep.*, vol. 6, no. 1, p. 35051, Dec. 2016.

[138] J. V. Barreras, T. Raj, D. A. Howey, and E. Schaltz, "Results of Screening over 200 Pristine Lithium-Ion Cells," in *2017 IEEE Vehicle Power and Propulsion Conference (VPPC)*, 2017, pp. 1–6.

[139] A. Devie, G. Baure, and M. Dubarry, "Intrinsic Variability in the Degradation of a Batch of Commercial 18650 Lithium-Ion Cells," *Energies*, vol. 11, no. 5, p. 1031, Apr. 2018.

[140] N. Lin, S. Ci, D. Wu, and H. Guo, "An Optimization Framework for Dynamically Reconfigurable Battery Systems," *IEEE Trans. Energy Convers.*, vol. 33, no. 4, pp. 1669–1676, Dec. 2018.

[141] S. Bender *et al.*, "Concept of an Electric Taxi for Tropical Megacities," in *Conference on future automotive technology*, 2014.

[142] G. Kakrinska, "Method for an Improved Battery Utilization through an Active Battery Interconnection Approach," M.S. thesis, Technical University Of Munich, 2018.

[143] K. Corzine, "Multilevel Converters," in *The power electronics handbook*, T. L. Skvarenina, Ed. Wisconsin: CRC press, 2002, pp. 6.1-6.23.

[144] N. Prabaharan and K. Palanisamy, "A comprehensive review on reduced switch multilevel inverter topologies, modulation techniques and applications," *Renew. Sustain. Energy Rev.*, vol. 76, pp. 1248–1282, Sep. 2017.

[145] Z. Yu, A. Mohammed, and I. Panahi, "A review of three PWM techniques," in *Proceedings of the 1997 American Control Conference (Cat. No.97CH36041)*, 1997, vol. 1, pp. 257–261 vol.1.

[146] A. Mohamed A. S., A. Gopinath, and M. R. Baiju, "A Simple Space Vector PWM Generation Scheme for Any General n-Level Inverter," *IEEE Trans. Ind. Electron.*, vol. 56, no. 5, pp. 1649–1656, May 2009.

[147] D. C. Rus, N. S. Preda, I. I. Incze, M. Imecs, and C. Szabo, "Comparative analysis of PWM techniques: Simulation and DSP implementation," in *2010 IEEE International Conference on Automation, Quality and Testing, Robotics (AQTR)*, 2010, vol. 3, pp. 1–6.

[148] K. Kumar Gupta and P. Bhatnagar, "Universal Control Scheme with Voltage-Level-Based Methods," in *Multilevel Inverters*, Elsevier, 2018, pp. 69–106.

[149] W. Yao, H. Hu, and Z. Lu, "Comparisons of Space-Vector Modulation and Carrier-Based Modulation of Multilevel Inverter," *IEEE Trans. Power Electron.*, vol. 23, no. 1, pp. 45–51, Jan. 2008.

[150] B. P. McGrath and D. G. Holmes, "Multicarrier PWM strategies for multilevel inverters," *IEEE Trans. Ind. Electron.*, vol. 49, no. 4, pp. 858–867, Aug. 2002.

[151] G. Carrara, S. Gardella, M. Marchesoni, R. Salutari, and G. Sciutto, "A new multilevel PWM method: a theoretical analysis," *IEEE Trans. Power Electron.*, vol. 7, no. 3, pp. 497–505, Jul. 1992.

[152] G. N. Rao, K. C. Sekhar, and P. S. Raju, “Neuro-Fuzzy Five-level Cascaded Multilevel Inverter for Active Power Filter,” *ACEEE Int. J . Electr. Power Eng.*, vol. 03, no. 01, pp. 49–54, 2012.

[153] Yiqiao Liang and C. O. Nwankpa, “A new type of STATCOM based on cascading voltage-source inverters with phase-shifted unipolar SPWM,” *IEEE Trans. Ind. Appl.*, vol. 35, no. 5, pp. 1118–1123, 1999.

[154] X. Shi, Z. Wang, L. M. Tolbert, and F. Wang, “A comparison of phase disposition and phase shift PWM strategies for modular multilevel converters,” in *2013 IEEE Energy Conversion Congress and Exposition*, 2013, pp. 4089–4096.

[155] H. Fundneider, “Identification and Simulation of Balancing Strategies for Battery Modules in Cascaded H-Bridge Multilevel Inverter considering Automotive Applications,” M.S. thesis, Technical University Of Munich, 2019.

[156] L. A. Tolbert, Fang Zheng Peng, T. Cunnyngham, and J. N. Chiasson, “Charge balance control schemes for cascade multilevel converter in hybrid electric vehicles,” *IEEE Trans. Ind. Electron.*, vol. 49, no. 5, pp. 1058–1064, Oct. 2002.

[157] M. Angulo, P. Lezana, S. Kouro, J. Rodriguez, and B. Wu, “Level-shifted PWM for Cascaded Multilevel Inverters with Even Power Distribution,” in *2007 IEEE Power Electronics Specialists Conference*, 2007, pp. 2373–2378.

[158] S. Thielemans, A. Ruderman, B. Reznikov, and J. Melkebeek, “Improved Natural Balancing With Modified Phase-Shifted PWM for Single-Leg Five-Level Flying-Capacitor Converters,” *IEEE Trans. Power Electron.*, vol. 27, no. 4, pp. 1658–1667, Apr. 2012.

[159] F. Chang, Z. Zheng, and Y. Li, “PWM strategy of a novel cascaded multi-level converter for battery management,” in *2014 17th International Conference on Electrical Machines and Systems (ICEMS)*, 2014, pp. 3208–3212.

[160] L. Maharjan, T. Yamagishi, H. Akagi, and J. Asakura, “Fault-Tolerant Operation of a Battery-Energy-Storage System Based on a Multilevel Cascade PWM Converter With Star Configuration,” *IEEE Trans. Power Electron.*, vol. 25, no. 9, pp. 2386–2396, Sep. 2010.

[161] Y. Zhang, W. Wang, Y. Kobayashi, and K. Shirai, “Remaining driving range estimation of electric vehicle,” in *2012 IEEE International Electric Vehicle Conference*, 2012, pp. 1–7.

[162] M. U. Cuma and T. Koroglu, “A comprehensive review on estimation strategies used in hybrid and battery electric vehicles,” *Renew. Sustain. Energy Rev.*, vol. 42, pp. 517–531, Feb. 2015.

[163] M. A. Roscher and D. U. Sauer, “Dynamic electric behavior and open-circuit-voltage modeling of LiFePO4-based lithium ion secondary batteries,” *J. Power Sources*, vol. 196, no. 1, pp. 331–336, Jan. 2011.

[164] F. Chang, Z. Zheng, Y. Li, and L. Peng, “A two-level SOC balance strategy for a novel hybrid energy storage topology,” in *2015 17th European Conference on Power Electronics and Applications (EPE’15 ECCE-Europe)*, 2015, no. 10, pp. 1–10.

[165] E. Chatzinikolaou and D. J. Rogers, “Cell SoC Balancing Using a Cascaded Full-Bridge Multilevel Converter in Battery Energy Storage Systems,” *IEEE Trans. Ind. Electron.*, vol. 63, no. 9, pp. 5394–5402, Sep. 2016.

[166] L. Zhang, H. Peng, Z. Ning, Z. Mu, and C. Sun, “Comparative Research on RC Equivalent Circuit Models for Lithium-Ion Batteries of Electric Vehicles,” *Appl. Sci.*, vol. 7, no. 10, p. 1002, Sep. 2017.

[167] K. S. Ng, C.-S. Moo, Y.-P. Chen, and Y.-C. Hsieh, “Enhanced coulomb counting method

for estimating state-of-charge and state-of-health of lithium-ion batteries," *Appl. Energy*, vol. 86, no. 9, pp. 1506–1511, Sep. 2009.

[168] A. Purwadi, A. Rizqiawan, A. Kevin, and N. Heryana, "State of Charge estimation method for lithium battery using combination of Coulomb Counting and Adaptive System with considering the effect of temperature," in *The 2nd IEEE Conference on Power Engineering and Renewable Energy (ICPERE) 2014*, 2014, pp. 91–95.

[169] C. Campestrini, M. F. Horsche, I. Zilberman, T. Heil, T. Zimmermann, and A. Jossen, "Validation and benchmark methods for battery management system functionalities: State of charge estimation algorithms," *J. Energy Storage*, vol. 7, pp. 38–51, Aug. 2016.

[170] D. G. Luenberger, "Observing the State of a Linear System," *IEEE Trans. Mil. Electron.*, vol. 8, no. 2, pp. 74–80, 1964.

[171] D. Luenberger, "An introduction to observers," *IEEE Trans. Automat. Contr.*, vol. 16, no. 6, pp. 596–602, Dec. 1971.

[172] M. A. Roscher, O. S. Bohlen, and D. U. Sauer, "Reliable State Estimation of Multicell Lithium-Ion Battery Systems," *IEEE Trans. Energy Convers.*, vol. 26, no. 3, pp. 737–743, Sep. 2011.

[173] G. L. Plett, "Extended Kalman filtering for battery management systems of LiPB-based HEV battery packs," *J. Power Sources*, vol. 134, no. 2, pp. 252–261, Aug. 2004.

[174] A. Lievre, S. Pelissier, A. Sari, P. Venet, and A. Hijazi, "Luenberger observer for SoC determination of lithium-ion cells in mild hybrid vehicles, compared to a Kalman filter," in *2015 Tenth International Conference on Ecological Vehicles and Renewable Energies (EVER)*, 2015, pp. 1–7.

[175] A. H. Ranjbar, A. Banaei, A. Khoobroo, and B. Fahimi, "Online Estimation of State of Charge in Li-Ion Batteries Using Impulse Response Concept," *IEEE Trans. Smart Grid*, vol. 3, no. 1, pp. 360–367, Mar. 2012.

[176] R. Zhang *et al.*, "State of the Art of Lithium-Ion Battery SOC Estimation for Electrical Vehicles," *Energies*, vol. 11, no. 7, p. 1820, Jul. 2018.

[177] W. Waag, C. Fleischer, and D. U. Sauer, "Critical review of the methods for monitoring of lithium-ion batteries in electric and hybrid vehicles," *J. Power Sources*, vol. 258, pp. 321–339, Jul. 2014.

[178] N. Lin, S. Ci, and D. Wu, "A novel low-cost online state of charge estimation method for reconfigurable battery pack," in *2016 IEEE Applied Power Electronics Conference and Exposition (APEC)*, 2016, pp. 3189–3192.

[179] Y. Zhang, W. Song, S. Lin, and Z. Feng, "A novel model of the initial state of charge estimation for LiFePO4 batteries," *J. Power Sources*, vol. 248, pp. 1028–1033, Feb. 2014.

[180] F. Leng, C. M. Tan, R. Yazami, and M. D. Le, "A practical framework of electrical based online state-of-charge estimation of lithium ion batteries," *J. Power Sources*, vol. 255, pp. 423–430, Jun. 2014.

[181] T. He, D. Li, Z. Wu, Y. Xue, and Y. Yang, "A modified luenberger observer for SOC estimation of lithium-ion battery," in *2017 36th Chinese Control Conference (CCC)*, 2017, vol. 53, no. 9, pp. 924–928.

[182] J. Pavlovic, B. Ciuffo, G. Fontaras, V. Valverde, and A. Marotta, "How much difference in type-approval CO2 emissions from passenger cars in Europe can be expected from changing to the new test procedure (NEDC vs. WLTP)?," *Transp. Res. Part A Policy Pract.*, vol. 111, pp. 136–147, May 2018.

[183] “Test Summary Sheet of BMW i3 BEV.” Advanced Powertrain Research Facility (APRF) at Argonne National Laboratory, Lemont, Illinois, US, 2014.

[184] “EPA Fuel Economy Estimates,” *United States Environmental Protection Agency*, 2019. [Online]. Available: https://www.fueleconomy.gov/feg/PowerSearch.do?action=noform&path=1&year1=1984&year2=2019&vtype=Electric. [Accessed: 03-May-2019].

[185] R. C. Karl, “Electrical Equivalent Circuit Model for Lead-Acid Batteries.” Unpublished Model, Institute for Electrical Energy Storage Technology, Technical University of Munich, Munich, Germany, 2014.

[186] C. Ni, “EC-based Modelling and Prediction of the Ageing Behaviour of Lithium-ion Cells,” M.S. thesis, Technical University Of Munich, 2014.

[187] S. W. Smith, *The Scientist and Engineer’s Guide to Digital Signal Processing*, Second Edi. San Diego, California: California Technical Publishing, 1999.

[188] M. Ahmad, “Active Interconnections of Battery Cells Using a Cascaded H-Bridge Inverter,” M.S. thesis, Technical University Of Munich, 2018.

[189] Roemer, Ahmad, Chang, and Lienkamp, “Optimization of a Cascaded H-Bridge Inverter for Electric Vehicle Applications Including Cost Consideration,” *Energies*, vol. 12, no. 22, p. 4272, Nov. 2019.

[190] M. Xiao, Q. Xu, and H. Ouyang, “An Improved Modulation Strategy Combining Phase Shifted PWM and Phase Disposition PWM for Cascaded H-Bridge Inverters,” *Energies*, vol. 10, no. 9, p. 1327, Sep. 2017.

[191] J.-S. Lee, H.-W. Sim, J. Kim, and K.-B. Lee, “Combination Analysis and Switching Method of a Cascaded H-Bridge Multilevel Inverter Based on Transformers With the Different Turns Ratio for Increasing the Voltage Level,” *IEEE Trans. Ind. Electron.*, vol. 65, no. 6, pp. 4454–4465, Jun. 2018.

[192] M. Miranbeigi, Y. Neyshabouri, and H. Iman-Eini, “State feedback control strategy and voltage balancing scheme for a transformer-less STATic synchronous COMpensator based on cascaded H-bridge converter,” *IET Power Electron.*, vol. 8, no. 6, pp. 906–917, Jun. 2015.

[193] J. Pereda and J. Dixon, “23-Level Inverter for Electric Vehicles Using a Single Battery Pack and Series Active Filters,” *IEEE Trans. Veh. Technol.*, vol. 61, no. 3, pp. 1043–1051, Mar. 2012.

[194] V. G. Monopoli, Y. Ko, G. Buticchi, and M. Liserre, “Performance Comparison of Variable-Angle Phase-Shifting Carrier PWM Techniques,” *IEEE Trans. Ind. Electron.*, vol. 65, no. 7, pp. 5272–5281, Jul. 2018.

[195] H. Vahedi, M. Sharifzadeh, K. Al-Haddad, and B. M. Wilamowski, “Single-DC-source 7-level CHB inverter with multicarrier level-shifted PWM,” in *IECON 2015 - 41st Annual Conference of the IEEE Industrial Electronics Society*, 2015, pp. 004328–004333.

[196] B. Xiao, L. Hang, C. Riley, L. M. Tolbert, and B. Ozpineci, “Three-phase modular cascaded H-bridge multilevel inverter with individual MPPT for grid-connected photovoltaic systems,” in *2013 Twenty-Eighth Annual IEEE Applied Power Electronics Conference and Exposition (APEC)*, 2013, pp. 468–474.

[197] Y. Yu, G. Konstantinou, B. Hredzak, and V. G. Agelidis, “Operation of Cascaded H-Bridge Multilevel Converters for Large-Scale Photovoltaic Power Plants Under Bridge Failures,” *IEEE Trans. Ind. Electron.*, vol. 62, no. 11, pp. 7228–7236, Nov. 2015.

[198] M. Ebadpour and M. B. B. Sharifian, “Cascade H-Bridge Multilevel Inverter with Low

Output Harmonics for Electric / Hybrid Electric Vehicle Applications," *Int. Rev. Electr. Eng. (I.R.E.E.),* vol. 7, pp. 3248–3256, 2012.

[199] B. Sarrazin, N. Rouger, J. P. Ferrieux, and Y. Avenas, "Benefits of cascaded inverters for electrical vehicles' drive-trains," in *2011 IEEE Energy Conversion Congress and Exposition*, 2011, pp. 1441–1448.

[200] "IPC-9592 Performance Parameters for Power Conversion Devices." IPC - Association Connecting Electronics Industries, 2007.

[201] D. Graovac, M. Pürschel, and K. Andreas, "MOSFET Power Losses Calculation Using the Data-Sheet Parameters," *Infineon Appl. Note*, vol. 1.1, 2006.

[202] R. Burkart and J. W. Kolar, "Component cost models for multi-objective optimizations of switched-mode power converters," in *2013 IEEE Energy Conversion Congress and Exposition*, 2013, pp. 2139–2146.

[203] G. Domingues-Olavarria, P. Fyhr, A. Reinap, M. Andersson, and M. Alakula, "From Chip to Converter: A Complete Cost Model for Power Electronics Converters," *IEEE Trans. Power Electron.*, vol. 32, no. 11, pp. 8681–8692, Nov. 2017.

[204] "Octopart - search engine for electronic parts," *Octopart Inc.*, 2019. [Online]. Available: https://octopart.com/. [Accessed: 06-May-2019].

[205] Y. Xiao, H. N. Shah, R. Natarajan, E. J. Rymaszewski, T. P. Chow, and R. J. Gutmann, "Integrated Flip-Chip Flex-Circuit Packaging for Power Electronics Applications," *IEEE Trans. Power Electron.*, vol. 19, no. 2, pp. 515–522, Mar. 2004.

[206] Xingsheng Liu, Xiukuan Jing, and Guo-Quan Lu, "Chip-scale packaging of power devices and its application in integrated power electronics modules," *IEEE Trans. Adv. Packag.*, vol. 24, no. 2, pp. 206–215, May 2001.

[207] B. Ozpineci, "Annual Progress Report for the Electric Drive Technologies Program," Oak Ridge National Laboratory, Washington, D.C., 2016.

[208] "The new BMW i3 94Ah," *BMW Group PressClub Press Release*, 2016. [Online]. Available: https://www.press.bmwgroup.com/united-kingdom/article/detail/T0259612EN_GB/the-new-bmw-i3-94ah?language=en_GB. [Accessed: 07-May-2019].

[209] "SERVICE AND WARRANTY INFORMATION 2016 BMW i3." BMW of North America, LLC, Woodcliff Lake, New Jersey 07677, 2016.

[210] "The new 2017 BMW i3 (94 Ah): More range paired to high-level dynamic performance," *BMW Group PressClub Press Release*, 2016. [Online]. Available: https://www.press.bmwgroup.com/usa/article/detail/T0259560EN_US/the-new-2017-bmw-i3-94-ah-more-range-paired-to-high-level-dynamic-performance. [Accessed: 17-Jun-2019].

[211] P. Lima, "Samsung SDI 94 Ah battery cell full specifications," *PushEVs*, 2018. [Online]. Available: https://pushevs.com/2018/04/05/samsung-sdi-94-ah-battery-cell-full-specifications/. [Accessed: 17-Jun-2019].

[212] F. Lambert, "Tesla buyer manages to get fully working Model S for just $15,000, thanks to single bad battery cell," *electrek.co*, 2020. [Online]. Available: https://electrek.co/2020/11/27/tesla-buyer-fully-working-model-s-single-bad-battery-cell/. [Accessed: 27-Nov-2020].

[213] G. K. Prasad and C. D. Rahn, "Model based identification of aging parameters in lithium ion batteries," *J. Power Sources*, vol. 232, pp. 79–85, Jun. 2013.

[214] C. Zhang, J. Jiang, L. Zhang, S. Liu, L. Wang, and P. Loh, “A Generalized SOC-OCV Model for Lithium-Ion Batteries and the SOC Estimation for LNMCO Battery,” *Energies*, vol. 9, no. 11, p. 900, Nov. 2016.

[215] K. Field, “Everything You Need To Know About Tesla’s New 4680 Battery Cell,” *CleanTechnica*, 2020. [Online]. Available: https://cleantechnica.com/2020/09/22/everything-you-need-to-know-about-teslas-new-4680-battery-cell/. [Accessed: 22-Nov-2020].

[216] F. Chang, F. Roemer, and M. Lienkamp, “Influence of Current Ripples in Cascaded Multilevel Topologies on the Aging of Lithium Batteries,” *IEEE Trans. Power Electron.*, vol. 35, no. 11, pp. 11879–11890, Nov. 2020.

[217] *ISO 11898-1: Road vehicles — Interchange of digital information — Controller area network (CAN) for high-speed communication*, 1st ed. Geneva, Switzerland: International Organization for Standardization, 1993.

[218] F. Roemer, M. Lamparter, and M. Lienkamp, “A method for masterless self-assigning CAN bus identifier,” in *2017 IEEE Transportation Electrification Conference and Expo (ITEC)*, 2017, pp. 119–123.

[219] B. Frieske, M. Kloetzke, and F. Mauser, “Trends in vehicle concept and key technology development for hybrid and battery electric vehicles,” in *2013 World Electric Vehicle Symposium and Exhibition (EVS27)*, 2013, pp. 1–12.

[220] H. Xiong, X. Zhu, and R. Zhang, “Energy Recovery Strategy Numerical Simulation for Dual Axle Drive Pure Electric Vehicle Based on Motor Loss Model and Big Data Calculation,” *Complexity*, vol. 2018, pp. 1–14, Aug. 2018.

[221] K. Jalali, T. Uchida, S. Lambert, and J. McPhee, “Development of an Advanced Torque Vectoring Control System for an Electric Vehicle with In-Wheel Motors using Soft Computing Techniques,” *SAE Int. J. Altern. Powertrains*, vol. 2, no. 2, pp. 261–278, Apr. 2013.

[222] P. M. Kelecy and R. D. Lorenz, “Control methodology for single inverter, parallel connected dual induction motor drives for electric vehicles,” in *Proceedings of 1994 Power Electronics Specialist Conference - PESC’94*, 1994, vol. 2, pp. 987–991.

[223] F. Helling, M. Kuder, A. Singer, S. Schmid, and T. Weyh, “Low Voltage Power Supply in Modular Multilevel Converter based Split Battery Systems for Electrical Vehicles,” in *2018 20th European Conference on Power Electronics and Applications (EPE’18 ECCE Europe)*, 2018, pp. 1–10.

[224] A. Meintz *et al.*, “Enabling fast charging – Vehicle considerations,” *J. Power Sources*, vol. 367, pp. 216–227, Nov. 2017.

Prepublication List

During the work on the dissertation topic, the author published, co-authored, or supervised the following papers and student theses, in which partial results of this dissertation are presented. The author is grateful for the contributions of the co-authors and the students.

Journals; Scopus/Web of Science listed (peer-reviewed)

[31] F. Chang, F. Roemer, M. Baumann, and M. Lienkamp, “Modelling and Evaluation of Battery Packs with Different Numbers of Paralleled Cells,” *World Electr. Veh. J.*, vol. 9, no. 1, p. 8, Jun. 2018.

[189] Roemer, Ahmad, Chang, and Lienkamp, “Optimization of a Cascaded H-Bridge Inverter for Electric Vehicle Applications Including Cost Consideration,” *Energies*, vol. 12, no. 22, p. 4272, Nov. 2019.

[216] F. Chang, F. Roemer, and M. Lienkamp, “Influence of Current Ripples in Cascaded Multilevel Topologies on the Aging of Lithium Batteries,” *IEEE Trans. Power Electron.*, vol. 35, no. 11, pp. 11879–11890, Nov. 2020.

Conferences, Magazines, etc.; Scopus/Web of Science listed (peer-reviewed)

[218] F. Roemer, M. Lamparter, and M. Lienkamp, “A method for masterless self-assigning CAN bus identifier,” in *2017 IEEE Transportation Electrification Conference and Expo (ITEC)*, 2017, pp. 119–123.

[-] F. Chang, F. Roemer, M. Baumann, and M. Lienkamp, “Modelling and evaluation of battery packs with different number of paralleled cells,” *EVS 2017 - 30th Int. Electr. Veh. Symp. Exhib.*, 2017.

Patents

[-] F. Roemer, M. Mrosek, and S. Schmalfuss, “ELECTRIC DRIVE UNIT FOR A BICYCLE,” WO Patent WO/2018/004462, 2018.

Journals, Conferences, Magazines, Articles, Conference presentations and poster, etc.; not Scopus/Web of Science listed

-

Dissertation irrelevant Publications; Scopus/Web of Science listed (peer-reviewed)

[-] F. Roemer, M. Mrosek, S. Schmalfuss, and M. Lienkamp, “New Approach for an Easily Detachable Electric Drive Unit for Off-the-Shelf Bicycles,” *World Electr. Veh. J.*, vol. 9, no. 3, p. 37, Aug. 2018.

[-] A. Ongel, E. Loewer, F. Roemer, G. Sethuraman, F. Chang, and M. Lienkamp, “Economic Assessment of Autonomous Electric Microtransit Vehicles,” *Sustainability*, vol. 11, no. 3, p. 648, Jan. 2019.

[-] M. Klöppel *et al.*, “Scube—Concept and Implementation of a Self-balancing, Autonomous Mobility Device for Personal Transport,” *World Electr. Veh. J.*, vol. 9, no. 4, p. 48, Dec. 2018.

[-] F. Roemer, M. Mrosek, S. Schmalfuss, and M. Lienkamp, “New Approach for an Easily Detachable Electric Drive Unit for Off-the-shelf Bicycles,” in *EVS 2017 - 30th International Electric Vehicle Symposium and Exhibition*, 2017.

Dissertation relevant Open-Source Software

-

Supervised Student Theses

[142] G. Kakrinska, “Method for an Improved Battery Utilization through an Active Battery Interconnection Approach,” M.S. thesis, Technical University Of Munich, 2018.

[155] H. Fundneider, “Identification and Simulation of Balancing Strategies for Battery Modules in Cascaded H-Bridge Multilevel Inverter considering Automotive Applications,” M.S. thesis, Technical University Of Munich, 2019.

[188] M. Ahmad, “Active Interconnections of Battery Cells Using a Cascaded H-Bridge Inverter,” M.S. thesis, Technical University Of Munich, 2018.

Appendix

Appendix A **Battery Cell Variations**

In this appendix, the detailed results of the cell variations are given. In Table A.1, a summary of all the key parameters of the cell variations of both capacity and internal resistance are given, as it is discussed in Subsection 4.1

Table A.1 Summary of key parameters and their attributes for both capacity and internal resistance

Attributes	CV_c in %	SOI_c in %	sp_c in %	p_c in %	s_c	k_c	CV_r in %	SOI_r in %	sp_r in %	s_r	k_r
Min	0.16	0.84	0.84	0.27	-1.53	1.66	0.72	3.43	3.49	-0.18	2.33
Max	6.69	17.39	19.31	9.85	1.25	13.0	25.9	67.12	80.10	2.40	10.8
Avg	1.22	5.17	5.61	2.87	0.09	3.33	5.04	18.76	18.89	0.47	4.04
Min (New)	0.16	0.84	0.84	0.27	-1.53	1.66	0.72	3.43	3.49	-0.18	2.33
Max (New)	6.69	17.39	19.31	9.85	1.25	13.0	25.9	67.12	80.10	2.40	10.8
Avg (New)	1.05	4.33	4.65	2.30	0.11	3.42	5.38	18.46	17.76	0.49	4.00
Min (Aged)	1.10	4.56	4.71	1.39	-0.58	2.07	2.56	14.27	15.56	0.14	2.99
Max (Aged)	2.80	10.97	11.40	8.31	0.92	3.97	5.00	23.98	27.52	0.14	5.35
Avg (Aged)	1.91	8.17	9.09	5.28	0.00	2.94	3.79	19.81	22.57	0.14	4.22

Appendix B **State Estimator Results**

In this appendix, the detailed results of the state estimator optimizations are presented. In Table B.1, the Pseudo-OCV sorting results depending on the different waiting times are shown, as discussed in Section 4.2.2.

Table B.1 Average maximum SOC differences depending on different waiting times

Waiting time	$\overline{\Delta SOC}_{\mathrm{max,new}}$	$\overline{\Delta SOC}_{\mathrm{max,aged}}$	$\overline{\Delta SOC}_{\mathrm{max,average}}$
0.125 s	0.0491 %	0.1666 %	0.1079 %
0.25 s	0.0388 %	0.1356 %	0.0872 %
0.5 s	0.0514 %	0.1285 %	0.0901 %
1 s	0.0749 %	0.1575 %	0.1162 %
2 s	0.1805 %	0.2595 %	0.2200 %
4 s	0.3294 %	0.3999 %	0.3647 %

In Table B.2, the Luenberger observer results are shown depending on the different parameter values, as discussed in Section 4.2.3.

Table B.2 Average maximum SOC differences depending on different parameter k_{B}

Parameter k_{B}	$\lvert\overline{\Delta SOC}_{\mathrm{new}}\rvert$	$\lvert\overline{\Delta SOC}_{\mathrm{aged}}\rvert$	$\lvert\overline{\Delta SOC}_{\mathrm{average}}\rvert$
0.0001	4.37 %	5.27 %	4.82 %
0.001	1.82 %	0.97 %	1.395 %
0.003	1.55 %	1.56 %	1.555 %
0.01	1.66 %	2.98 %	2.32 %
0.1	1.69 %	3.91 %	2.8 %